Ph. D. Thesis

INSTITUTE OF PHYSICAL CHEMISTRY

Polish Academy of Sciences

Kostyantyn Nikiforov

M.Sc., Chem.Eng.

HYDROGEN EMBRITTLEMENT AND STRESS CORROSION CRACKING OF BAINITE HIGH STRENGTH STEELS IN Cl^- CONTAINING ENVIRONMENT

Ph. D. Thesis

Supervisor: Professor **Ellina Lunarska**

D.Sc., Ph.D., M.Sc., Met.Eng.

Warsaw 2004

Kostyantyn Nikiforov, M. Sc.

HYDROGEN EMBRITTLEMENT AND STRESS CORROSION CRACKING OF BAINITE HIGH STRENGTH STEELS IN CL^- CONTAINING ENVIRONMENT

Abstract

The variation of the chemical composition, microstructure, heat treatment and cold work considerably alter the susceptibility of low carbon low alloy high strength steels used in aircraft industry to stress corrosion cracking. Increased aggressiveness of the environment, as appearance of "acid rain" and "acid dew" also affects the susceptibility and the mechanism of stress corrosion cracking of high strength steel.

In present work, the mechanism of stress corrosion cracking of bainite high strength aircraft (30HGSNAŻ) steel of high purity has been investigated and the effects of the variation of carbon content and heat treatment, as well as the effect of shot peening and fatigue pretreatment on the structure and on the susceptibility to stress corrosion cracking in Cl^- containing solutions have been evaluated.

Analysis of failure cases of aircraft parts and results of the laboratory tests have shown that corrosion cracks nucleate at corrosion pits and propagate according to hydrogen embrittlement mechanism. Therefore, susceptibility to pitting corrosion, hydrogen behavior, susceptibility to hydrogen embrittlement and to stress corrosion cracking has been studied using the specially modified methods.

Resistance to stress corrosion cracking under the open circuit conditions has been stated to be associated with the resistance to pitting corrosion, established in the specially elaborated test. Resistance to pitting and to stress corrosion cracking increases with decreasing carbon content and with the application of shot peening. Uneven deformation produced during fatigue pretreatment affects the pitting but the intensity of pitting corrosion is much lower in the case of application of shot peening before the fatigue test.

Susceptibility to hydrogen embrittlement depends on the hydrogen trapping efficiency, which in turn is associated with the carbon segregation at the boundaries of bainite laths and parent austenite grains. Decrease in the carbon content decreases the hydrogen trapping and thus increases the resistance to the hydrogen embrittlement.

Shot peening increases the trapping efficiency within deformed layer and hampers the hydrogen transport through the layer. Presence of the shot peened layer decreases the hydrogen flux entering the core and thus decreases susceptibility of core to the hydrogen embrittlement. The hydrogen induced cracking in the shot peened or in the fatigue pretreated metal follows the local deformation paths and the kind of the applied cold work determines the mode of the hydrogen assisted damage.

The higher aggressiveness of Na_2SO_4 + NaCl solution simulating the "acid rain" or "acid dew" in comparison with NaCl one manifests itself mainly under the open circuit conditions.

The bainite 30HGSNAŻ type steel with decreased carbon content, subjected to appropriate heat treatment and surface modification by shot peening exhibits the mechanical properties required by the Polish Standard and the resistance to pitting corrosion, to stress corrosion cracking and to hydrogen embrittlement higher than the standard steel.

Mgr inż. Kostyantyn Nikiforov

KRUCHOŚĆ WODOROWA I KOROZJA NAPRĘŻENIOWA WYSOKOWYTRZYMAŁYCH STALI BAINITYCZNYCH W ŚRODOWISKU ZAWIERAJĄCYM Cl^-

Streszczenie

Zmiana składu chemicznego, mikrostruktury, obróbki cieplnej i mechanicznej znacząco wpływa na podatność niskowęglowej, niskostopowej stali wysokiej wytrzymałości, stosowanej w przemyśle lotniczym, na korozję naprężeniową. Wzrastająca agresywność środowiska, jak występowanie „kwaśnych deszczy" i „kwaśnej rosy", również wpływa na podatność i na mechanizm korozji naprężeniowej stali wysokowytrzymałej.

W niniejszej pracy zbadano mechanizm korozji naprężeniowej bainitycznej wysokowytrzymałej lotniczej stali (30HGSNAŻ) o wysokiej czystości, oraz określono wpływ zmian zawartości węgla i obróbki cieplnej, jak również kulowania i wstępnej próby zmęczeniowej, na strukturę i na podatność stali na korozję naprężeniową w środowiskach zawierających Cl^-.

Analiza powypadkowa części lotniczych oraz badania laboratoryjne wykazały, że pęknięcia korozyjne są zarodkowane na korozyjnych wżerach i rozprzestrzeniają się zgodnie z mechanizmem kruchości wodorowej. Dlatego też, przy pomocy specjalnie zmodyfikowanych metod badano podatność materiałów na korozję wżerową, zachowanie się wodoru w metalu, podatność na kruchość wodorową i na korozję naprężeniową.

Stwierdzono, że odporność na korozyjne pękanie w warunkach obwodu otwartego jest związana z odpornością na korozję wżerową, określoną w specjalnie opracowanych testach. Odporność na korozję pitingową i naprężeniową wzrasta z obniżeniem zawartości węgla i z zastosowaniem kulowania. Nierównomierne odkształcenie wprowadzone w trakcie wstępnego testu zmęczeniowego, wpływa na korozję pitingową, intensywność której jest znacznie niższa w przypadku materiału poddanego kulowaniu przed testem zmęczeniowym.

Podatność na kruchość wodorową zależy od efektywności pułapkowania wodoru, która z kolei jest związana z segregacją węgla na granicach płytek bainitu i rodzimych ziaren austenitu. Obniżenie zawartości węgla zmniejsza pułapkowanie wodoru i tym samym zwiększa odporność na kruchość wodorową.

Kulowanie zwiększa efektywność pułapkowania wodoru w warstwie odkształconej i hamuje transport wodoru przez tę warstwę. Obecność warstwy kulowanej obniża strumień wodoru do wnętrza i tym samym obniża podatność na kruchość wodorową części wewnętrznej. Wodorowe pękanie kulowanego lub wstępnie zmęczonego metalu zachodzi wzdłuż pasm lokalnego odkształcenia, a zatem rodzaj odkształcenia określa przebieg wodorowego niszczenia.

Większa agresywność roztworu Na_2SO_4 + NaCl, symulującego „kwaśny deszcz" lub „kwaśną rosę", w porównaniu z NaCl uwidacznia się głównie w warunkach obwodu otwartego.

Bainityczna stal typu 30HGSNAŻ o obniżonej zawartości węgla, poddana odpowiedniej obróbce cieplnej i modyfikacji powierzchni przez kulowanie wykazuje własności mechaniczne wymagane przez Polską Normę, oraz odporność na korozję pitingową, na korozję naprężeniową i na kruchość wodorowe wyższą aniżeli standardowa stal.

The Author wishes to express his sincere thanks

to ***Professor ELLINA LUNARSKA***

for introduction into the new interesting scientific field, constant inspiration, constructive discussions, care and parent attitude. Without her continued encouragement and kind assistance this thesis would not have been possible.

to ***Dr. E. Sitko***

for his encouragement and the valuable discussions.

to ***Ms J. Pyrza***

for her assistance at experimental work.

to ***Professor J. Flis*** and to ***Professor T. Zakroczymski*** and to ***all of the Colleagues*** from the Department of Electrochemistry, Corrosion and Applied Surface Science of the Institute of Physical Chemistry, PAN

for their support and friendly attitude.

CONTENTS

1. INTRODUCTION

The highly loaded parts of the airplanes are made of steels of the strength about 2000 MPa. During the exploitation, those parts are subjected simultaneously to the high stresses and aggressive environment. In the case of the aircraft parts, stress may be residual resulted from the production process or externally applied at static and cyclic loading. As the aggressive environments in the aircraft exploitation the industrial and sea shore atmosphere, the acid rain, acid dew, fertilizers, as well as fire extinguish chemicals may be considered. Under the combine action of the stress and the environment, the stress corrosion cracking of the aircraft parts may occur.

The mechanism of the stress corrosion cracking has not been completely understood yet, because of its complex and involved nature. Susceptibility of high strength steel to stress corrosion cracking is determined by the chemical composition of steel, its microstructure and mechanical properties, as well as by the environment parameters and the stresses. The change of any factor affecting the stress corrosion cracking can significantly alter the susceptibility of material to this type of damage.

At present, the aircrafts exploited in Poland have some highly loaded elements made of the 30HGSNA high strength steel. Although the susceptibility of this steel to stress corrosion cracking has been studied and recognized, modification and modernization of the steel making processes, variation of the steel chemistry and microstructure within the range allowed by the appropriate Standards may affect susceptibility of material to stress corrosion cracking. On the other hand, the increase in the aggressiveness of the environment (acid rain and dew) affects susceptibility to the corrosion damage of currently used steel parts, especially of those being still in exploitation and revealing some traces of fatigue.

The deeper investigation of effect of the material state and the aggressive environment on susceptibility to the stress corrosion cracking of 30HGSNA type steel should be undertaken. The obtained results impact the knowledge of the mechanism of the stress corrosion cracking of high strength steels. The systematic and clear data may also allow elaborate the effective methods to prevent the failures caused by the stress corrosion of steel providing the increase in exploitation time of the aircraft equipment and safety of flying.

2. LITERATURE REVIEW

2.1 Environment induced cracking

Environment induced cracking (EIC) is a general term for a brittle mechanical failure that results from a synergism between the tensile stress and the aggressive environment. Failures are not observed in the case of action of one of these factors. However, when stress and corrosion environment are combined, EIC may occur. EIC includes:

- stress corrosion cracking (SCC)
- corrosion fatigue cracking (CFC)
- hydrogen induced cracking (HIC) or hydrogen embrittlement (HE)

Modern alloys of high strength and the corrosion resistance are often more susceptible to EIC. SCC, CFC, and HIC are perhaps the most pernicious forms of corrosion because of the elusiveness of their mechanism and the resultant of their occurrence.

Some parameters affecting the SCC, CFC and HIC are summarized in Table 2.1 [1].

Table 2.1

Parameters affecting the SCC, CFC and HIC

Characteristics	Stress corrosion cracking	Corrosion Fatigue Cracking	Hydrogen Induced Cracking
Stress	static tensile	cyclic with some tensile constituents	static tensile
Aqueous corrosive environment	specific to the alloy	any	any
Temperature increase	accelerates	accelerates	increases to RT, then decreases
Pure metal	more resistant	susceptible	susceptible
Crack morphology	- TG or IG branched - sharp tip	- TG unbranched - blunt tip	- TG or IG unbranched - sharp tip
Corrosion product in crack	absent (usually)	present	absent (usually)
Crack surface appearance	cleavage like	beach marks and/or striations	cleavage like
Cathodic polarization	suppresses (usually)	suppresses	accelerates
Strength level	susceptible, but HIC often predominates	accelerates	accelerates

2.2 Stress corrosion cracking

Stress corrosion cracking (SCC) is a form of localized damage that refers to the cracking under the combined influence of stress and corrosive environment. The macroscopic fracture appearance tends to be of the "brittle" type, even if the metal/alloy is of a mechanically ductile variety. Cracking can have a transgranular or intergranular morphology.

Generally three conditions must be present simultaneously to produce the SCC: a critical environment, a susceptible alloy and a tensile stress. Aggressive environment is often specific to the alloy system and may not have effects on other alloys. Stress, that can contribute to SCC, includes the residual stress from manufacturing processes (welding, brazing, casting, surface and heat treatment, forming and shaping, machining, cutting and shearing), assembly stress (poor fit up, torqueing), operational stress (applied), thermally induced stress (temperature gradients, different thermal expansion and contraction) and stresses induced by the build-up of the voluminous corrosion products.

2.2.1 Course of the stress corrosion cracking

The following stages at the material failure due to the SCC are distinguished:

- incubation of the crack;
- propagation of the corrosion crack;
- mechanical failure of material in the crack affected zone.

Multiple variables such as the stress level, the alloy composition, microstructure, concentration of corrosive species, the surface finish, micro-environmental surface effects, temperature, electrochemical potential, etc affect the stress corrosion cracking phenomena.

The main metallurgical and environmental factors affecting the SCC of the low alloy steels are shown in Table 2.2. Some of these factors will be shortly described below.

2.2.2 Incubation of the SCC crack

According to the present knowledge, initiation of SCC has been mainly caused by the corrosion process on the metal surface. The local corrosion or the local destruction are especially dangerous in the case of SCC.

Local corrosion. The local material losses due to the local corrosion (pitting, crevice, selective etc) lead to the formation of the notch causing, the stress concentration up to the critical level for the crack propagation.

Table 2.2.
Structure factors and environment parameters affecting the incubation and the propagation of the stress corrosion cracks.

SCC	Structure parameters	Environment parameters
Incubation of crack		
	- nonmetallic inclusions; - segregation of elements; - non uniform material structure; - damage of protective layers	- Cl^- ions; - non uniformity of electrolyte; - non uniform thickness of electrolyte layer
Propagation of crack		
Anodic dissolution	- presence of carbon and nitrogen; - segregation on grain boundaries; - spheroidizing of structure	- entering of cations to the protective layers - decrease in solution pH
Hydrogen mechanism	- factors affecting hydrogen transport - inclusions as inner notches	- cathodic polarization - decrease in solution pH
Vacancy mechanism	- difficulties in the dislocation creation	- decrease in general corrosion

Formation and destruction of protective layer. Protective (passive) layers formed on the surface of the material due to the interaction with aggressive environment may hamper the further harmful actions of environment and the corrosion processes. But these layers (usually oxide or hydroxide) have lower mechanical strength or higher brittleness in comparison with the bulk material. Therefore, they can be easily destroyed even at the action of the low mechanical stresses. This results in the local exposure of the material surface to the aggressive environment, which leads to the local material loss and the crack initiation.

Generally, susceptibility of materials to the initiation of stress corrosion cracking in given environment has been determined by the susceptibility to the local corrosion, by the repassivation rate and by the mechanical properties of the protective (passive in the given environment) layers.

2.2.3. SCC propagation

Presence of the notches on the metal surface provides the local stress concentration and leads to the change of the environment parameters inside the notch. Both factors promote the crack grown to the size causing the failure of the installation. According to the present knowledge there are few different mechanisms of the crack propagation for different environment-material systems. Combination of various mechanisms (so called the mixed mechanism) is also possible.

Anodic dissolution. This mechanism has been proposed to operate in the low alloy steels in nitrate solutions [2]. The side walls of the crack undergo repassivation, but due to the stress concentration at the crack tip the passive layer may break and the active dissolution of the metal occurs. Crack propagates when the metal in this environment is in the active-passive state and the environment has the moderate repassivation ability.

Vacancy generation. This mechanism supposes the generation of vacancies in a process of iron dissolution. Iron ions diffuse through existing passive layer to solution at the crack tip causing the generation of vacancies in the metal lattice. Under influence of tensile stress the random distribution of vacancies became organized in the stream [3]. Following organization of vacancies into the clusters and their orientation towards to the stress vector cause the intergranular crack propagation.

Hydrogen embrittlement. According to many researches hydrogen is the main deteriorating factor in the SCC of the low alloy high strength steels. Due to the decrease of pH of solution inside the crack, hydrogen can easily evolve from the electrolyte. Evolved hydrogen interacts with the metal causing the hydrogen embrittlement.

The hydrogen assisted degradation of materials has been the aim of intensive studies and discussions on the special conferences, as, for instance, on the recently held ones: "Corrosion-Deformation Interaction" (CDI'96 at EUROCORR, 1996), "Environmental Degradation of Engineering Materials" - EDEM'99 (Gdansk, 1999), EDEM-2003 (Bordeaux, 2003), "Environment-Induced Cracking of Metals" – EICM- 1 (USA, 1999), EICM-2 (Banff, Canada, 2004). However, no united mechanism of hydrogen embrittlement has been elaborated and several possible mechanisms (including the ones proposed earlier) of the hydrogen embrittlement have been still considered.

Decohesion of the metal lattice. According to this mechanism [4], hydrogen atoms adsorbed at the crack tip or moving to the crack tip from the metal [5] decrease the binding strength of the metal atoms, cf. Figure 2.1. As a result, the stress required for the crack propagation decreases. Formation of the internal cracks occurs due to the metal lattice decohesion produced by the hydrogen segregated at the sites with the locally increased hydrostatic stress [6].

Adsorption mechanism. According to this approach, the hydrogen atoms adsorbed at the crack tip and walls decrease the metal surface energy, and thus facilitate the Orowan's crack opening and propagation [7].

Adsorption-induced localized-slip model. This model [8] is generally applicable to the cleavage-like and intergranular cracking. In the inert environment the crack growth occurs predominantly by the egress of dislocations at the crack tips, cf. Figure 2.2. Adsorption of the

hydrogen atoms weakens the interatomic bounds and thereby facilitates the injection of dislocations from the crack tip, which produces the crack growth by an alternate-slip process.

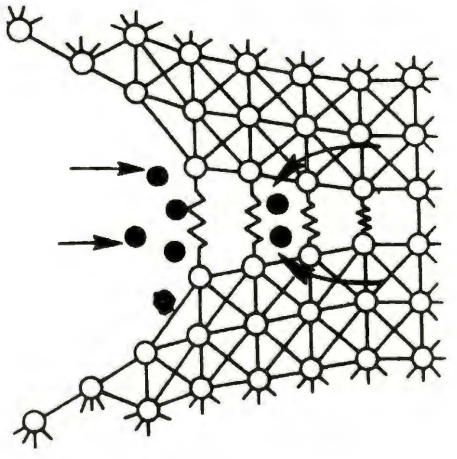

Figure 2.1. Model of hydrogen interaction with the metal lattice at the crack tip. • - hydrogen atoms, ° - metal atoms [6].

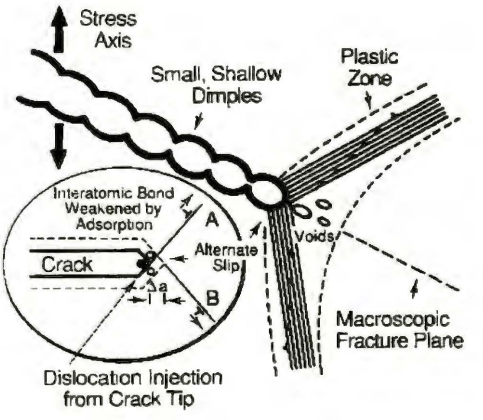

Figure 2.2. Schematic diagrams illustrating crack growth by the adsorption-induced localized-slip model [8].

Suppression of dislocation motion. In the case of iron the dislocation pile-ups are relaxed by the cross-slip of dislocations and no brittle cracks are formed at ambient temperature. However, hydrogen suppresses the cross-slip of dislocations making relaxation at the crack tip impossible. As a result, the brittle cracking occurs [9].

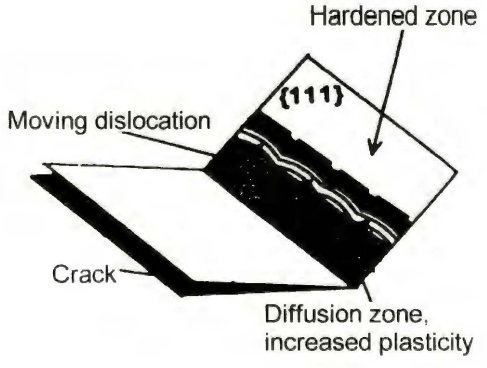

Figure 2.3. Model of the crack tip with the zone of increased plasticity and with the hardened zone, formed under the action of hydrogen [11].

Local plasticity of metal. Hydrogen increases the screw dislocation mobility [10], producing the softening effect. However, this leads to the concentration of dislocations at the obstacles, and the initial hydrogen induced local plasticity leads to subsequent hardening and final embrittlement.

The other model of the crack propagation due to the hydrogen induced softening is based on the effect of the localized corrosion at the crack tip [11]. The plasticity of the metal enhances

because of the generation of vacancies and hydrogen due to the localized anodic dissolution at the crack tip. Away from the crack tip the emitted dislocations interact with the previously formed obstacles, cf. Figure 2.3. The diffusion zone (enhanced plasticity) and hardened zone in the front of the crack tip impose the microscopic zigzag propagation of crack.

2.3. Factors affecting susceptibility to SCC of high strength steels

2.3.1 Crack initiation

The main factors determining the crack initiation in the high strength steels exposed tp the atmosphere are:

- mechanical defects;
- nonmetallic inclusions, especially sulfides;
- nonuniformity of environment.

2.3.1.1. Mechanical defects

In the case of the parts made of high strength steel, especially the airplane parts, the special precautions have to be preserved to avoid any possible surface defects, which can serve as the notches for the fatigue and local corrosion initiation. However, such defects as scratches, fissures, microcracks can form during the exploitation due to the accumulative damage, erosion or ageing processes. At exposition of such parts to the aggressive environment those sites serve as the corrosion cracks nuclei and the stress corrosion cracking may start to appear.

2.3.1.2 Nonmetallic inclusions

The nonmetallic inclusions occurring in steel vary by their chemical composition and morphology as well as by their mechanical and physical properties. In the carbon and low-alloy steels, the major inclusions are silicates, sulfides (mainly {Mn, Fe}S) of different shapes [12], oxides and complex oxides with the sulfide shell.

The most important properties of the nonmetallic inclusions from the standpoint of corrosion are their ability to deteriorate in aqueous media. Sulfides are known to disintegrate in aqueous solution. The dissolution of the surface sulfides provides the pitting nucleation sites [13] and micro notches. Depending on the solution pH as a result of sulfide disintegration, H_2S or HS^- and S^- ions are produced. Accelerating effect of these compounds on the corrosion rate has been established by many investigators [14, 15, 16].

Shape of nonmetallic inclusions plays significant role in the pit nucleation. Spheroidized

particles are less susceptible to corrosion than elongated and plastically deformed ones [17, 18].

Another factor accounting for the detrimental effects of inclusions on the local corrosion and cracks initiation is the presence of the micro fissures at the inclusions. Since sulfides exhibit a much higher thermal expansion coefficient than the steel matrix, the voids between the sulfide or sulfide shielded oxide and the metal base are formed during cooling and may additionally promote the local crack initiation. Because of the nonuniformity of the surface chemistry and the phase composition the presence of the nonmetallic particles of other inclusions (silicates, oxides) may also plays detrimental role in the corrosion and stress corrosion nucleation processes [19].

2.3.1.3. Nonuniformity of environment

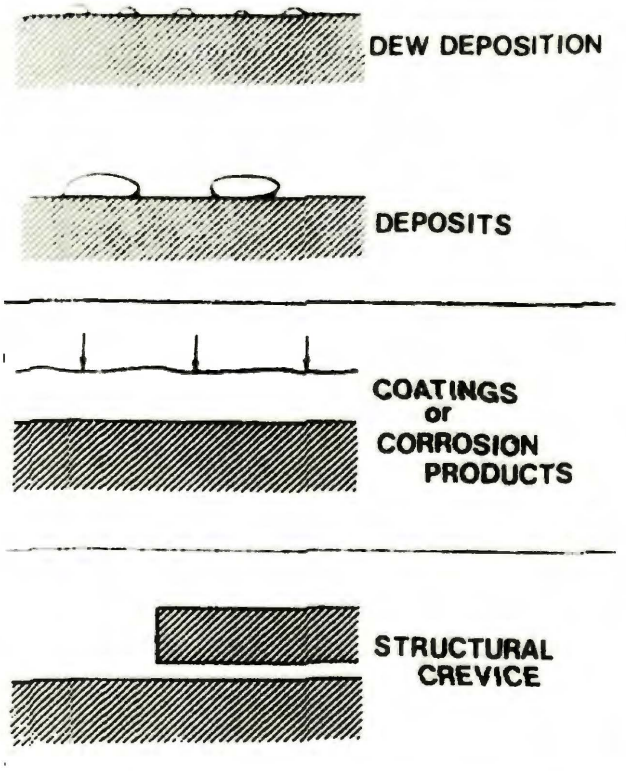

Figure 2.4. Schematic presentation of the nonuniformity of the environment on the surface of machine parts exposed to air [20]

The local degradation of the metal, even having the uniform surface may occur due to the action of the nonuniform environment. The metal parts exposed to the air are usually covered by the film of water. Different thickness of the film and its nonuniform drying differ the access of air oxygen to the surface, accelerating the local corrosion. The similar effect may produce droplets of rain and dew, especially the acid rain and acid dew. Formation and accumulation of corrosion products, including the Cl containing hydroxides, especially within the kinks and crevices of the apparatus promote the local corrosion (Figure 2.4 [20]). In the case of the agricultural airplanes the droplets of fertilizer might also be the cause for the pit formation.

2.3.2 Crack propagation

Since the process of the crack propagation in the low carbon low alloy high strength steels has been governed by the hydrogen mechanism, the similar factors should determine the susceptibility to both: the hydrogen embrittlement and the corrosion cracks propagation.

The effects of the most important factors affecting the crack propagation in the low carbon low alloy high strength steels will be shortly exemplified.

2.3.2.1 Effect of the steel strength

With the increase in the strength of the low carbon low alloy steels the critical stress intensity decreases (Figure 2.5) [21] and the crack propagation velocity increases (Figure 2.6) [22], as measured in the water [21] and in the Cl^- containing solutions of various pH [22]. This has been associated with the hydrogen effects, since the similar relationships have been found at the steels testing in gaseous hydrogen [23, 24, 25]. As discussed in [25], all the parameters characterizing the susceptibility of high strength steels to HE deteriorate more eager at the increase in the metal strength. The detrimental effect of hydrogen on the loss of plasticity by the steel of different strength is shown in Figure 2.7 [26]: the same amount of hydrogen produces the more pronounced decrease in plasticity in the case of the steel of higher strength.

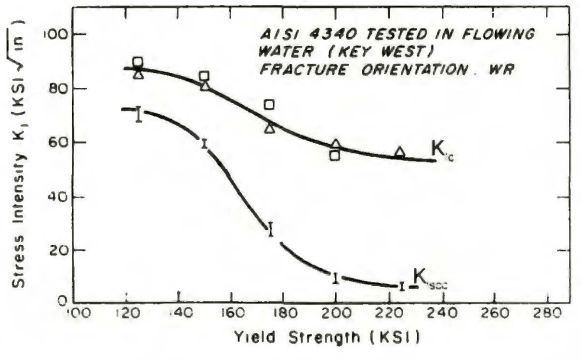

Figure 2.5. Effect of the strength level on K_{Ic} and K_{Iscc} for AISI 4340 steel [21].

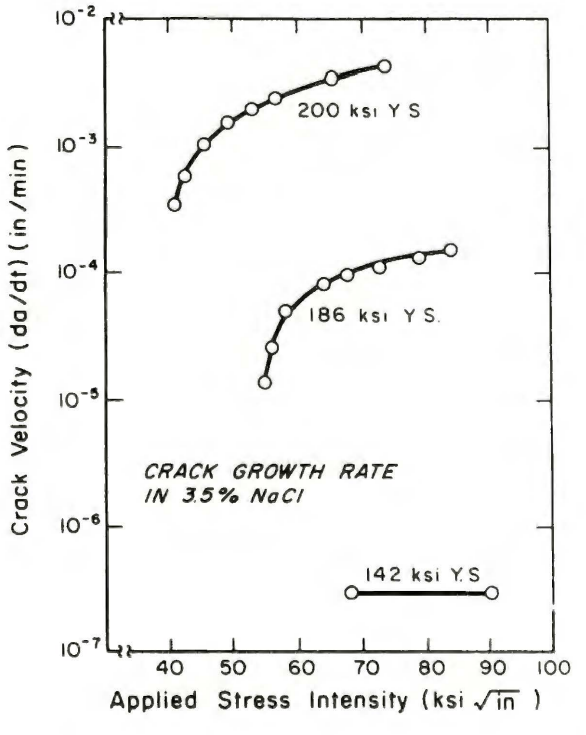

Figure 2.6 Effect of the applied stress intensity on the crack growth rate for AISI 4340 [22] for different level of steel strength.

However, the above relationships have not been always strictly observed because of the influence of other factors, especially the microstructure of steels.

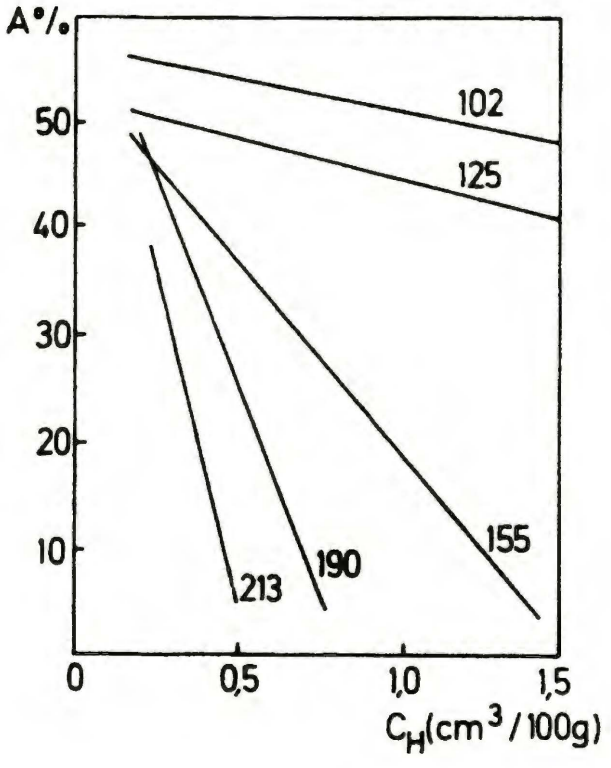

Figure 2.7. Effect of the steel strength on decrease in plasticity, depending on the hydrogen content. Numbers at curves represent the specimen strength in kg/mm^2 [26].

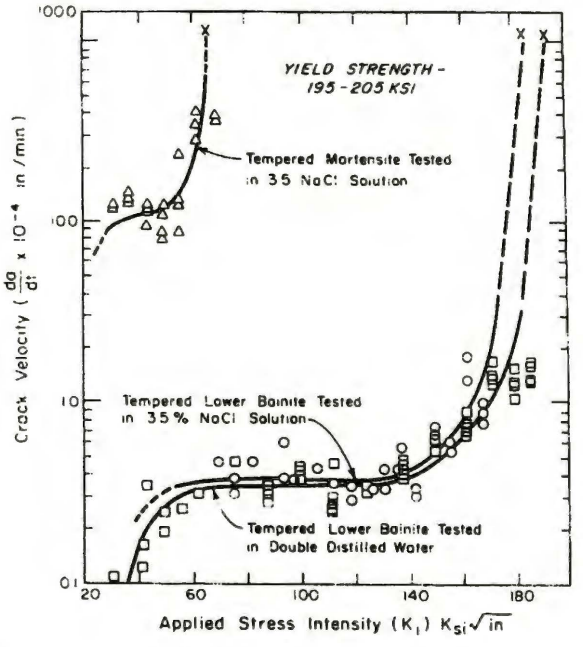

Figure 2.8 Crack velocity vs. stress intensity for AISI 4340 steel (tempered martensite and tempered bainite structures) in 3.5% NaCl and double distilled water [27].

2.3.2.2 Effect of the microstructue

High strength steels have structure of tempered martensite or bainite. In the case of uniform structure the crack propagation is faster in the martensite steel, cf. Figure 2.8 [27]. It has been also shown in several works [28-31] that the bainite structure is more resistant to HE than the martensite one. For example, the crack propagation rate has been significantly greater in the high strength steel with the tempered martensite structure than in that with the lower bainite structure [32]. However, some recent studies of the effect of the microstructure of the low carbon alloy steels of increased strength (26H2MF and 34HMN) [33] on hydrogen embrittlement in NaCl solution have revealed that the bainite is more susceptible than the tempered martensite, while the least susceptible is ferrite with the small dispersed carbides.

Generally, the following order of decreasing susceptibility to hydrogen embrittlement has been suggested [34, 35]: martensite → bainite → pearlite → tempered martensite → sorbite.

The higher susceptibility to HE of martensite structure in comparison to the bainite one may be accounted for the following reasons:

- the higher internal stresses in martensite structure;
- the more effective hydrogen trapping in the plate martensite structure [18];
- different effect on hydrogen segregation by the coherently twinned interfaces in the plate martensite, as opposed to the incoherent bainite laths [32].

It should be noted, however, that there are no systematic studies of the effect of the morphology of the bainite structure on the hydrogen behavior in high strength steels.

Material with nonuniform structure is more susceptible to SCC [36]. The banded ferrite-pearlite structure has been reported to be more susceptible to HE than the acicular ferrite or bainite [37]. In the case of the nonuniform martensite-bainite structure the martensite areas are more susceptible to the hydrogen cracking [38].

The retained austenite, which may be present in the high strength low alloy steels also affect the susceptibility to HE. In the case of the steels heat treated to obtain the different microstructure but the similar strength level, the presence of the retained austenite [39] has been found to produce the beneficial effect, despite the kind of the main constituents of the structure. The origin of these phenomena might be the ability of austenite to be a sink and a trap for hydrogen. However, according to above authors the effect of retained austenite depends on its relative distribution and stability.

Among the other structure features affecting susceptibility to SCC and HE of high strength steels the refining of structural features plays an important role.

The ausforming processes (plastic deformation of steel at austenising temperature, prior to quenching) of high strength steel [40] refine the martensite platelet, which leads to the significant increase in the delayed fracture time, as tested in distilled water environment (Figure 2.9). The refining of ferrite/bainite structure has been shown [41] to improve the resistance to HE.

An intergranular fracture of high strength steels observed in the both neutral or acidic [42, 43, 44] and gaseous [45, 46] environments, the cracking occurs along the prior austenite grain boundaries. Therefore, effect of the grain size and the grain boundary chemistry should be considered. As seen in Figure 2.10 [47] the coarse grains result in the shorter failure time. The segregation of impurities, as S and P at the grain boundaries also affects the susceptibility to HE [48].

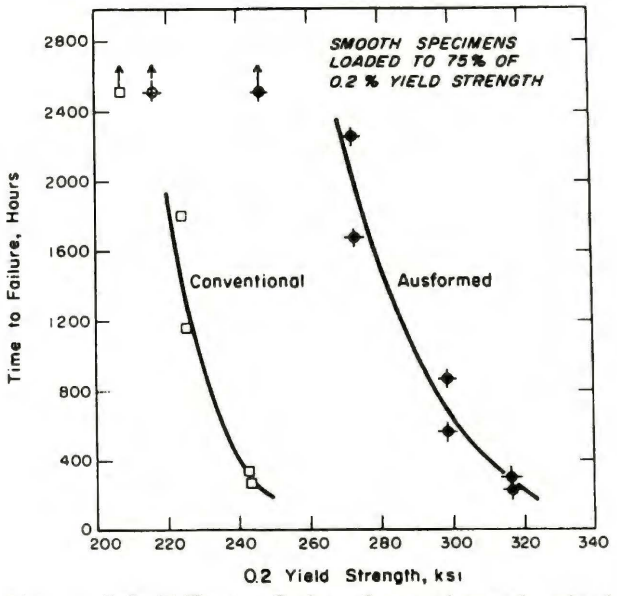

Figure 2.9 Effect of the thermal-mechanical processing on the time to fracture of D6AC steel in distilled water [40].

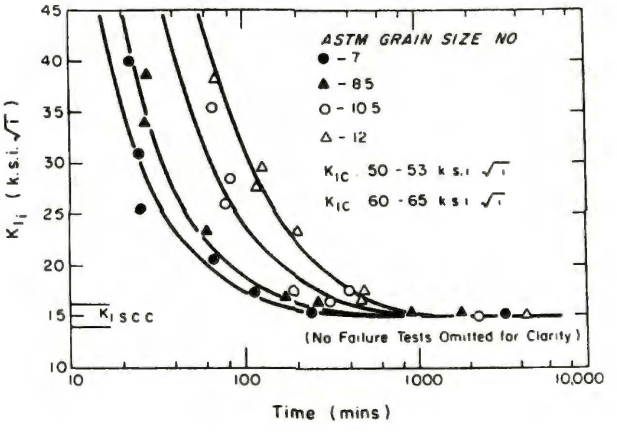

Figure 2.10 Effect of the grain size and the initial stress intensity on delayed failure time of AISI 4340 steel in 3.5% NaCl [47].

2.3.2.3. Effect of nonmetallic inclusions

From the standpoint of nonmetallic inclusion effect on hydrogen embrittlement, two aspects should be considered. First, surface inclusions may facilitate the entry of hydrogen into the steel and thus may promote the cracking. The six fold increase in the amount of absorbed hydrogen has been estimated in the case of the presence of elongated sulfides as compared with the spherical one, the overall sulfides content being the same [49]. On the other hand, inclusions distributed in the metal bulk may play a role in the hydrogen trapping and thus may assist the nucleation and development of internal crevices and cracks.

The elongated silicates, weakly bound with the matrix of the low carbon mild steel [50], or sulfides surrounded by the micro voids because of their considerable contraction at cooling may serve as the nucleation sites for hydrogen blisters formation [39]. In the pipeline steels [51] the cracks initiate at the elongated MnS inclusions. Internal cracks have been found [52] to form at the large oxide-sulfide inclusions during the tensile tests of hydrogen-precharged steel, whereas in similar and similarly treated steel which contains only small amount of sulfides no such crack has been observed.

Inclusions having the thermal expansion coefficient lower than steel (as oxides) produce the local stress concentration during cooling. Dissolved hydrogen diffuses to these sites causing the local decohesion of metal lattice, which leads to the formation of internal cracks [6, 53]. In the quenched unloaded steel the cracks have been observed to develop at the oxide inclusions, while no crack initiation has been noted at the sulfides [54]. This has been explained by the difference in tessellated stresses set up around the both kind of inclusions during quenching.

2.3.2.4. Effect of the chemical composition

C, Mn, Cr, Ni, and Si are the main alloying elements in the high strength steels. S and P are present as impurities. In Table 2.3 the possible beneficial and detrimental effects of the alloying elements on the SSC and HE, as discussed in [39] are presented. It is seen that the data are quite scattered and in many cases contradictory.

Table 2.3
Detrimental and beneficial effects of typical alloying elements on HE and sulfide stress cracking (SSC) of ferrite and high strength steels [39]

Element	Beneficial	Detrimental
C	no effect up to 0.5% beneficial to SSC at 0,45%	detrimental for SSC
Cr	at low % for SSC up to 1-2%	up to 2.4-5%
Mn	No	high strength steel - from 01%-2.7% for SSC
Ni	no effect up to 1%	for SSC, above 1%
Si	in high strength steel - up to 2% For SSC 0.3-0.9%	0.25-2%

Decrease in the **S** and **P** content substantially improves the resistance of high strength steel to HE [41]. Segregation of S, similarly as P, on the boundaries of the martensite laths and the prior austenite grains [55] accelerates the hydrogen crack propagation, the effect being thoroughly discussed in [48]. Effect of S has been associated with the mention above effects of the number, distribution and morphology of the formed sulfides. Amount of S in the steel affects the HE through the formation of different number and shape of sulfides [39].

The negative effect of **Mn** (2.5%) on susceptibility of AISI 4340 steel to SCC has been shown in [24, 56]. Addition of P, S, Cr, Mn and Ni has been found to produce no substantial effect on stress corrosion cracking behavior [56]. This seems to be in contradiction with other literature data concerning the effect of the nonmetallic inclusion on the stress corrosion behavior.

The effect of **Si** addition on the stress corrosion crack propagation has been found [57] to depend on its content. At Si < 1.5% no effect of the increased Si concentration has been observed in AISI 4340 steel tested in 3.5% NaCl solution. In the case of increase in the Si content from 0.03 to 0.36%, accompanied by the increase of Mn from 0.02% to 0.9%, the substantial decrease in the threshold stress intensity has been stated [48]. However, with the increase in Si content higher than 1.6%, the time to fracture increases and the crack propagation velocity significantly decreases (Figure 2.11) [57].

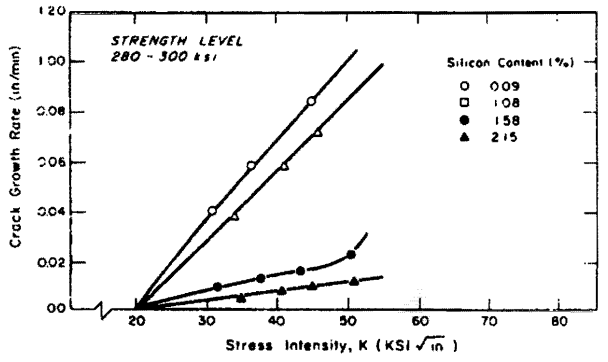

Figure 2.11 Effect of the Si content on the crack velocity in AISI 4340 steel, as tested in 3.5% NaCl[57]

Ni (similarly as Si) promotes the segregation of P at the grain boundaries of the high strength steel [48] leading to the hydrogen induced cracking. On the other hand, the addition of Ni (about 0.8%) has been shown to decrease the hydrogen induced cracking [37] and the hydrogen absorption [58] by the low alloy steels.

Carbon. Just after quenching, decarburized iron has the low susceptibility to SCC which increases due to the following tempering [59]. This has been explained by the increasing carbon concentration at the grain boundaries [60] during tempering.

Decrease in the carbon content has been known to produce a beneficial effect on resistance of high strength steels to SCC [28]. In the case of the HE there are controversies in the literature: tendency to increase the resistance to hydrogen cracking (for example, [25, 28, 56, 61,), no effect [39] or decrease of the resistance [28, 39] have been reported at the increase of the carbon content. It should be noted, however, that the effect of the carbon content is highly involved since its variation affects the various parameters influencing resistance to hydrogen embrittlement, such as the material strength and microstructure.

In [62] the negative influence of carbon on HE has been suggested to occur because of the cracks nucleation at carbides, which undergo decohesion at the early stage of mechanical test. The effect of the carbide size and their distribution can also overshadow the effect of microstructure (martensite, tempered martensite, bainite) on corrosion cracking [37]. Refinement of the carbides and their more uniform distribution due to the ausforming process [40] assists the increase of the resistance of steel to the HE (Figure 2.9). Also in [33] the increase in resistance of high strength steel to the HE has been associated with the presence of small dispersed carbides. Effect of the carbide morphology may be traced by the effect of the tempering temperature on the susceptibility to SCC and HE. However, in that case the effect is also involved since the change of the material strength in the course of tempering and the possibility of the temper brittleness [63].

The effect of the segregation of carbon at the grain boundaries has been also found [59]

to produce the detrimental effect on the hydrogen embrittlement.

The effect of carbon manifests itself also through the effect of carbides on the corrosion rate, and thus on the hydrogen evolution. In the case of the low-alloy steel in acidic solution, the effect of the tempering temperature has been associated with the controlled by the temperature area of carbides at the metal free surface, where hydrogen evolution predominantly occurs [64].

2.3.2.5 Effect of the cold work

Cold work modifies the susceptibility of steels to hydrogen embrittlement and to SCC. As has been discussed in [65], the role of the cold work on the SCC and HE behavior is rather ambiguous. The beneficial effect on the resistance to HE [65, 66] (especially observed in the case of cold drawn wires) has been mainly related to the eliminating of the surface defects produced at heat treatment and to the formation of specific dislocation structure and texture [66]. However, the increase in susceptibility to HE due to the cold work has been also stated [67, 68]. Deterioration of the resistance to SCC and HE has been always stated in the case of heterogeneous cold work [65].

It should be also noted that the plastic deformation at the crack tip contributed to the crack propagation process. For example, the correlation between the plastic deformation and the crack extension rate due to the hydrogen embrittlement has been stated in [69]. Considering the effect of the cold work on HE, its influence on the subsurface microstructure and on the strength of materials [65] should be also taken into account.

In the case of the airplane parts the following kind of the cold work may be considered: the applied shot peening and the plastic deformation occurred in the course of exploitation. Shot peening is widely used in the aircraft industry to modify the surface layer of steel in order to increase the resistance to fatigue [70, 71]. In the course of exploitation, the local concentration of plastic deformation (for example due to the fatigue processes) occurs in the metal parts. Those sites may promote the hydrogen induced cracking [20].

Shot peening. As a result of the shot peening, the surface layer of the quite complex state has been formed. Beside the plastic deformation and the change of the microstructure, the nonuniform distribution of stresses and the formation of compressive stresses are observed within the modified layer [72]. Such a modifying should also has the influence on the corrosion resistance of material [72-74]) including the resistance to SCC.

According to [75], the effect of the shot peening on the susceptibility to SCC depends on the kind of steels. In ferrite steel it eliminates SCC, whereas in the case of martensite steels shot peening only delays the onset of SCC, not totally eliminating it. In stainless duplex steel [76] the

shot peened layer has been found to decrease susceptibility to SCC due to the increasing crack incubation time. The effect has been explained by inhibiting the crack initiation and propagation by the compressive stresses in the cold worked surface layer.

In the case of differently surface treated low alloy AISI 4130 steel [77] the shot peened one reveals the higher resistance to hydrogen embrittlement as measured in the constant load rupture tests than the as-received, the laser surface hardened and the cold rolled steel. This has been explained by the restricted movement of the dislocation in the shot peened layer, which makes hydrogen movement by dislocation impossible and diffusion becomes the main mechanism of hydrogen transport.

It should be noted that the effect of shot peening on hydrogen behavior and hydrogen embrittlement has not been fully investigated and it may differ from that produced by the other types of cold work [77]. The reason is the formation of compressive stresses at shot peening, which have been known [78] to improve the resistance to hydrogen action.

Fatigue pretreatment. The quite specific appearance of the deformation structure forms during the fatigue processes [79]. Such a structure consists of the persistent slip bands, within which the dislocations are collected in the strips and boundaries, defining the ladder like structure. As has been shown in [80] the hydrogen cracks propagate along the deformation bands. Therefore, the dislocation structure formed during the fatigue influences the further processes of the hydrogen induced cracking. This formation of specific dislocation structure due to fatigue may be important in the case of exposition of the airplane parts being in service, to the aggressive environments.

2.3.2.6. Environmental effects

Among the various environmental factors influencing the hydrogen embrittlement of steels the most important in the case of the exploitation of the airplane parts are: presence of water solution film, pH of the solution film, presence of Cl^- ions and cathodic poisons (H_2S). The machine parts may be also subjected to the anodic or cathodic polarization as a result of cathodic protection. Galvanic elements or static electric charge may also form.

Presence of the water film on the metal surface causes the evolution of hydrogen which vanishes at the film drying (Figure 2.12) [20]. At the splashing of metal by the aqueous solution the hydrogen permeation has been similar to that measured for the part immersed in the solution [58]. The factors affecting the formation of the films on the parts exposed to the air, as humidity and temperature, possibility for splashing with rain or sea water can also affect the hydrogen charging of steel.

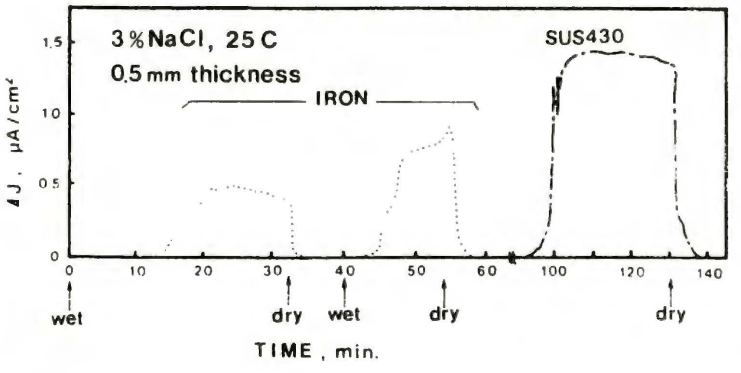

Figure 2.12. Effect of the wetting and drying of the metal surface on the hydrogen permeation current through the metal membranes [20].

pH and potential. The delayed fracture of the high strength steels in aqueous media is accelerated by decrease in the solution pH [81, 82]. The effect of pH on crack growth kinetics in AISI 4340 steel has been shown [44] to be significant only at the high cathodic potential. However, the other studies of the crack propagation rate [83] have shown some effect of pH in the range from 1 to 14. It has been also shown that even in the case of alkaline environment the crack can propagate by the hydrogen embrittlement mechanism.

Applied potential (both cathodic and anodic) has been found to accelerate the delayed fracture of various high strength steels [21] and [84], as well as in the type 410 stainless steel [85]. The effect of anodic polarization is the promotion of the corrosion pits formation within which the hydrogen evolves, the effect of cathodic polarization is the acceleration of hydrogen evolution [84, 85].

Cathodic poisons (mostly the elements from Groups V and VI of periodic table) promote the hydrogen entry into the steel from the aqueous media. As has been stated in [86] addition of As, Se, Te to 0.1 N H_2SO_4 increases the hydrogen entry into the high strength steel and decreases the stress required for delayed fracture. Similar results have been obtained for P and CS_2 [87]. Hydrogen sulfide addition to the neutral and acidic aqueous environments also accelerates the delayed fracture kinetics, as for example it has been shown in [82] and [88].

Cl^- concentration is a detrimental factor promoting the pitting corrosion of stainless steel [89]. Increase of the Cl^- content in the water solutions also accelerates the rate of the propagation of cracks of the low carbon low alloy steels [83].

2.4. Effects of hydrogen behavior on susceptibility to HE of high strength steels.

2.4.1. Hydrogen distribution in steel structure

In the iron alloys hydrogen may exist in the following states:

- as dissolved in the lattice, diffusible hydrogen;
- trapped at the various structure features, reversibly or irreversibly.

2.4.2. Hydrogen trapping

The boundaries of the phase constituents (carbides) and inclusions (sulfides, oxides, silicates), the boundaries of the prior austenite grains, the boundaries of the martensite and bainite laths, the dislocation pileups [39, 90] and the dissolved atoms of alloying elements [91] may serve as the hydrogen traps in the low alloy high strength steels. It is obvious that the variation in the steel chemistry affects the solid solution composition and the phase composition and thus affects the hydrogen diffusivity, hydrogen lattice solubility and hydrogen trapping. All the metal heat or mechanical treatments altering the metal structure also influence the hydrogen trapping.

Among the main alloying elements of the low alloy high strength steels, Mn and Cr atoms serve as the hydrogen traps, the atoms of Ni has the repulsive effect [91] and the hydrogen trapping by C atoms is negligible [91]. The ability of hydrogen trapping by the different mictrostructure features is shown in Table 2.4 [68, 92].

The effectiveness of the hydrogen trapping can be evaluated by the application of the various modifications of hydrogen permeation measurement techniques [90, 93-97]. Decrease in permeability of hydrogen under the similar charging conditions reveals the hydrogen trapping. In Table 2.5 [98] the hydrogen permeability and thus the hydrogen trapping is shown for various microstructures in relation to the martensite one, exhibiting the lowest permeability. The increasing effect on permeability produces the bainite, troostite and sorbite structure. Bainitic structure generally has the lower permeability than the pearlite. A very general conclusion from this is that the refining of lamellae promotes the permeability and that the more massive forms of the carbide particles offer the considerably less resistance to the hydrogen passage.

Table 2.4

Parameters of hydrogen trapping by various microstructure features.

Nature of trap	Character of the trap at room temperature	Energy of trapping, eV	Reference
TiC	irreversible	0.98	[39]
Fe_3C	irreversible reversible?	0.87 0.20	[39] [99]
MnS	irreversible	0.80 0.75	[39] [100]
Grain boundary	reversible	0.27-0.61 018	[39] [99]
Internal free surface	irreversible	0.72-1.0	[39]
Dislocation	reversible	0.25 0.28	[39] [99]
Microvoids		0.54 0.37	[39] [99]
Lattice site	very reversible, diffusion site	0.08	[101]

It should be noted that the above findings have been supported by the more resent studies revealing the effect martensite [31], carbide coarsening [41, 102-104,], MnS inclusions [41, 97, 105,], morphology of the oxide [38] and sulfide [106] inclusions.

Table 2.5

Permeation of hydrogen through the steels of various microstructure

Investigator	Steel	Microstructure	Relative Permeability
Nosyreva [107]	0.84% C 0.5% Mn	Martensite Lower Bainite Globular cementite Troostite (fine, globular carbides) Annealed steel Sorbite (growth of troostite) Normalized steel	1 1 3.59 3.91 4.78 7 7.43
Baht and Lloyd [108]	0.59% C	Martensite Coarse lamellar pearlite and ferrite Very fine pearlite and ferrite	1 1.57 2.79
Amiot [107]	0.26% C 0.25% C	Martensite Tempered Martensite (at 550 C) Fine bainite Coarse bainite Coarse lamellar pearlite Fine lamellar pearlite Spheroidized	1 1.04 1.57 1.95 2.16 2.98 3.25

In the case of the nonuniform, martensite-bainite structure the permeation kinetics is related to the fraction of martensite [31] since the trapping capacity of the bainite and ferrite-pearlite areas of the structure being lower than that of the martensite one.

The steel strength has been suggested to have an influence on the hydrogen trapping. With the increase in the yield stress the amount of hydrogen dissolved in interstitial position of the lattice does not change but the concentration of trapped hydrogen increases [109].

The effects of the internal stresses and the modification of the microstructure of the high strength steel on hydrogen diffusivity and solubility have been studied in [63]. The similar complex changes of the micro strain (Figure 2.13a) and of the hydrogen diffusion coefficient (Figure 2.13 b) with the increase in the tempering temperature have been accounted for the change of the stresses in martensite during its decomposition and for the precipitation and then coarsening of the carbides. The hydrogen diffusivity has been found to increase with the structure transformation in order: quenched martensite – bainite+martensite - very fine carbide in ferrite –fine pearlite – coarse lamellar pearlite. The hydrogen solubility decreases in order: fine carbides in ferrite – bainite + martensite – quenched martensite – fine pearlite – coarse lamellar pearlite.

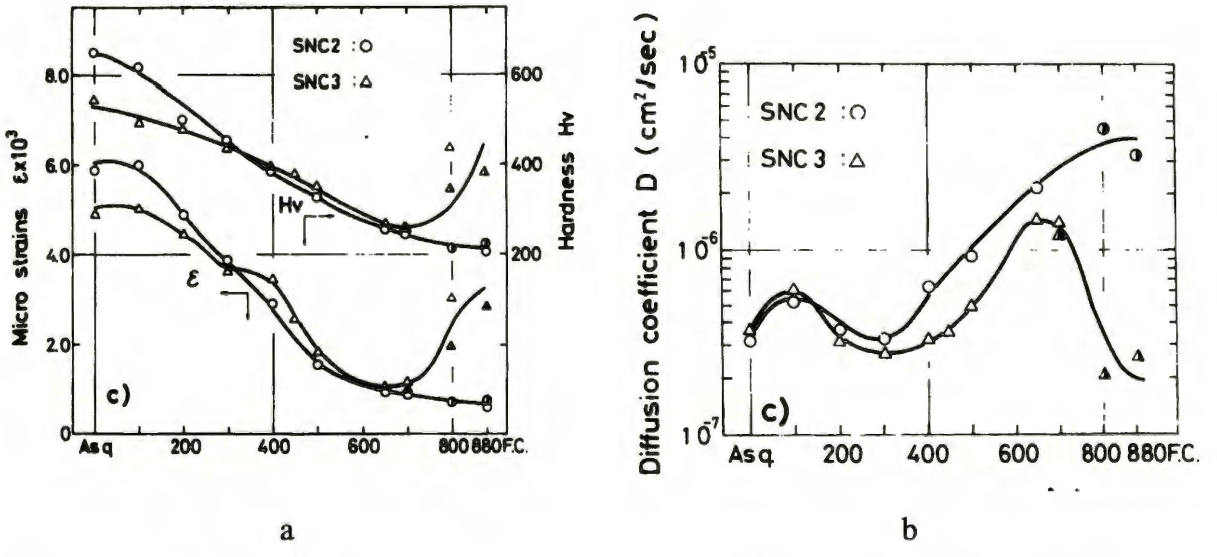

a b

Figure 2.13. Effect of the tempering temperature on microstrain and hardness (a) and on the hydrogen diffusivity (b) in the high strength steels [63].
SNC 2 – C - 0.3%, Si -0.2%, Mn - 0.50%, Ni - 2.75%, Cr - 0.8%;
SNC 3 – C - 0.35%, Si -0.2%, Mn – 0.50%, Ni - 3.25%, Cr - 0.8%.

2.4.3. Effect of different state of hydrogen on HE of steel

Despite the many studies, the problem concerning the state of hydrogen being decisive for the hydrogen embrittlement of the low carbon low alloy high strength steels has not been settled yet. Diffusive, reversibly and irreversibly trapped hydrogen has been accounted for the susceptibility to HE, Table 2.6.

Table 2.6

Hydrogen state responsible for the HE

Hydrogen state in steel	Reference
Diffusible (lattice) hydrogen	27, 110, 111, 112
Reversibly trapped hydrogen	38, 39, 90, 113, 114, 115
Irreversibly trapped hydrogen	27, 29, 39, 59, 67, 68, 92, 104, 116, 117

If cracks are initiated in the sites of the local stress concentration, the diffusible hydrogen should be mainly accounted for the cracking. When mobile hydrogen is driven into the traps it cannot contribute to embrittlement. From this point of view, the hydrogen trapping should prevent the cracking. For example, the beneficial effect of the cold work has been explained by the hydrogen trapping by defects created at metal plastic deformation [65]. Such approach suggests the creation of hydrogen traps in the steels structure to be the possible viable solution to HE problem. In fact the formation of coherent particles of TiC, which are the strong traps, has been shown to increase the resistance of high strength steel to hydrogen embrittlement [39]. The beneficial effect of VC carbides has been also observed in the case of high strength steels [39, 41].

On the other hand, in many cases the increased susceptibility to HE has been associated with the trapping ability of steel, as shown in Table 2.6. The intensive hydrogen trapping in martensite structure at the carbide and parent austenite grain boundaries has been stated as the cause for the hydrogen cracking.

It should be also taken into account that traps filled with hydrogen serve as the hydrogen sinks. Hydrogen from the sinks may redissolve in the metal and promote the cracking at the metal loading. It has been stated in [118] that the mobile hydrogen is responsible for the ductility loss during the straining, while hydrogen irreversibly trapped on inclusions does not affect steel ductility but causes the degradation by cracking (HIC).

It has been also found that the formation of BN or NbBN, being the strong hydrogen traps does not produce the beneficial effect on the resistance to HE of high strength steels [41] because their precipitation on the grain boundaries of prior austenite deteriorates the boundary structure.

Therefore, the care should be taken to ensure that addition of traps does not lead to a degradation of mechanical properties, or that the beneficial ability of traps is not deteriorated by the used thermal or mechanical treatment.

The complex effect of traps on susceptibility to HE should be accounted by variation of their number, trapping activation energy, kinetic parameters of the capture and release. The problem has been thoroughly analyzed by Pressouyare and coauthors [39, 101, 119]. According to their suggestions, to produce the beneficial effect on the susceptibility to HE, the traps should meet the certain requirements:

- traps should have a high critical concentration for hydrogen;
- traps should be present in a high quantity;
- traps should be irreversible;
- traps should be distributed homogeneously in the matrix;
- traps are beneficial when they are far away from the saturation.

From the above approach it follows that all the changes in the steel chemistry, heat or mechanical treatment varied the dislocation structure, internal stress distribution, microstructure would strongly affect the hydrogen behavior, and thus the susceptibility of high strength steel to hydrogen action. Therefore, the very detailed studies should be done in order to evaluate the influence of the critical parameters of the steel structure on the susceptibility to HE for each kind of high strength steels.

It has been generally accepted that the susceptibility to hydrogen induced cracking of the high strength steel has been affected by the hydrogen diffusivity, which determines the rate of hydrogen to reach the hydrogen traps, and by the hydrogen entry flux, which determined the build-up the local concentration of trapped hydrogen to some critical level, necessary to initiate and propagate the cracking [68, 90, 114]. However, the share of those parameters in susceptibility to hydrogen embrittlement has been still under the question [68, 90] and may differ depending on the chemistry, heat and mechanical treatment of steels [68].

2.5 Susceptibility to SCC and HE of 30HGSNA type steel

30HGSNA steel is the high strength steel (strength level σ_{uts}=1600-2000 MPa) designed in USSR in 1949. The specific feature of this steel is the presence of about 1%Si and 1%Mn, which before the elaborating of this steel have been recognized as impurities. The western, later elaborated steels with the addition of Si and Mn as alloying elements (4340M, 300M, and H11) have higher amount of C as well as some addition of Mo and V.

According to PN-72/H-84025, the 30HGSNA steel has following chemical composition: 0.27 - 0.34% C, 1.00-1.30% Mn, 0.9-1.2% Si, 0.9-1.2%Cr, 1.4-1.89% Ni. Special type of 30HGSNA steel used in aircraft industry is 30HGSNAŻ (Ż - stands for electroslag melting) steel characterized by lower contents of S and P and the better mechanical properties (see Table 2.7).

Table 2.7

Mechanical properties of different casts of 30HGSNA steel.

Cast	R_{02}, MPa	R_m, MPa	A_5, %	Z, %	U, J/cm^2
Standard, L	1640	1750	10,9	47	56
Standard, T	1640	1780	9,5	32,3	42
Electroslag, L	1610	1790	10,6	46,7	61
Electroslag, T	1640	1800	10,0	33,2	50
Vacuum, L	1650	1780	10,2	51,2	65
Vacuum, T	1630	1780	10,6	43,5	52

L – longitudinal; T - transverse direction

The 30HGSNA type of steel has been widely used in the Russian and Polish aircraft industries to produce the highly loaded parts of airplanes because of its good combination of the strength and toughness properties. Although the above properties are critical for the use in the airplane parts, the susceptibility of the 30HGSNA and similar steels to the environment assisted cracking has been also studied.

The extensive investigation of the susceptibility to SCC and HE of 30HGSNA steel in 3% NaCl solution was done by Dr E. Sitko in his PhD made under the supervision of Prof. M.Smialowski [36]. Steel used in the Polish airplane industry was investigated in the humid air, distilled water and 3.5% NaCl solution.

From the data obtained in electrochemical tests, electrochemical measurements of hydrogen permeation, tensile static (at constant strain rate and constant load) and fatigue tests with the use of flat and notched cylindrical specimens, vacuum extraction of hydrogen and microscopic examination, the following conclusions have been made:

- Cracking of the 30HGSNA steel in water environment under the tensile stress is the results of following processes:

1) incubation of pitting at the triple phase boundary: metal - sulfide inclusion - water;

2) hydrogen evolution within the pits and its absorption on the pit bottom;

2) hydrogen assisted crack propagation.

- Main reason of high susceptibility of 30HGSNA steel to SCC is the presence of sulfide inclusions. They serve as pitting sites within which the hydrogen evolved and therefore the HE occurs even at anodic polarization.
- Cl^- ions do not play an essential role in this case.
- No cracking was observed below the critical value of stress and within the certain potential range.
- At testing in air of humidity up to 50% the good mechanical durability and low SCC have been stated.

Later on, the 30HGSNA steel for the aircraft industry has been produced by the slag melting and the special conditions have been observed in order to decrease the S content and to decrease the number and the size of sulfides (30HGSNAŻ steel). The lack of the sulfides in the structure of 30HGSNAŻ steel has been found to cause the higher permeability of this steel to hydrogen, in comparison with the steels 41, 15G2Nb and 17HMBVA as tested at cathodic polarization in the synthetic sea water [120]. However, the improved steel can also be embrittled by hydrogen.

In [121] the formation of pitting on the 30HGSA and 30HGSNA steels subjected to the tensile stretching in 4M HCl solution has been accounted for the selective dissolution of Cr and Mn from the steel. The incubation of pitting under those conditions can be hampered by the addition of some cation-active inhibitors. The inhibition of the erosion- corrosion degradation of 30HGSNA steel in the tap water has been described in [122].

It has been also shown in [123] that pitting accelerates the initiation of the fatigue cracks in 3% NaCl solution because of the stress concentration. Acceleration of the fatigue crack propagation occurs due to the intensification of hydrogen evolution at the pit (crack) tip [119].

Kinetics of corrosion cracking of 30HGSN3A steel in H_2SO_4 + NaCl solution at cathodic polarization has been compared with that for 40H steel [124]. The more uniform hydrogen distribution in the bulk of the metal due to the lower amount of impurities at grain boundaries in 30HGSN3A steel has been accounted for its higher resistance.

The resistance to HE of quenched and ausforming 30HGSNA steel has been accounted for the effect of the impurities distribution [125]. The fracture stress exhibited by the differently treated steel and the type of the fracture surface are shown in Table 2.8. The highest resistance of tempered ausformed steel has been explained by the decrease in the impurities content at the prior austenite grain boundaries as well as by the formation of the zigzag shape of those boundaries.

Table 2.8
Effect of the 30HGSN2A steel treatment on the fracture stress and the fracture mode [125]

Steel treatment	Fracture stress, MPa		Fracture mode
	Without hydrogen charging	After hydrogen charging (0.1N H_2SO_4 + 1.5g/l thiourea, 0.05mA/cm^2, 2hrs)	
Quenched from 900°C	2730	1720	IG
Quenched from 900°C, tempered at 200°C, 1hr	3700	3280	IG + TG
30% deformation at 880°C	3680	2190	TG
30% deformation at 880°C tempered at 200°C, 1hr	4090	3550	TG + ductile

The variation in the heat treatment (resulting in the similar mechanical properties) of 30HGSNAŻ steel and the presence of the surface layer formed due to the exposition in oil, has been found to affect the hydrogen absorption and permeation, as tested in the NaCl+Na_2SO_4 solution [126]. Susceptibility to hydrogen induced cracking of steel in Cl^- containing solutions has been also affected by the variation of the heat treatment and the carbon content (both being in the accordance with the Standard) [127].

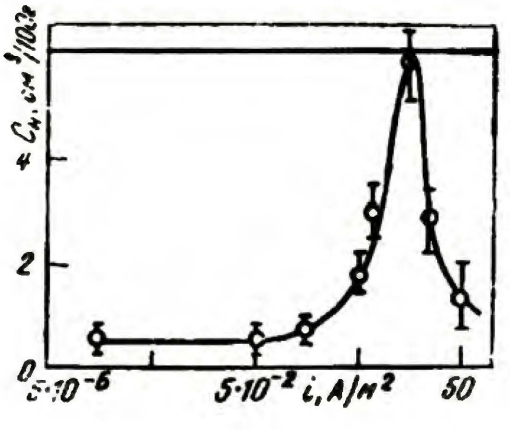

Figure 2.14. Diffusible hydrogen content vs. cathodic polarization current density in 0.1N H_2SO_4 with thiourea for 30HGSNA steel [128].

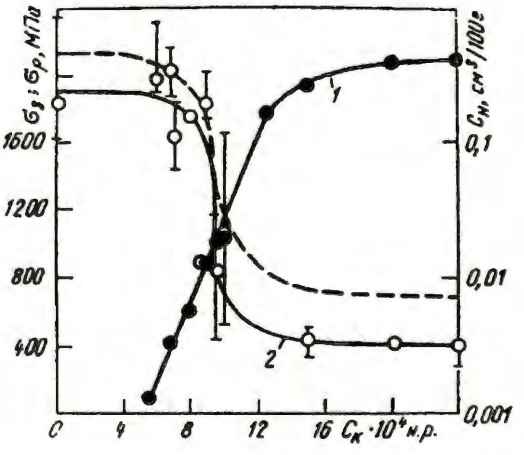

Figure 2.15. Change of the mechanical properties and the hydrogen content in 30HGSNA steel vs. H_2SO_4 concentration. 1 - hydrogen content, 2 - solid line: crack initiation stress, dashed line: destruction (critical) stress. [128]

The content of mobile (diffusion) hydrogen permeated through the membranes of martensite 30HGSA steel has been compared with the loss of the mechanical properties and with the change of the fracture mode [128]. As seen in Figure 2.14 the content of diffusible hydrogen vs. the cathodic current exhibited maximum. At low polarization almost no hydrogen permeation has been recorded, similarly as at the high one. The latter finding authors explained by the

masking of the surface with the gas bubbles or by the formation of internal voids. The maximum concentration has been accounted as the critical concentration causing the dramatic decrease in the mechanical properties, Figure 2.15. At the same content of hydrogen the TG cracking transforms to the IG one.

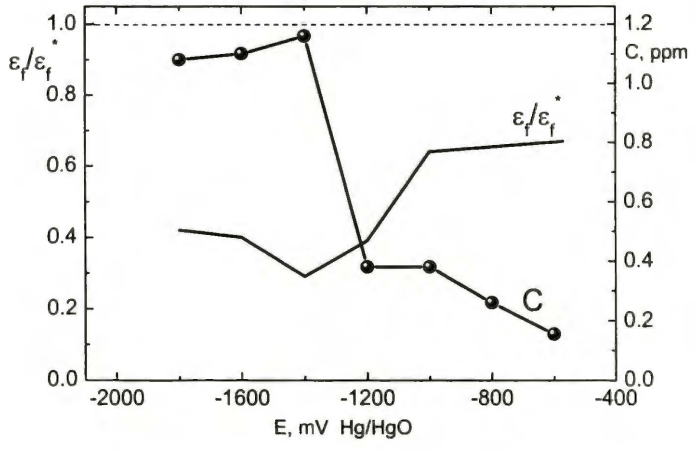

Figure 2.16. Effect of polarization on the plasticity loss, and on the content of permeable hydrogen (C) for 30HGSNAŻ steel tested in NaCl+Na_2SO_4 solution [127]

Quite similar results have been obtained at testing of 30HGSNAŻ steel in the NaCl + Na_2SO_4 solution [127], cf. Figure 2.16. The decrease in plasticity has been associated with the increase in the movable hydrogen content. In [128] authors attribute the observed decrease in mechanical properties to the segregation of the diffusion hydrogen at the grain boundaries. In the case of studies done in [127] the pronounced decrease in plasticity has been accounted for the creation of new traps by hydrogen of increased fugacity after the filling of the traps already existing in the metal.

Good resistance of 30HGSN steel to the fatigue at cathodic polarization within the range -900 up to -1150mV_{HSE} in 3% NaCl solution has been stated, despite the significant hydrogen permeation at those potential. The corrosion potential was E_c =-670mV_{HSE} [123].

In [129] the susceptibility of 30HGSNAZ steel to pitting and the higher susceptibility of the same steel to SCC have been stated at testing in NaCl + Na_2SO_4 than in NaCl solutions. The results confirm the assumption that the decrease in pH of Cl^- containing solution produces the detrimental effects.

Some information provides also the analysis of the field failure cases [130]. At examination of the material taken from the airplane parts failed during exploitation and unfailed parts being in exploitation the following features have been stated:

- presence of micro cracks accompanied by the corrosion pits,
- some traces of local corrosion on the surface of unfailed parts,
- higher hydrogen content in the vicinity of the crack walls than in unfailed metal.

Detailed analysis has showed that the material of the failed parts contained the carbon content close to the upper limit stated by the Standard.

3. AIM

From the results of the failure case analysis of the aircraft parts and from the data reported in the literature it can be concluded that the formation of the bainite structure and the decrease in carbon content, close to or even below the lower limit for the 30HGSNAŻ steel, should improve the resistance of the steel used in the aircraft industry to the local corrosion and the hydrogen embrittlement, and thus should improve the resistance to the stress corrosion cracking in Cl^- containing environments. However, it also follows from the literature review that the variation of structure and carbon content produces the complex and highly involved effects.

The influence of the bainite morphology on the stress corrosion cracking has not been fully recognized.

At decrease in the carbon content the strength of the steel would not fulfill the requirements for the aircraft parts. In such a case the shot peening, widely used in the aircraft industry in order to increase the resistance to fatigue, might be applied. Highly deformed shot peened surface layer affects, in turn, susceptibility to pitting corrosion and to the hydrogen embrittlement.

The local plastic deformation of parts being in service occurred as a result of the fatigue processes should also influence the susceptibility to pitting corrosion, stress corrosion cracking and hydrogen embrittlement of material at the exposition to the aggressive environment.

The increased aggressiveness of the environment ("acid rain" and "acid dew") to which the high strength steel has been exposed not only affects the susceptibility to the corrosion but also may alter the mechanism of the stress corrosion processes.

The aim of the present work is to elucidate the effects of the variation of the carbon content, the heat treatment, the surface mechanical treatment and fatigue pretreatment of the bainite 30HGSNA (0.3C-1Cr-1Mn-1Si-1Ni) type steel on susceptibility to pitting corrosion, hydrogen behavior and the stress corrosion cracking in Cl^- containing solutions.

To fulfill the above tasks the following research program has been established:

1. In order to evaluate the effect of the carbon content the different heats of the 30HGSNAŻ type steel with the carbon content from 0.25 to 0.31%C have been used.

2. In order to check the effect of the variation of the chemistry of the Cl^- containing ıggressive solution the 3.5% NaCl and solution simulating the "acid rain" have been used.

3. In order to check the effect of the microstructure steels have been subjected to various heat treatments, according to the technical requirements of the aircraft industry.

4. In order to study the effect of the kind of the cold work on the stress corrosion cracking the shot peening and the tensile-compressive fatigue pretreatments have been applied.

5. In order to evaluate the structure features, which govern the susceptibility to pitting corrosion, stress corrosion cracking and hydrogen embrittlement, the systematic analysis of the microstructure of the steels, including optical and scanning microscopy and the X-ray diffraction has been done.

6. In order to check the susceptibility of differently treated materials to general corrosion and to evaluate their electrochemical parameters the potentiodynamic tests have been carried out at anodic and at cathodic polarization.

7. In order to evaluate the susceptibility of the low alloy high strength steels to the pitting corrosion the special test has been elaborated and applied.

8. In order to establish the hydrogen parameters, responsible for the susceptibility of steel to hydrogen action, the electrochemical hydrogen permeation measurements have been used and the test procedure has been modified accordingly.

9. In order to investigate the microstructure change of materials after the hydrogen charging the scanning electron microscopy has been used.

10. In order to evaluate susceptibility to stress corrosion cracking the tensile tests have been carried out in studied electrolytes with application of appropriate polarization.

11. To measure the total hydrogen content in the material subjected to various tests the vacuum extraction method has been applied.

4. MATERIALS AND EXPERIMENTAL PROCEDURES

4.1. Materials

4.1.1. Chemical composition of studied materials

Chemical composition of studied high strength aircraft steels of the 30HGSNA type is given in Table 4.1, together with the composition required by the Polish Standards (PN 72/H-84035 and PN 80/H-94011). The special forging procedure was applied in the case of all the heats in order to decrease the amount of S and P.

Table 4.1

Chemical composition of studied steels.

Steel code	Chemical composition, wt%							
	C	Mn	Si	P	S	Cr	Ni	Cu
Polish standard for 30HGSNA steel	0.27-0.34	1.00-1.30	0.9-1.2	max 0.030	max 0.25	0.9-1.20	1.40-1.80	max. 0.20
31	0.31	1.13	1.02	0.023	0.003	1.03	1.50	0.15
28	0.28	1.09	0.91	0.02	0.003	1.01	1.56	0.09
25	0.253	1.13	1.04	0.017	0.004	1.12	1.65	

4.1.2. Steel heat treatment

All studied steels were produced in the Baildon Steelmill Factory in the frame of KBN grants T12 97 13 [130] and T12C 06219 [131] by electroslag melting and treated according the requirements of the airplane industry. Heat treatment operations were done under the protective atmosphere. The slabs of steels (100x25x1000 mm) were normalized at 900°C, then annealed at 780°C, cooled with oven to 650°C, kept for 2 hr. and cooled down in air (heat treatment N). The specimens for mechanical tests and for hydrogen permeation measurements were machined from the slabs along the rolling direction. After machining, specimens were heat treated. The treatment was done in the airplane factory PZL-WSK Okęcie.

Steels 31 and 28 were subjected to following treatments:

- isothermal quenching from 900°C in oil at 200°C, then aging at 210°C for 2 hrs. (heat treatment I);

- quenching from 900°C in oil at RT and tempering at 210°C for 2 hrs. (heat treatment QT).

Specimens of 25 steel were isothermally quenched from 910°C in oil at 80°C and then aged at 190°C for 3 hrs. and cooled in oil at 40 – 50°C (heat treatment I*).

After heat treatment and final preparation, all the specimens were mechanically polished to attain the surface roughness lower than 0.64 μm (Polish Standard $^{0.64}\sqrt{}$) and were additionally aged at 120°C in oil for 3 hrs, according to the airplane industry requirements.

4.1.3. Shot peening

Heat treated specimens of steel 25N and 25I* were subjected to shot peening by means of cast iron shots (0.43mm mesh and 470 HV of hardness), pneumatically injected for 60s at pressure 0.5MPa. Those parameters provided the surface coverage higher than 100%. Since shot peening can produce some surface defects, especially in the case of normalized steel (Figure 4.1) the shot peened surface of the specimens was mechanically polished to remove the possible surface defects and to obtain the smooth surface, according to requirements.

4.1.4. Fatigue pretreatment

Specimens of the low carbon steel were subjected to the axial tension fatigue tests at RT at loading frequency 20Hz. Treatment was done according to Polish Standard PN-76/H-04325 in the Institute of Nuclear Research (Swierk) using the INSTRON 8501 machine with the special attachments.

Specimens were tested at two levels of the maximum stress: 1100MPa (code 25I*F-1 for not shot peened specimens and code 25I*sF for shot peened specimens in Table 4.2) and 1300MPa (code 25I*F-2 in Table 4.2). The number of cycles was $2*10^5$ and $9.2*10^4$ in the case of specimens 25I*F-1 and 25I*F-2, respectively. After fatigue pretreatment, specimens were used for the other tests.

The code, the heat, surface and fatigue pretreatment of used specimens, as well as the kind of tests, which underwent the respective specimens are given in Table 4.2.

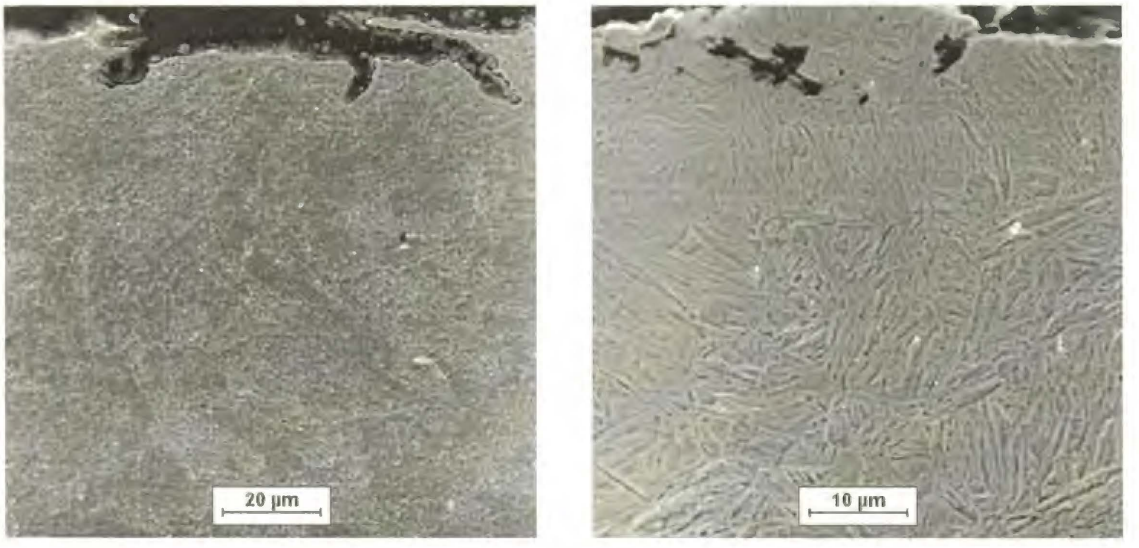

Figure 4.1 Surface defects produced by shot peening.

4.1.5. Specimens dimensions

For electrochemical and hydrogen permeation measurements, the membranes, 10x40x2mm and 10x40x1mm in size, were cut along the rolling direction, as shown in Figure 4.2. The 1mm thick membranes were polished after the heat treatment to obtain the thickness 0.5 mm.

The 2mm thick membranes were subjected to two side surface treatments. After that, one side of the membrane was mechanically polished to obtain the membrane thickness of 0.5 mm.

Specimens for tensile tests were cut along the rolling direction, cf. Figure 4.2. The non standard specimens, 30mm in gauge length and 3mm in gauge diameter were tensile tested.

Specimens for fatigue pretreatment tests (shown in Figure 4.3) were cut along the rolling direction. For hydrogen permeation measurements through fatigue pretreated specimens, the membranes, 0.5 mm thick, were cut perpendicular to the specimen axis in the middle part of the specimen gauge, as shown in Figure 4.3.

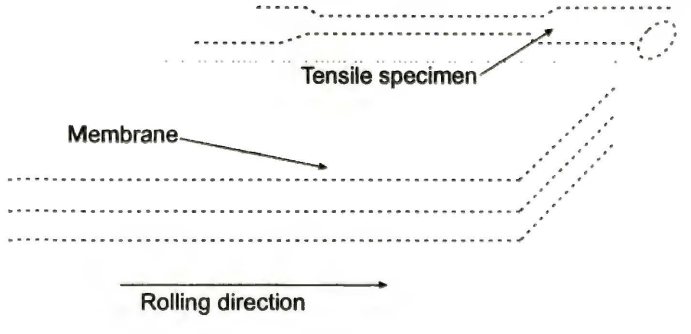

Figure 4.2 Scheme of the specimens preparation for hydrogen permeation an tensile experiments.

Table 4.2

Code, applied treatments and the kind of tests done for studied steels.

Specimen Code	Heat treatment	Surface and mechanical treatment	Tests
25N	normalized steel 25		electrochemical, pitting corrosion, SCC, H permeation, vacuum extraction
25Ns	normalized steel 25	shot peened	electrochemical, pitting corrosion, SCC, H permeation, vacuum extraction
25I*	heat treated steel 25		electrochemical, pitting corrosion, SCC, H permeation, vacuum extraction
25I*s	heat treated steel 25	shot peened	electrochemical, pitting corrosion, SCC, H permeation, vacuum extraction
25I*F-1	heat treated steel 25	fatigue pretreated	pitting corrosion, H permeation,
25I*F-2	heat treated steel 25	fatigue pretreated	pitting corrosion, H permeation
25I*sF	heat treated steel 25	shot peened fatigue pretreated	pitting corrosion
28I	isothermally quenched steel 28		electrochemical, pitting corrosion, SCC, H permeation, vacuum extraction
28QT	quenched and tempered steel 28		electrochemical, pitting corrosion, SCC, H permeation, vacuum extraction
31I	isothermally quenched steel 31		electrochemical, pitting corrosion, SCC, H permeation, vacuum extraction
31QT	quenched and tempered steel 31		electrochemical, pitting corrosion, SCC, H permeation, vacuum extraction

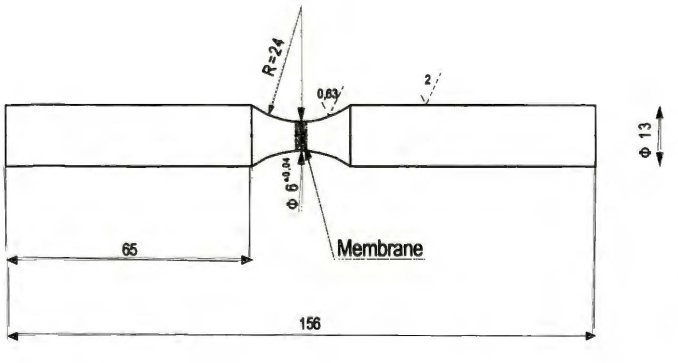

Rys.4.3. Specimen for fatigue pretreatment tests. The site of cutting the membrane for hydrogen permeation measurements is shown.

4.1.6. Test solutions

In order to compare the results obtained for studied steels with the previously obtained ones, and with the literature data, the 3% NaCl (pH=5.5) was used. This solution may also simulate the sea shore atmosphere and dew. Taking into account the increased aggressiveness of the environment, and especially the effect of "acid rain " and "acid dew", the solutions containing 30g/l NaCl + 71g/l Na_2SO_4 in distilled water (acidified to pH=3 by addition of H_2SO_4) simulating the "acid rain" [132] was used for electrochemical and hydrogen permeation measurement. Both solutions were non deaerated.

4.2. Experimental procedures

4.2.1. Structure examination

Microstructure of used materials was observed by a NEOPHOT 2 metallographic microscope, using bright, dark and asymmetrical lightening, at magnification up to 2,000 X and by the scanning electron microscope. To evaluate the steel microstructure, the cross section of sample was etched for 3 – 5 s in (10g $FeCl_3$ + 100ml HCl + 100ml H_2O) solution after its aging for 24 hrs. The size of parent austenite grains, the size of bainite laths and diameter of carbide precipitates were evaluated by quantitative metallography methods [133]. The relative length of the parent austenite grains and bainite laths were measured on scanning microscope pictures of etched specimens using specially elaborated program.

The depth of the microstructure revealing the changes in comparison with the bulk microstructure was adopted as a thickness of the shot peened layer.

Surface topography of the shot peened and fatigue pretreated specimens in as received condition and after pitting corrosion test, the side and the fracture surface of tensile tested specimens and the ingress surface of membranes subjected to hydrogen permeation measurements were observed on scanning electron microscope Hitachi S 4200 at magnification up to 10,000X with attached ESEM-50 Philips EDS analyzer.

The X-ray diffraction was done by a Brucker AXS D8 diffractometer, using $Cu_{k\alpha}$ radiation and Ni filter. X-ray spectra were recorded for as received and for surface treated specimens. The bainite and ferrite lattice parameters were calculated by routine procedure.

4.2.2. Pitting corrosion tests

To measure the susceptibility to pitting corrosion of studied low alloy steels, the special rocedure has been elaborated [134].

The test solution for pitting corrosion tests had to fulfill the following requirements:

- to model the typical industrial corrosion environments;
- to provide the preferential pitting corrosion without prevailing general corrosion;
- to provide the similar type of corrosion of different kinds of steels, including the steels with modified surface layer;
- time of test can not be longer than 24 hours.

The following solutions containing different concentration of Cl^- ions were tested:

- 3% NaCl ($C_{Cl^-} = 0,5M$)
- 30g/l NaCl + 71g/l Na_2SO_4 ($C_{Cl^-} = 0,5M$)
- 0.1 M $FeCl_3$ ($C_{Cl^-} = 0,3$ M)
- 0.05 M $FeCl_3$ ($C_{Cl^-} = 0,15$ M)
- 1 M $FeCl_3$ ($C_{Cl^-} = 3$ M)

Specimens were placed into the corrosion cell (0.5 dm^3) filled with tests solution and kept for 12 to 24 hrs. After removing the corrosion products in ultrasonic cleaner filled with (16%HCl+urotropine) solution, specimens were weighted and the general corrosion rate was calculated according to Polish Standard PN-78/H-04610. The density and the diameter of pits were estimated using quantitative metallography methods at observation of surface on microscope. The pit depth was evaluated on the specimen cross sections.

As seen in Figure 4.4, the rate of general corrosion was few orders of magnitude lower in NaCl and in NaCl+Na_2SO_4 solutions than that in $FeCl_3$ solutions of different concentration. Pitting corrosion was observed only in $FeCl_3$ solutions. As seen in Figure 4.5, the number and the diameter of the pits did not depend on Cl^- ion concentration for exposition longer than 20 hours. On the other hand, the influence of exposition time was not so pronounced in the case of higher concentration of Cl^- ions. Taking into account the preliminary results shown in Figures 4.4 and 4.5, the immersion in non deaerated solution containing 0.1M $FeCl_3$ (C_{Cl^-}=0.3 M) for 22 hrs was decided to fulfill the above mentioned requirements and those parameters were selected to evaluate the susceptibility to pitting corrosion of studied materials.

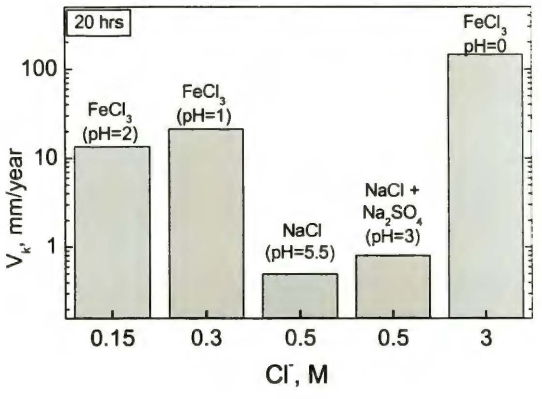

Figure 4.4. General corrosion rate estimated for steel in solutions of different Cl^- ions concentration.

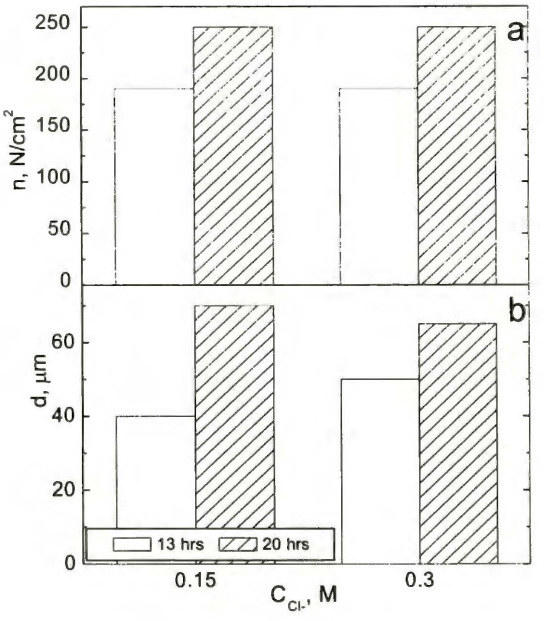

Figure 4.5. Effects of Cl^- ions concentration and exposition time on pits density (a) and pits diameter (b).

In the case of the shot peened specimens, the pitting corrosion was evaluated on the shot peened surface of the specimen.

For evaluation the susceptibility to pitting corrosion of the fatigue pretreated specimens, the gauge part of the specimens after fatigue pretreatment was subjected to pitting corrosion tests.

4.2.3. Electrochemical measurements

Electrochemical measurements were done at RT using the specially designed microcell with the working area about 0.1 sm^2 (Figure 4.6). The microcell was fixed on the surface (including the modified ones) of the membrane. Test solution was poured into the microcell and the open circuit potential (E_{ocp}) was measured until the steady state value has been achieved. Then the cathodic polarization curves were recorded from the open circuit potential into the cathodic direction up to -2000 mV Hg/Hg0, with the scan rate 1 mV/s. All the values of potential are given vs. the Hg/HgO reference electrode.

The anodic polarization curves were recorded from potential, 300mV more cathodic than E_{ocp}, into the anodic direction, up to +1000mV with the scan rate 1 mV/s. The corrosion current density (i_c) was evaluated as the current density corresponding to the intersection of cathodic and anodic branches of the polarization curve.

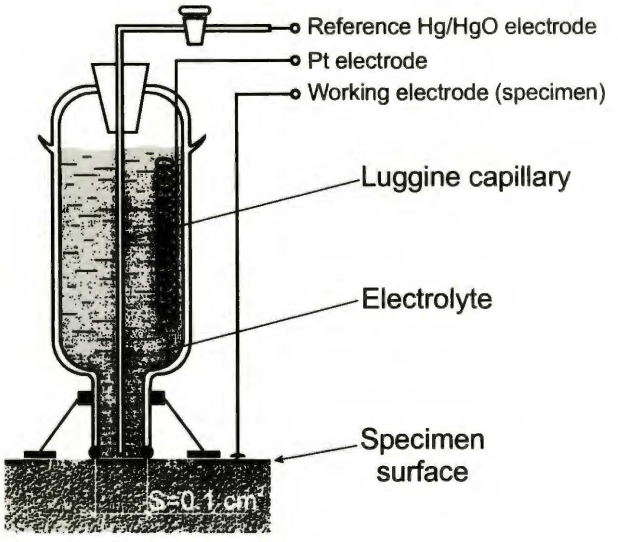

Figure 4.6. Microcell for electrochemical measurements.

4.2.4. Electrochemical hydrogen permeation measurements

Electrochemical measurements of hydrogen permeation were done by Devanathan – Stachurski [93] method using the specially designed double cell enabling the Pd coating of membrane surface. Membranes of the studied materials were degreased with ethanol and clamped between two electrochemical cells (the ingress and the egress ones), as shown in Figure 4.7. Generally, the area exposed to the permeation was 0.5 cm^2, however, in the case of fatigue pretreated material, the working area was 0.1 cm^2. In the case of surface treated membrane, the treated side served as the ingress one.

After fixing the membrane, the egress cell was filled with the (0.8g $PdCl_2$+60g NaOH)/l H_2O solution and the egress side of membrane was cathodically coated with palladium. After coating, electrolyte was removed, the cell was rinsed with distilled water and filled with 0.1N NaOH solution. The anodic potential +150mV was applied to the egress side of a membrane and the anodic current, being the measure of hydrogen permeation rate, was recorded. This procedure allowed achieving the background current of 0.5μA at the empty ingress cell.

After achieving of the such background current, the test solution was poured into the ress cell. The ingress side of membrane was polarized potentiostatically. The following des of polarization have been applied:

- step by step increased anodic potential between E_{ocp} and +100mV;
- step by step increase cathodic potential between E_{ocp} and -2400 mV;
- polarization with the constant cathodic potential.

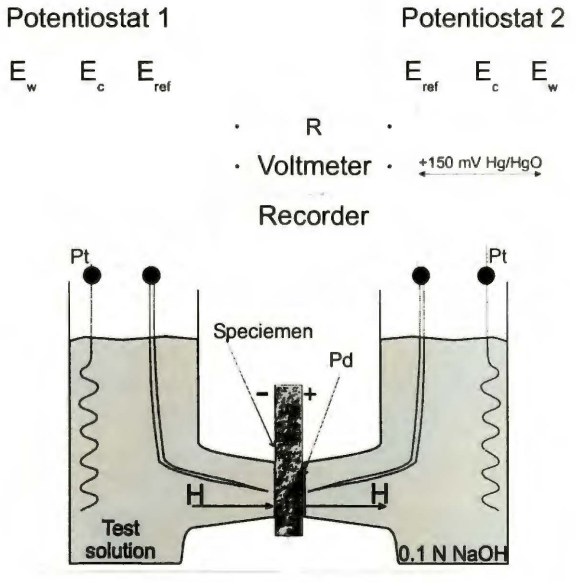

Figure 4.7. Scheme of the double cell for the hydrogen permeation measurements.

The buildup transient of the anodic permeation current in the egress cell was recorded up to the steady state value corresponding to the each applied polarization to the ingress side (Figure 4.8). At the end of the experiments, polarization of the ingress side was switched off, and the decay permeation transient was recorded in the egress cell.

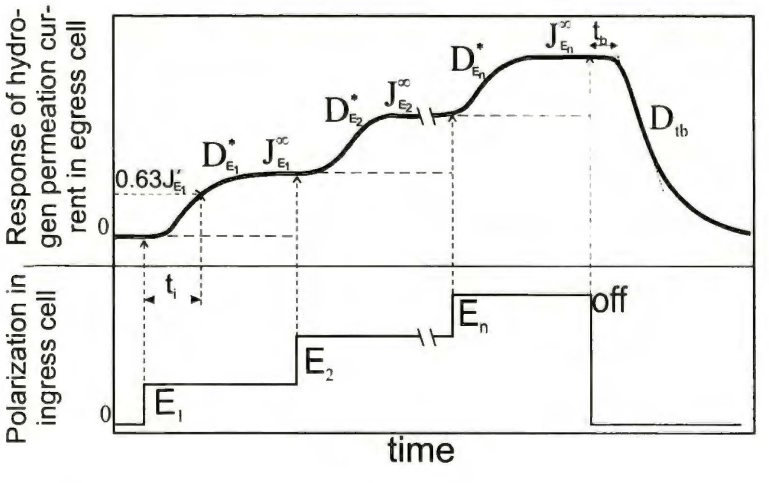

Figure 4.8. Schematic presentation of the run of the hydrogen permeation measurements at step by step increased cathodic polarization.

For each applied polarization, the values of the steady state hydrogen permeation current (J_l^{∞}) was recorded. The values of the hydrogen apparent diffusivity ($D^*_{E_n}$) and the hydrogen concentration at the ingress side of membrane (C_{E_n}) were calculated according to the following equations [93, 135-137]:

$$D^*_{E_n} = \frac{l^2}{6 \cdot t_n} \tag{4.1}$$

$$C_{E_n} = \frac{J^{\infty}_{E_n} \cdot l}{D^*_{E_n}} \tag{4.2}$$

where: l - the membrane thickness,

J^{∞}_{E}- the steady state value of the permeation current;

t_n - the time required to reach the 0.63 of J^{∞}_{E} (Figure 4.8).

In the case of the permeation transient revealing the maximum, the permeation current corresponding to the maximum was taken into account.

From the decay hydrogen permeation transient recorded after cessation of hydrogen charging (Figure 4.8), the hydrogen diffusivity was calculated, according to equation [138]:

$$D_{tb} = \frac{0.051 \cdot l^2}{t_b} \tag{4.3}$$

where: t_b - the break-through time between the cessation of the hydrogen charging and intersection of the decay current line with the initial steady state level [139] (Figure 4.8).

4.2.5. Vacuum hydrogen extraction

The amount of absorbed hydrogen was measured using the modified vacuum extraction facility shown in Figure 4.9.

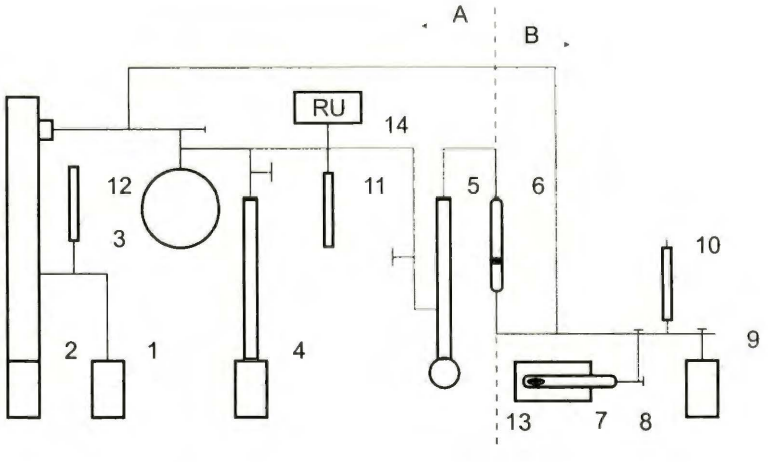

Figure 4.9. Scheme of the hydrogen vacuum extraction facility.
1, 2, 5 and 9 - vacuum pumps; 3 - hydrogen collector of a certain volume; 4 - McLeod gauge; 6 - palladium filter; 7 - electric furnace; 8 - quartz ampoule; 10, 11 and 12 - vacuummeter heads; 13 - specimen; 14 - resistance vacuummeter connected with the computer.
A – measurement part; B – heating part.

The heating part B and the measuring part A of the system were divided by the palladium ter heated to 675 K allowing the permeation of hydrogen. The increase in the hydrogen ,ressure in the part A during specimen heating at constant temperature was detected as a change of the resistance of Pt wire in vacuummeter head. The data were computer collected and

displayed. The measurement was stopped when the pressure-time relationship attended the plateau, corresponding to the full extraction of hydrogen from the specimen at given temperature. The hydrogen content in specimen was calculated according to the equation:

$$V_H = V_n \cdot \frac{p_{H_2}}{760} \cdot \frac{273}{T} \cdot \frac{100}{m} \tag{4.4}$$

where: V_H - the hydrogen content in specimen, ppm; V_n - the volume of the measured part A; P_{H2} - the hydrogen pressure, Torr; T - surrounding temperature, K; m - the weight of specimen, g.

4.2.6. Tensile tests

Tensile tests were carried out on the computerized INSTRON machine at the straining in air and in the test solutions at the open circuit potential and at cathodic polarization. Specimen was placed into the electrochemical cell mounted in the jaws of the tensile machine. After pouring the electrolyte, specimen was kept for 30 min at the open circuit potential or at the given cathodic polarization and then stretched until the fracture at the strain rate 5.5×10^{-6} s^{-1} without changing polarization.

Susceptibility to the stress corrosion cracking was determined as the ratio of elongation to the fracture of the specimens tested in the solution to that tested in air ($\varepsilon_f^{sol}/\varepsilon_f^0$).

For all the measurements the mean values from 3 to 5 tests carried out under the similar conditions were taken into the account.

5. RESULTS

5.1. Microstructure of studied steels

5.1.1. Evaluation of the steel microstructure

The number and size of all the nonmetallic inclusions in all the studied steels were lower than grade #1 of the appropriate scale, according to Polish Standard PN-64/H-04510. At high magnification the small (about 1 μm in size) individual (Fe, Mn)S inclusions have been found.

X-ray analysis of the studied steels did not reveal the presence of retain austenite in the metal structure. As followed from the X-ray analysis, metallographic examination and comparison of the microstructure of studied steels with the microstructures shown in [140], the microstructure of isothermally quenched and quenched and tempered steels was the bainitic one with the acicular bainite ferrite and the cementite precipitates. Normalized steel exhibited the spheroidized pearlite structure.

Figure 5.1 presents the microstructure of the bainite steels, as seen in optical microscope.

5.1.2. Qualitative metallography

It is known that the bainitic structure is very difficult for qualitative determination, as confirms Figure 5.1. In order to do the qualitative analysis, the special procedure has been evaluated. The surface of the specimen cross-section, prepared similarly as for optical microscopy was subjected to the SEM observations at magnification up to 5000X. The obtained pictures were then electronically processed using the special graphic program to develop the boundaries of the parent austenite grains and the bainite laths as exemplifies the Figure 5.2. The mean values of the size of the parent austenite and pearlite grains, of the length and width of the bainite laths and of the size of carbide precipitates, evaluated by means of the qualitative metallography methods are shown in Table 5.1.

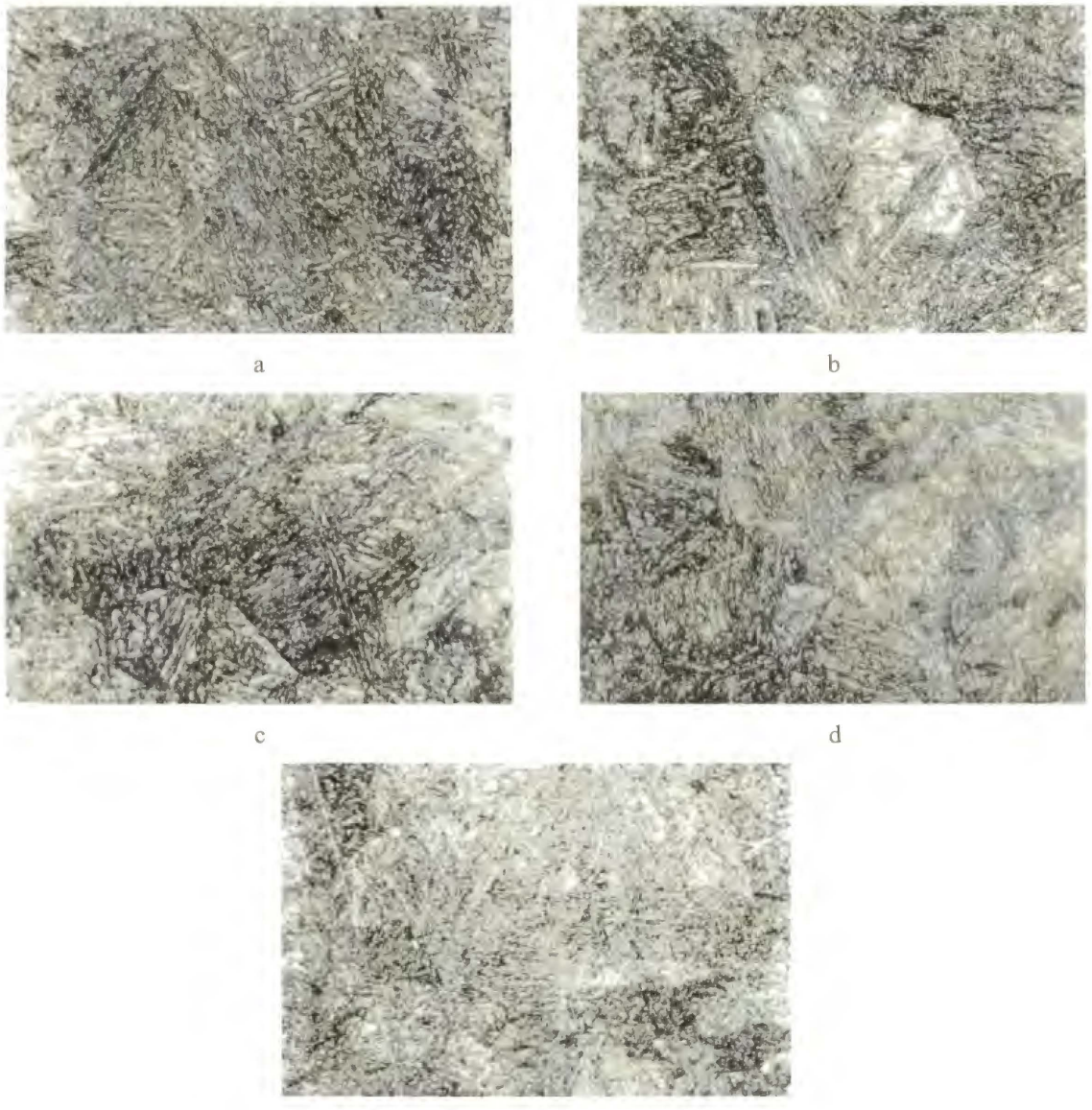

Figure 5.1. Microstructure of studied steels (OM):
a – 31I; b – 31QT; c – 28I; d – 28QT; e – 25I*.

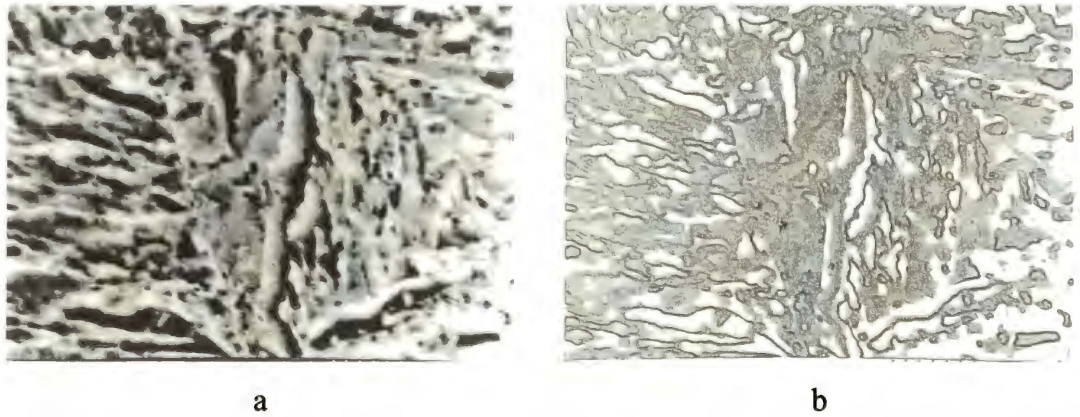

Figure 5.2. Processing of SEM micrograph for qualitative determination of the structure of studied steels. a – original SEM image; b – processed image.

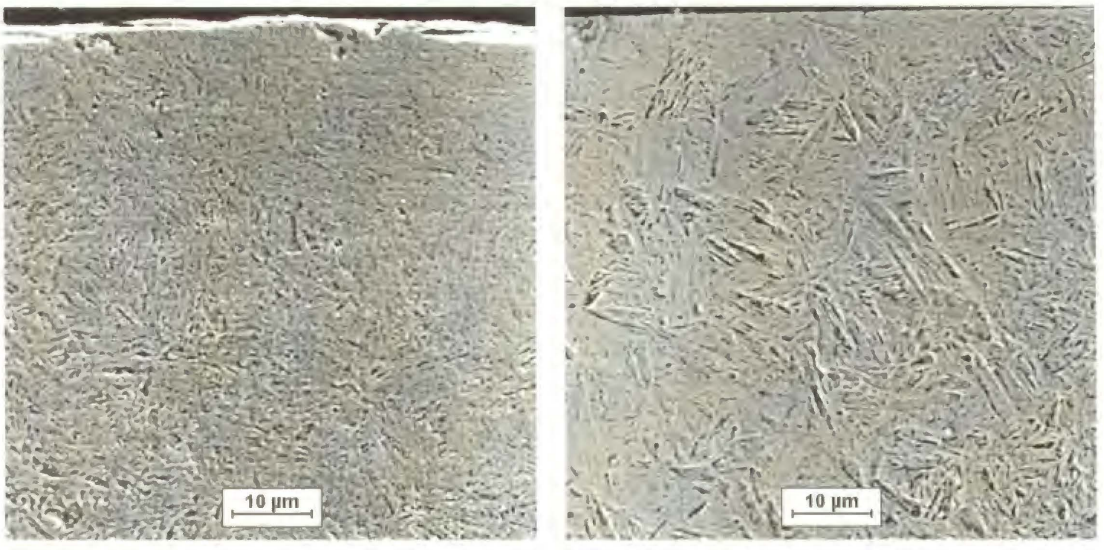

a b

Figure 5.3. Change of the microstructure of subsurface layer of 25I* steel due to the shot peening: a – shot peened material, b – bulk material (SEM).

a b

Figure 5.4. Change of the microstructure of subsurface layer of 25N steel due to the shot peening: a – shot peened layer; b- bulk material (SEM).

Table 5.1

The size of the pearlite and the parent austenite grains, the length and the width of bainite laths and the size of carbide precipitates in studied steels.

Material code	Parent austenite (pearlite) grain size, d. μm	Bainite lath length a, μm	Bainite lath width b, μm	Carbide size μm
25N	40	-	-	0.4-0.5
25I*	32	10	0.4	0.2
28I	32	8	0.8	0.2
28QT	27	6	0.6	0.2
31I	31	16	1.6	0.2
31QT	30	9	1.0	0.3

5.1.3. Microstructure of modified surface layers

Shot peening of steels changed the microstructure of the subsurface layer. In the case of isothermally quenched steel 25I* the decrease in the bainite laths in comparison with the bulk material occurred, cf. Figure 5.3. In the case of normalized steel, shot peening produced the heavy plastic deformation (Figure 5.4a) of the normalized pearlite-ferrite structure (Figure 5.4b). In all the cases there was no apparent boundary between the deformed layer and the bulk. The depth of metal surface layer exhibiting the microstructure, different from that of the core, was adopted as the thickness of shot peened layer and shown in Table 5.2.

Table 5.2.

Thickness of shot peened layer.

Material code	Thickness of modified layer, X, μm
25Ns	180
25I*s	120

5.1.4. X-ray analysis

The lattice parameters of the bainite and pearlite ferrite were calculated from the obtained X-ray spectra. The results are presented in Table 5.3.

Table 5.3.

Lattice parameters of pearlite and bainite ferrite in studied steels.

Steel code	Ferrite lattice parameters, Å
25N	2.8471
25Ns	2.8666
25I*	2.86741
25I*s	2.86583
25I*F-1	2,85703
25I*F-2	2,86551
28I	2.8768
28QT	2.8752
31I	2.8798
31QT	2.8767

5.2. Pitting corrosion

In the case of bainite steels the round pits of different size and depth were formed (Figure 5.5a and 5.5c). In normalized steel (not shot peened, as well as shot peened) no pits were formed, only some uneven corrosion was detected. Although the pits have not been associated with the carbides, the increase in the carbon content in the steels resulted in the more intensive pitting corrosion.

The cross sections of specimens corroded in $FeCl_3$ solution are shown in Figures 5.5 b and d. It is seen that the deeper pits were formed on specimens with not modified layer (Figure 5.5b) than on the shot peened one (Figure 5.5d). The number of pits, their mean diameter and maximum depth for studied steels are shown in Table 5.4.

Figure 5.6 shows the appearance of the side surface of 25I* and 25I*s specimens subjected to fatigue pretreatment and then to the pitting corrosion tests. In the case of the not shot peened steel, fatigue produced the plastic deformation bands (Figure 5.6a), which, however have not been observed in the case of the shot peened material (Figure 5.6b).

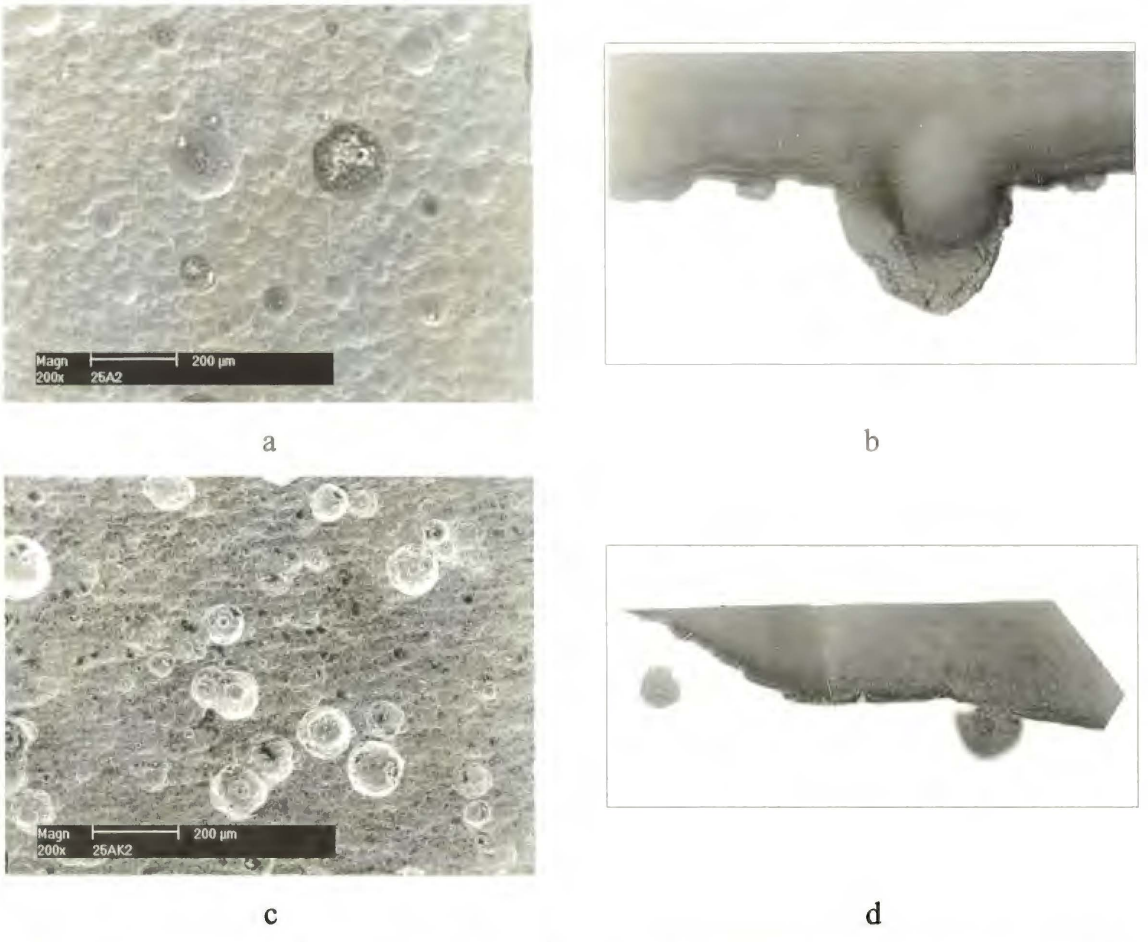

Figure 5.5. Appearance of the surface (a- 25I*, c – 25I*$_S$) and the cross section (b - 25I*, d- 25I*$_S$) of studied steels subjected to pitting corrosion.

Table 5.4

Density (N), mean diameter (d) and maximum depth (h_{max}^{pit}) of pits formed on studied steels during the exposition in Cl^- containing test solution

	N,cm^{-2}	d, mm	h_{max}^{pit}, mm
25I*	30-40	0,1	0,08
25Is*	220	0,15	0,008
25I*F-1	20	0.13	0.06
25Is*F	30	0.10	0.03
28I	50	0,09	0,14
28QT	180	0,12	0,32
31I	40-50	0,4	0,31
31QT	35-40	0,4	0,21

After the pitting corrosion test of fatigue pretreated specimens, the pits situated along the plastic deformation bands were seen on not shot peened specimens (Figure 5.6c). In the case of shot peened and fatigue pretreated specimens some elongated pits, similar in appearance to those

on the not shot peened surface were observed (Figure 5.6d). The deeper pits were formed on the not shot peened fatigue pretreated specimens in comparison with shot peened fatigue pretreated ones (cf. Table 5.4).

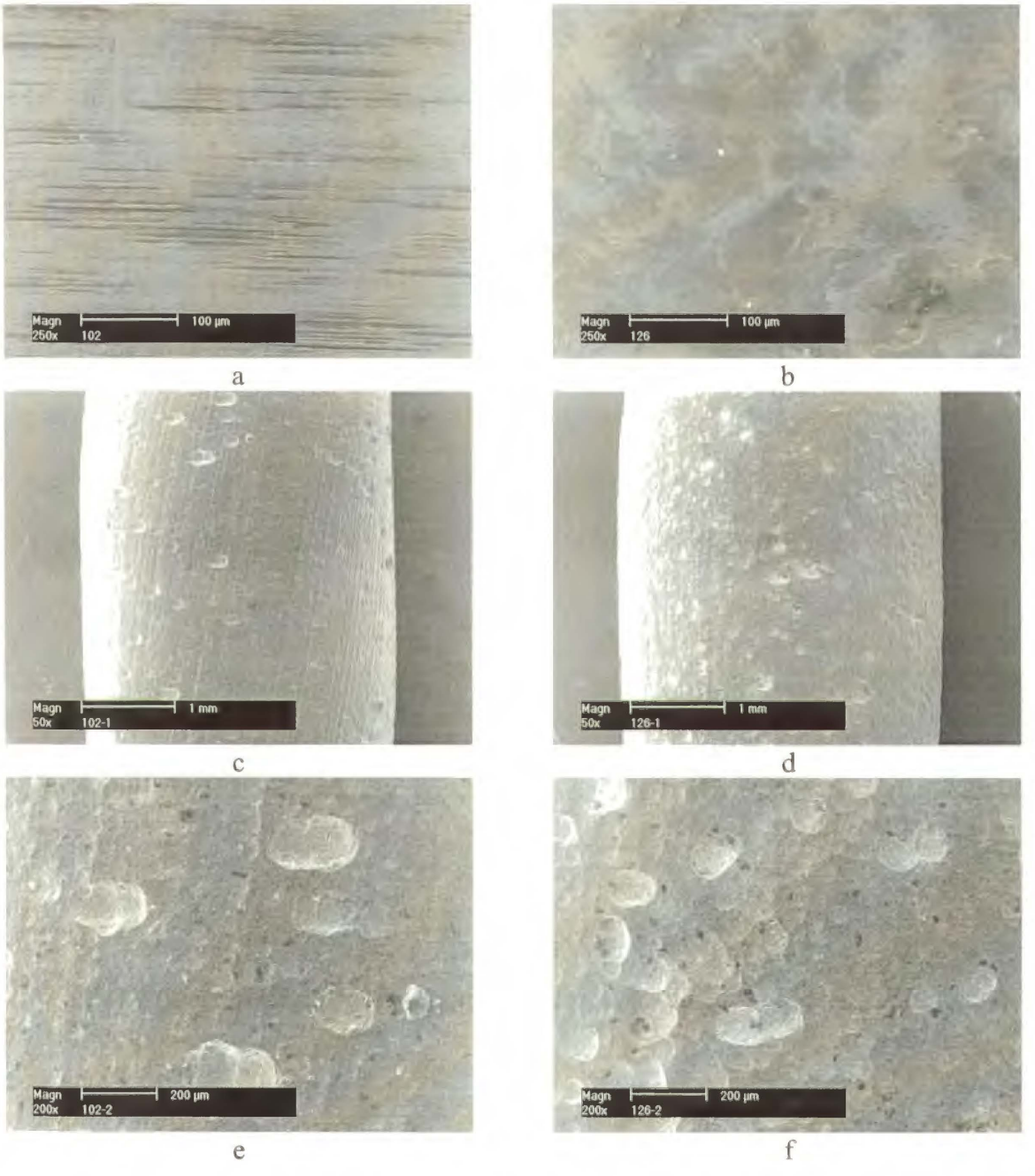

Figure 5.6. Appearance of the side surface of the fatigue pretreated not shot peened specimens of 25I* (a, c, e) and of the fatigue pretreated shot peened specimens of 25I*s (b, d, f).
a, b - side surface of the specimens after fatigue pretreatment test;
c, d, e, f - side surface of the fatigued pretreated specimens after pitting corrosion test

5.3. Electrochemical measurements

The values of the open circuit potential for studied materials and solutions are shown in Table 5.5. It is seen that the NaCl+Na_2SO_4 solution was more aggressive than the NaCl one. In the case of NaCl+Na_2SO_4 solution, the studied materials exhibited generally the more cathodic potentials and the higher corrosion current densities.

Table 5.5

Open circuit potential (Eocp) and corrosion current density for studied materials and electrolytes.

	NaCl		NaCl+Na_2SO_4	
	E_{ocp}, mV Hg/HgO	i_c , μA/cm^2	E_{ocp}, mV Hg/HgO	i_c , μA/cm^2
25N	-445	0.9	-515	2.1
25Ns	-330	4.2	-500	1.5
25I*	-430	1.6	-500	5.7
25I$_S$*	-340	5.1	-530	11
28I	-490	2.4	-570	6
28QT	-490	3.2	-440	12
31I	-420	6	-430	14
31QT	-350	12	-390	28

Figure 5.7 shows the appearance of cathodic polarization curves for isothermally quenched steels. In both studied solutions polarization curves exhibited the limit current for cathodic polarization up to about -1000 ~ -1150mV. The values of the limit current depended on the carbon content in steels and on the shot peening. At the increasing carbon content the current increased (Figure 5.7a). The lower limit of current may be observed for the shot peened steel in comparison with the not shot peened one (Fig. 5.7b).

At higher cathodic polarization the values of the polarization current are quite similar for given potential for all the studied steels.

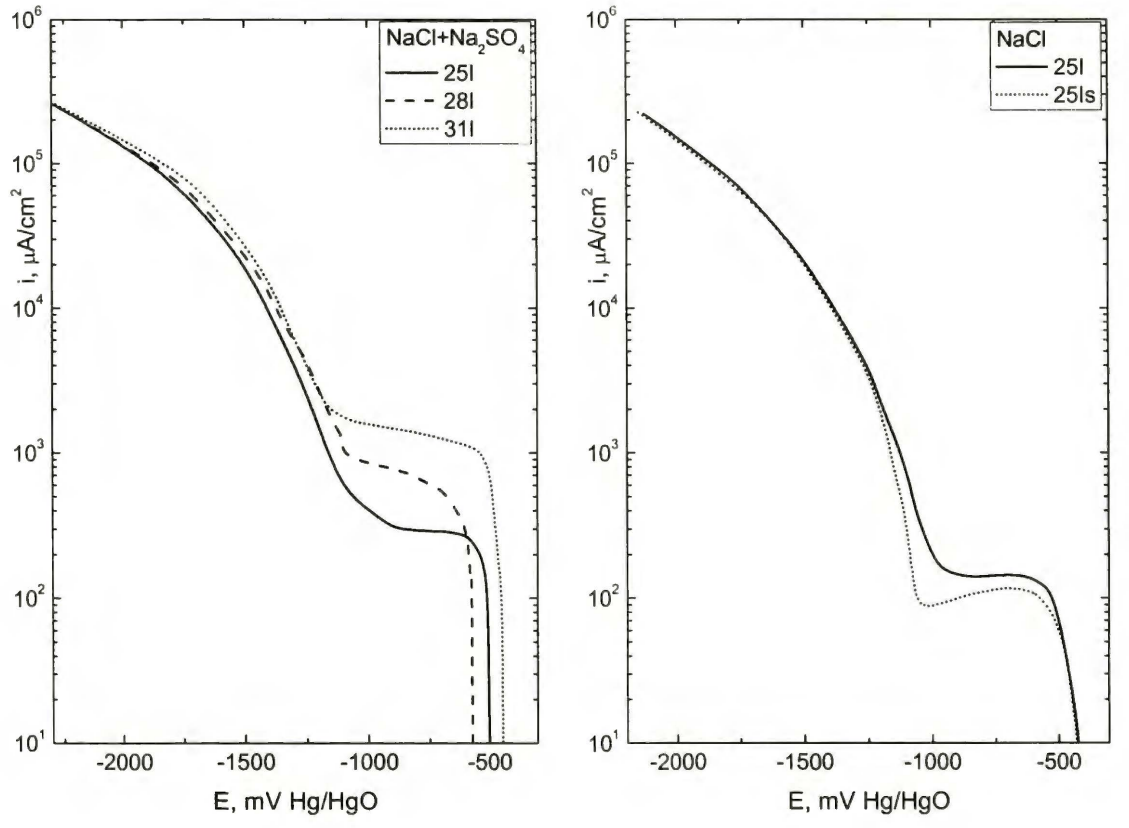

Figure 5.7. Cathodic polarization curves for isothermally quenched steels in $NaCl+Na_2SO_4$ (a) and NaCl (b) solutions.

5.4. Electrochemical measurements of hydrogen permeation rate

5.4.1. Anodic polarization

In contrast to the data reported in [36], no hydrogen permeation through all the studied steels has been detected at the open circuit potential and at anodic polarization of the ingress side within the potential range between E_{ocp} and +100mV Hg/HgO.

5.4.2. Cathodic polarization

At application of step by step increasing potentiostatic cathodic polarization, the different appearance of the buildup permeation transients has been observed. Figure 5.8 exemplifies the appearance of the consequent buildup transients at increasing cathodic potential (the steady state permeation of preceding transient is adopted as the zero point for the next one). It is seen that at certain polarization the unusual transient with a very low slop approaching the high steady state

permeation appeared. This transient may be associated with the hydrogen induced irreversible changes in the metal microstructure, as has been stated in [141, 142].

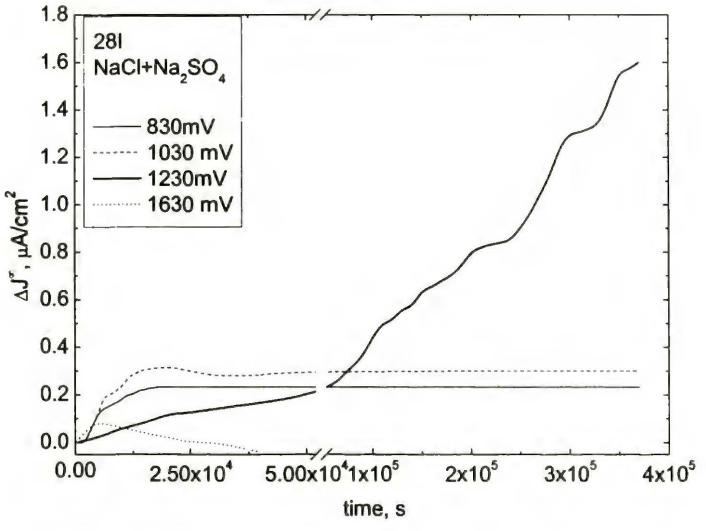

Figure 5.8. Consequent hydrogen permeation buildup transients recorded at application of increased cathodic potential.

At still higher polarization the transients exhibiting maximum of permeation occurred. Such an appearance of the permeation transient has been associated with the formation of microcracks and microvoids within the metal [113]. Indeed, the cross section of the membranes subjected to such polarization showed the presence of microcracks, as seen in Figure 5.9. Microcracks are situated along the boundaries of the parent austenite grains and the bainite laths.

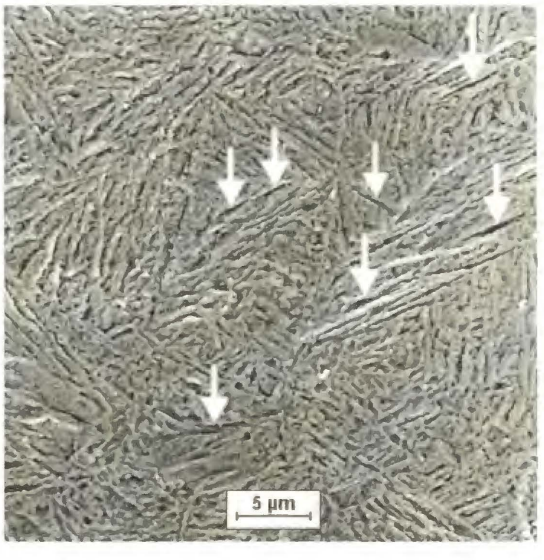

Figure 5.9. Cross section of the membrane subjected to high cathodic polarization. Microcracks marked with arrows.

Membranes subjected to the very high prolonged polarization exhibited the peeling-off of the ingress side. Figures 5.10 – 5.12 present the appearance of the peeled-off ingress surface of the studied steels. The delamination of the surface layers proceeded along the deformation bands in the case of shot peened 25Ns steel (Figure 5.10). The microvoids resembling the boundaries of

the parent austenite and the bainite laths are seen in the case of peeled-off surface of membrane made of 25I* steel (Figure 5.11). The brittle cracking occurred in the case of 28I steel resembled the bainite microstructure (cf. Figure 5.1 and Figure 5.12).

It should be noted that no sulfide inclusion has been observed on the peeled off surface of the studied membranes.

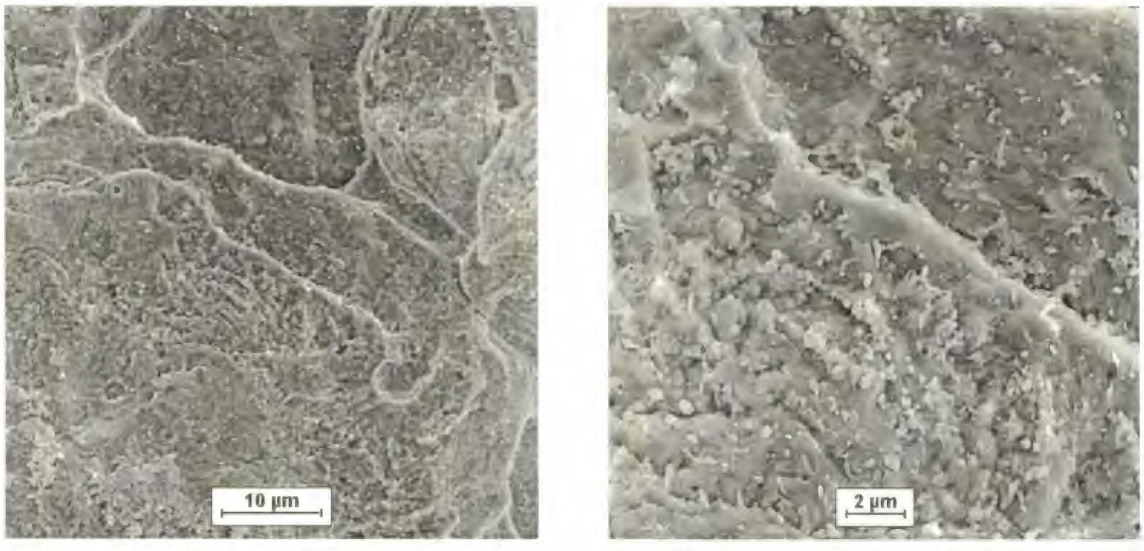

a b

Figure 5.10. Appearance of the peeled-off ingress surface of the membrane subjected to high cathodic polarization. Steel 25Ns.

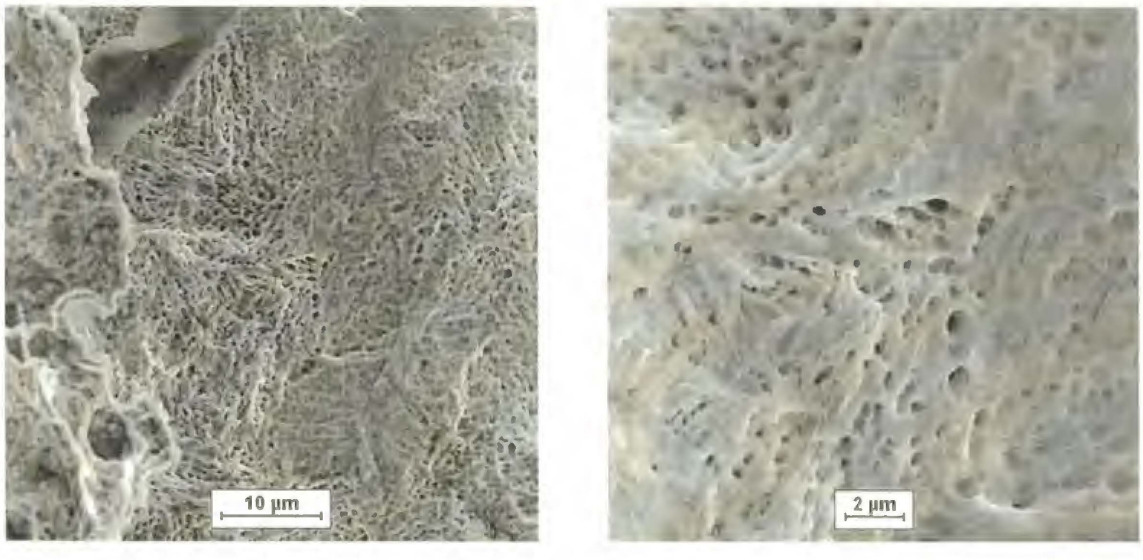

a b

Figure 5.11. Appearance of the peeled-off ingress surface of the membrane subjected to high cathodic polarization. Steel 25I*.

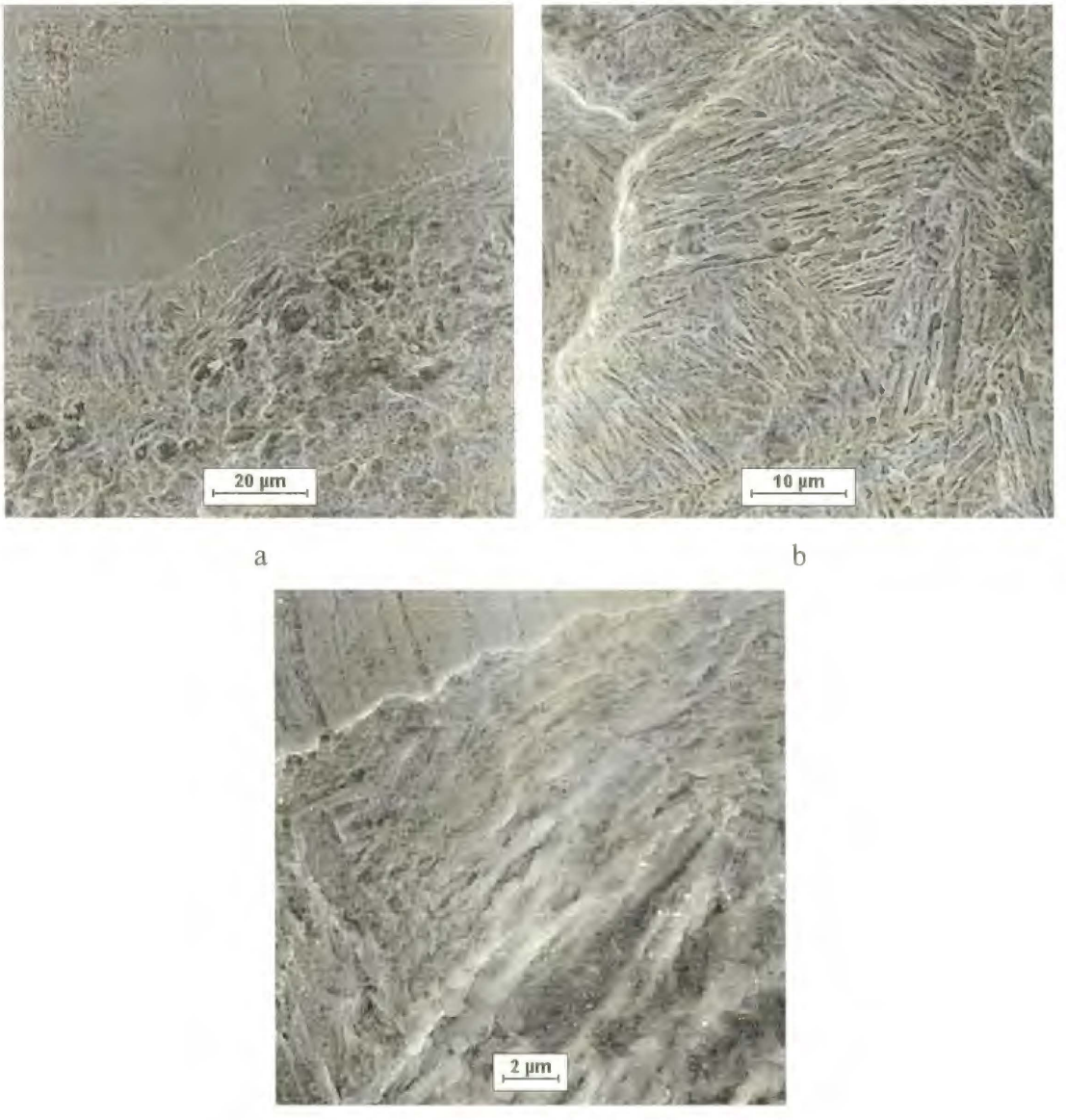

a b

c

Figure 5.12. Appearance of the peeled-off ingress surface of the membrane subjected to high cathodic polarization. Steel 28I.

Figure 5.13 shows the effect of material, chemistry and heat treatment on the steady state (or maximum) hydrogen permeation at applied polarization. With decrease of carbon content the hydrogen steady state permeation increased in the case of quenched and tempered steel (Figure 5.13a), as well as in the case of isothermally quenched one (Figure 5.13b).

The hydrogen behavior in the studied steels may be compared under the following conditions:

- similar polarization current;
- no formation of voids.

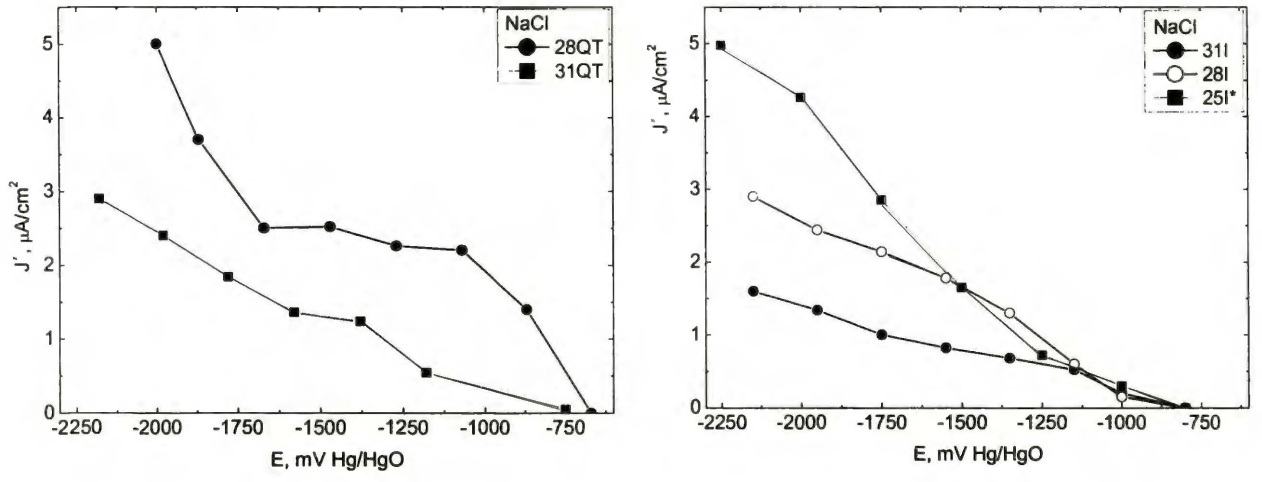

a b

Figure 5.13. Steady state hydrogen permeation current recorded for quenched and tempered (a) and isothermally quenched (b) steels at applied cathodic potentials.

The effect of polarization current on hydrogen permeation is shown in Figure 5.14, where cathodic polarization current in the ingress cell and the corresponding steady state hydrogen permeation in the egress cell are plotted vs. applied potential. The observed increase in the hydrogen steady state permeation might be associated with the increase in the cathodic polarization current. Therefore, the relationship of steady state (or maximum) hydrogen and applied potential may be caused not only by the intrinsic properties of the studied metal, but also by the effect of the limit polarization current, as has been shown in Figure 5.7.

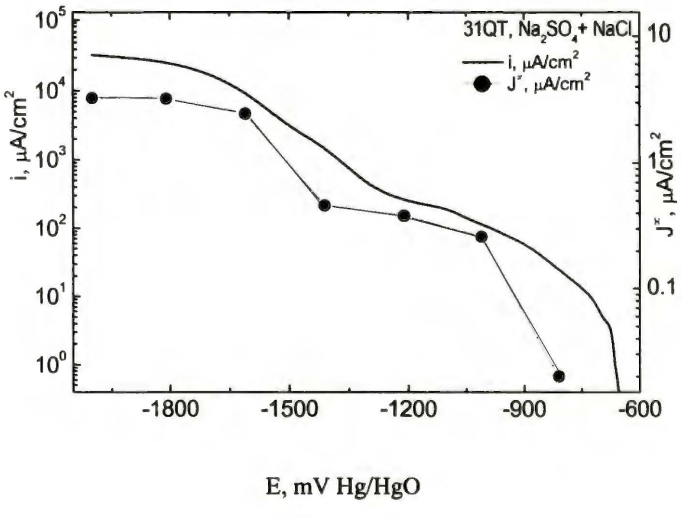

Figure 5.14. The steady state hydrogen permeation current (J^{∞}) and polarization current (i) recorded at applied cathodic potentials for 31QT steel in Na_2SO_4+NaCl solution.

To avoid the effect of the formation of microvoids and the effect of the limiting current, polarization potential of -1500 mV was adopted as the reference one. At this potential, the cathodic current is quite similar for all studied steels (Figure 5.7) and no permeation transients with the maximum occurred (Figure 5.8). Table 5.6 summarizes the mean values of steady state permeation current densities, as recorded for studied materials and solutions at -1500 mV.

Table 5.6

Values of the steady state hydrogen permeation J^{∞}_{-1500} at polarization of -1500 mV.

Steel code	NaCl	NaCl + Na_2SO_4
25N	2.56 +/- 0.49	3.5 +/- 0.10
25Ns	0.80 +/- 0.02	0.96 +/- 0.10
25I*	2.16 +/- 1.55	2.4 +/- 0.20
25I*s	0.59 +/- 0.16	0.69 +/- 0.12
28I	1.2 +/- 0.57	1.7 +/- 0.07
28QT	2.4 +/- 0.6	2.5 +/- 0.03
31I	1.3 +/- 0.2	0.8 +/- 0.06
31QT	1.25 +/- 0.07	1.4 +/- 0.03

5.4.3. Effect of modified layer on hydrogen permeation

As seen in Figure 5.15 shot peening decreased the steady state hydrogen permeation. The effect of shot peening on hydrogen permeation at polarization at potential -1500mV in both solutions is shown in Table 5.6.

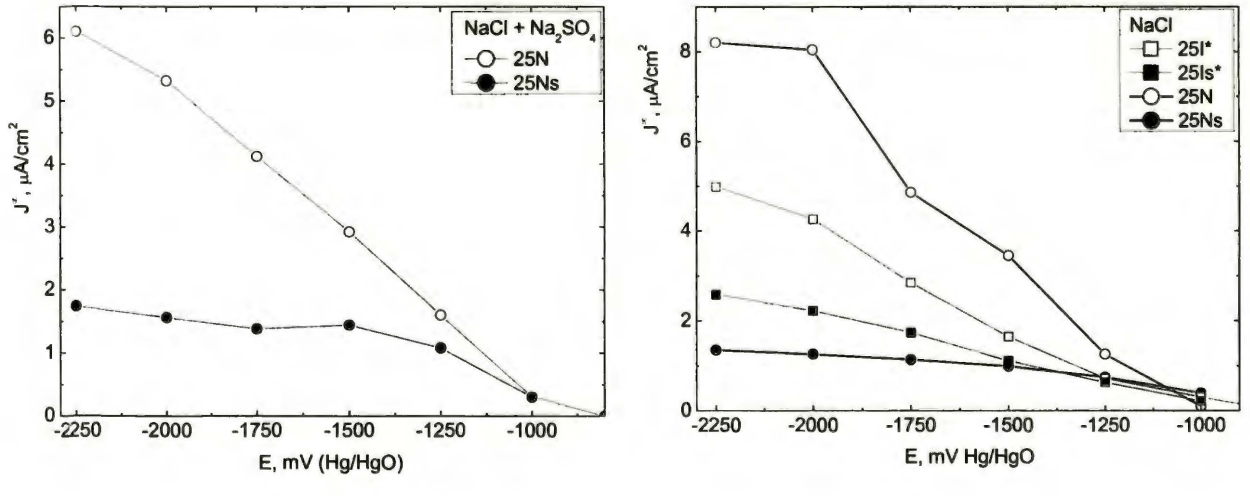

a b

Figure 5.15. Effect of shot peening on the steady state hydrogen permeation current as recorded at cathodic polarization of 25N and 25I* steels in studied electrolytes.

5.4.4. Effect of fatigue pretreatment on hydrogen permeation

Figure 5.16 presents the steady state hydrogen permeation recorded for the membranes cut from the fatigue pretreated specimens. The values of hydrogen permeation at polarization -1500 mV of fatigue pretreated specimens are shown in Table 2.7.

Table 5.7

The steady state hydrogen permeation in $NaCl + Na_2SO_4$ solution at -1500 mV for fatigue pretreated membranes.

Sample code	J^{∞}_{-1500}, $\mu A/cm^2$
25I*F-1	0,07
25I*F-2	0,05

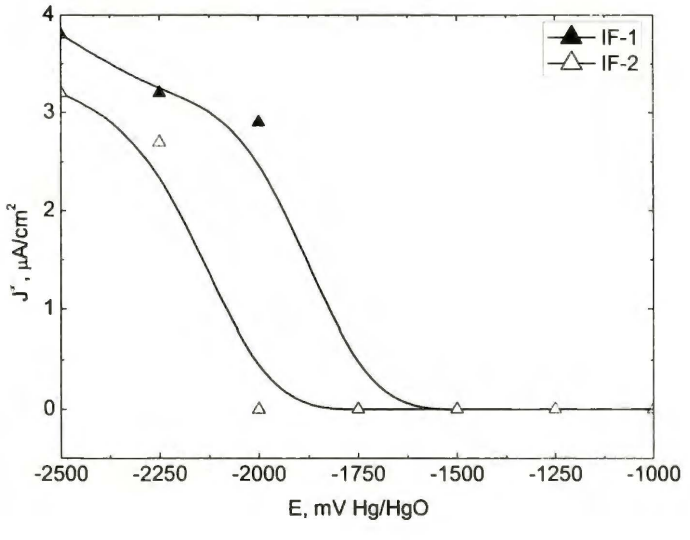

Figure 5.16. The steady state hydrogen permeation recorded for fatigue pretreated specimens at cathodic polarization in $Na_2SO_4 + NaCl$ solution.

Figure 5.17 shows the appearance of the ingress side of fatigue pretreated membranes subjected to high cathodic polarization. Beneath the peeled-off layer surface had a very specific appearance (Figure 5.17a and b). The formation of the ladder-like structure is observed (Figure 5.17b and 5.17c). At higher magnification (Figures 5.17d and 5.17e) the specific deformation of bainite ferrite as well as the deformation of carbide precipitates can be also noticed.

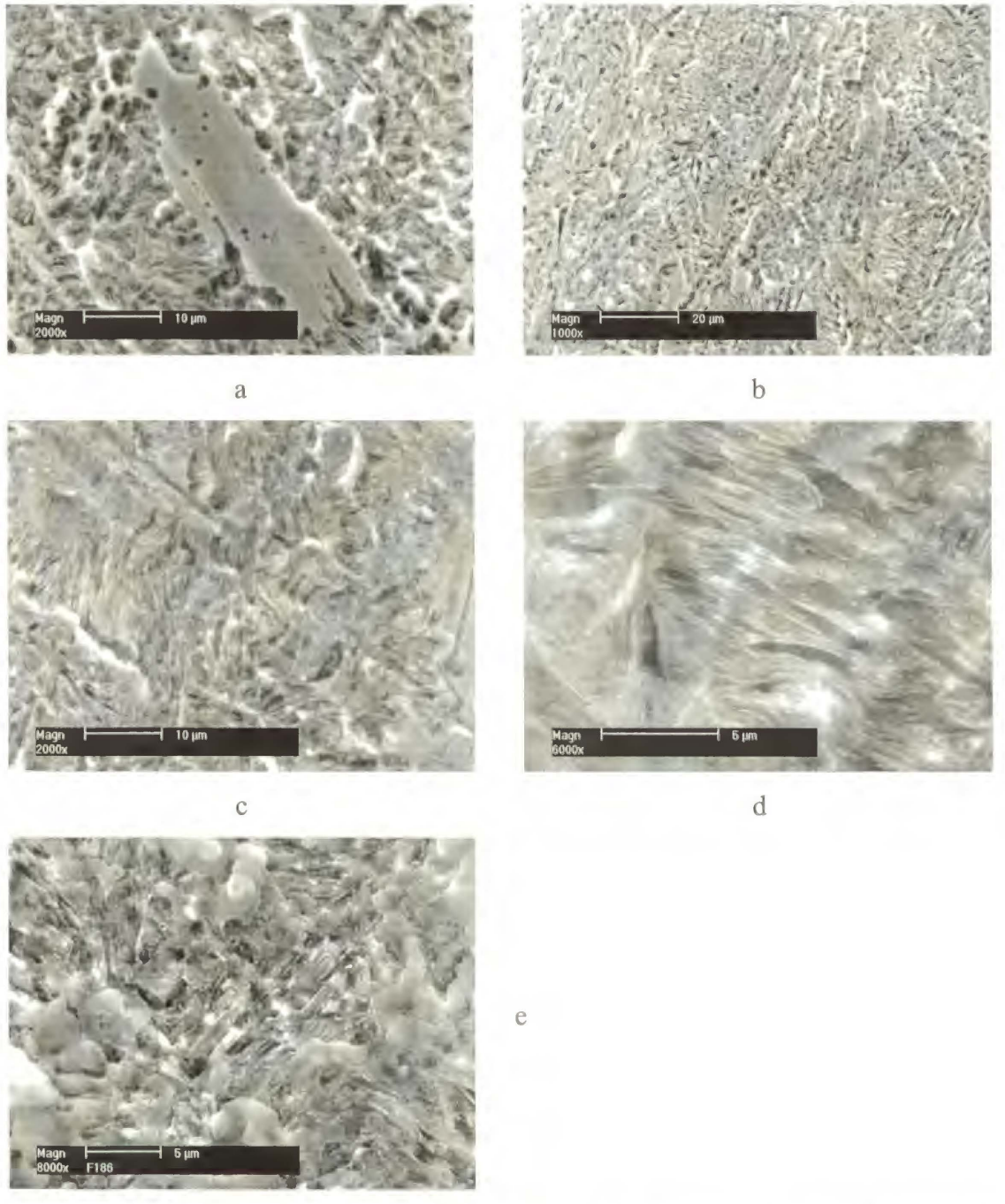

Figure 5.17. Appearance of the ingress side of the fatigue pretreated membranes subjected to high cathodic polarization.

5.4.5. Hydrogen apparent diffusivity

In Table 5.8, the values of apparent hydrogen diffusivity calculated from the buildup permeation transients recorded at polarization -1500 mV (D^*_{-1500}) (equation 4.1.) and from the decay transients (D_{tb}) (equation 4.2.) are collected. Normalized 25N steel exhibited the highest hydrogen diffusivity. Increase in the carbon content, heat treatment, application of shot peening and fatigue pretreatment decreased the both parameters characterizing the hydrogen diffusivity.

Table 5.8

Hydrogen apparent diffusivity as calculated from buildup permeation transient recorded at polarization -1500mV in NaCl + Na_2SO_4 solution (D^*_{-1500}) and hydrogen apparent diffusivity calculated from the decay permeation transients (D_{tb}) for studied steels.

Material code	D^*_{-1500} cm^2/s	D_{tb} cm^2/s
25N	$1.63*10^{-6}$	$3.5*10^{-6}$
25Ns	$6.8*10^{-7}$	$1.2*10^{-6}$
25I*	$3.4*10^{-7}$	$4.7*10^{-7}$
25I*s	$1.7*10^{-7}$	$3.4*10^{-7}$
25I*F-1	$4.2*10^{-8}$	$6.9*10^{-7}$
25I*F-2	$2.3*10^{-9}$	$3.5*10^{-7}$
28I	$2*10^{-7}$	$3.3*10^{-7}$
28QT	$2.3*10^{-7}$	$4.4*10^{-7}$
31I	$0.9*10^{-7}$	$2.2*10^{-7}$
31QT	$1.3*10^{-7}$	$2.9*10^{-7}$

5.5. Vacuum extraction measurements

After the completing the hydrogen permeation tests (after recording of the decay transients) membranes were subjected to vacuum extraction measurements. Since the mobile hydrogen escaped from the membrane at the decay cycle, and at remounting of membrane, its cleaning and preparation for vacuum extraction, the residual hydrogen left in the membranes was measured. The mean values of residual hydrogen measured for the similarly treated membranes made of studied materials are shown in Table 5.9.

It is seen that materials with the shot peened layers exhibited the higher amount of residual hydrogen than the same materials with not treated surface.

Table 5.9

The mean content of residual hydrogen (V_H) left in membranes after the completing the permeation tests in NaCl + Na_2SO_4 solution.

Specimen code	V_H, ppm
25N	0.32
25Ns	0.63
25I*	0.58
25I*s	1.34
25I*F-1	2.2
25I*F-2	3.5
28I	0.73
28QT	0.65
31I	1.12
31QT	0.55

5.6. Stress corrosion cracking

5.6.1. Mechanical properties of the studied materials

Table 5.10 shows mechanical properties of the studied materials as established in tensile tests done in air. As follows from the Table 5.10 the low carbon steel subjected to shot peening exhibited mechanical properties as required by the Standard for aircraft steel 30HGSNA.

Shot peening did not change the appearance of fracture surface of steels.

5.6.2. Stress corrosion cracking

The effect of test solution, heat treatment, shot peening and carbon content on susceptibility to stress corrosion cracking are exemplified in Figures 5.18-5.20.

As seen in Figure 5.18 under the open circuit conditions the NaCl+Na_2SO_4 solution produced the more detrimental effect than NaCl one. This effect is especially seen on the change of reduction of area. At cathodic polarization no dramatic difference between the effect of both solutions could be seen. Isothermal quenching provided the higher resistance to SCC than the quenching and tempering (Figure 5.19). The resistance to SCC increased with decrease in the

carbon content (Figure 5.20). The data characterizing susceptibility of studied steels to stress corrosion cracking (ratio of elongation to fracture in solution to that in air) at the open circuit potential and at the cathodic polarization -1500 mV (adopted as the reference one) in studied solutions are collected in Table 5.11.

Table 5.10.

Mechanical properties established for studied steels and as required by the Polish Standard for 30HGSNA steel.

Steel code	σ_{UTS}, MPa	ϵ_f	RA, %
25N	570	0.22	57
25Ns	1090	0.19	53
25I*	1590	0.11	47.6
25I*s	1700	0.116	47
28I	1620	0.22	41
28QT	1640	0.28	51
31I	1760	0.26	46
31QT	1740	0.26	46
Polish Standard for 30HGSNA	min. 1650	min. 0.09	min 45

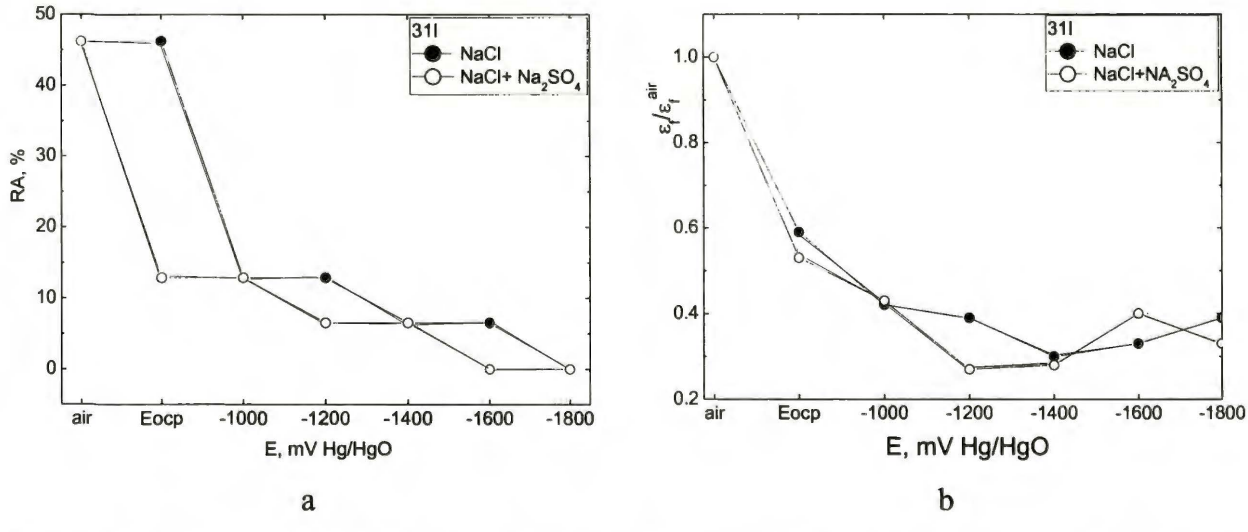

Figure 5.18. Effect of the test solution on reduction in area (a) and elongation to fracture (b) measured at the open circuit potential (Eocp) and at the different cathodic polarization.

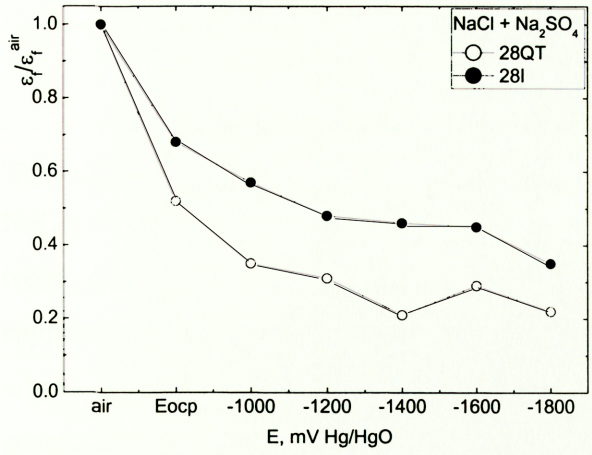

Figure 5.19. Effect of heat treatment on elongation to fracture at the testing in solution, at open circuit potential (Eocp) and at different cathodic polarization.

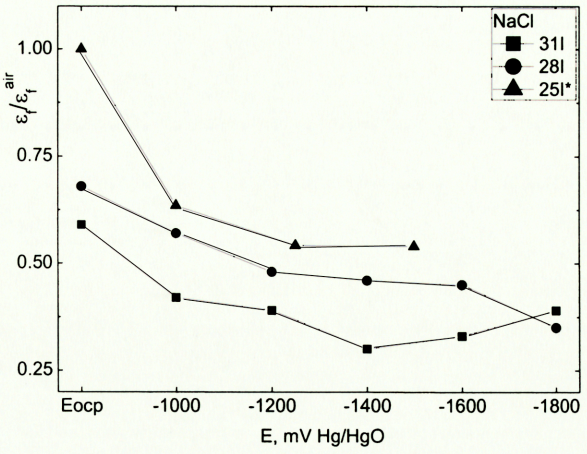

Figure 5.20. Effect of carbon content on elongation to fracture at the testing in solution at open circuit potential (Eocp) and at cathodic polarization.

Table 5.11

Susceptibility to SCC (ratio of elongation to fracture in solution to that in air) of studied steels under the open circuit conditions (Eocp) and at cathodic polarization -1500mV in NaCl and in NaCl + Na_2SO_4 solutions.

material code	$\varepsilon_f^{Eocp}/\varepsilon_f^o$		$\varepsilon_f^{-1500}/\varepsilon_f^o$	
	NaCl	NaCl + Na_2SO_4	NaCl	NaCl + Na_2SO_4
25N	1.0	0.945	0.55	0.61
25Ns	0.93	0.936	0.52	0.56
25I*	1.0	0.74	0.47	0.54
25I*s	0.96	0.93	0.44	0.35
28I	0.68	0.68	0.44	0.46
28QT	0.53	0.52		0.29
31I	0.59	0.53	0.25	0.32
31QT	0.54	0.63		0.27

5.6.3. Fractography

Open circuit conditions. Figure 5.21 show the appearance of the side surface of the specimens fractured under the open circuit conditions in NaCl (Figures 5.21a and 5.21b) and in NaCl+Na_2SO_4 (Figures 5.21c and 5.21d) solutions. It is obvious that in both solutions, the cracks were associated with the pits formed on the side surface of tensile tested specimens. This is supported by the appearance of the fracture surface of specimen tested in solution (Figure 5.22a), where pit can be seen. The cracks propagated from the pits into the bulk of the tensile tested specimens, as seen on the cross section, cf. Figure 5.22b.

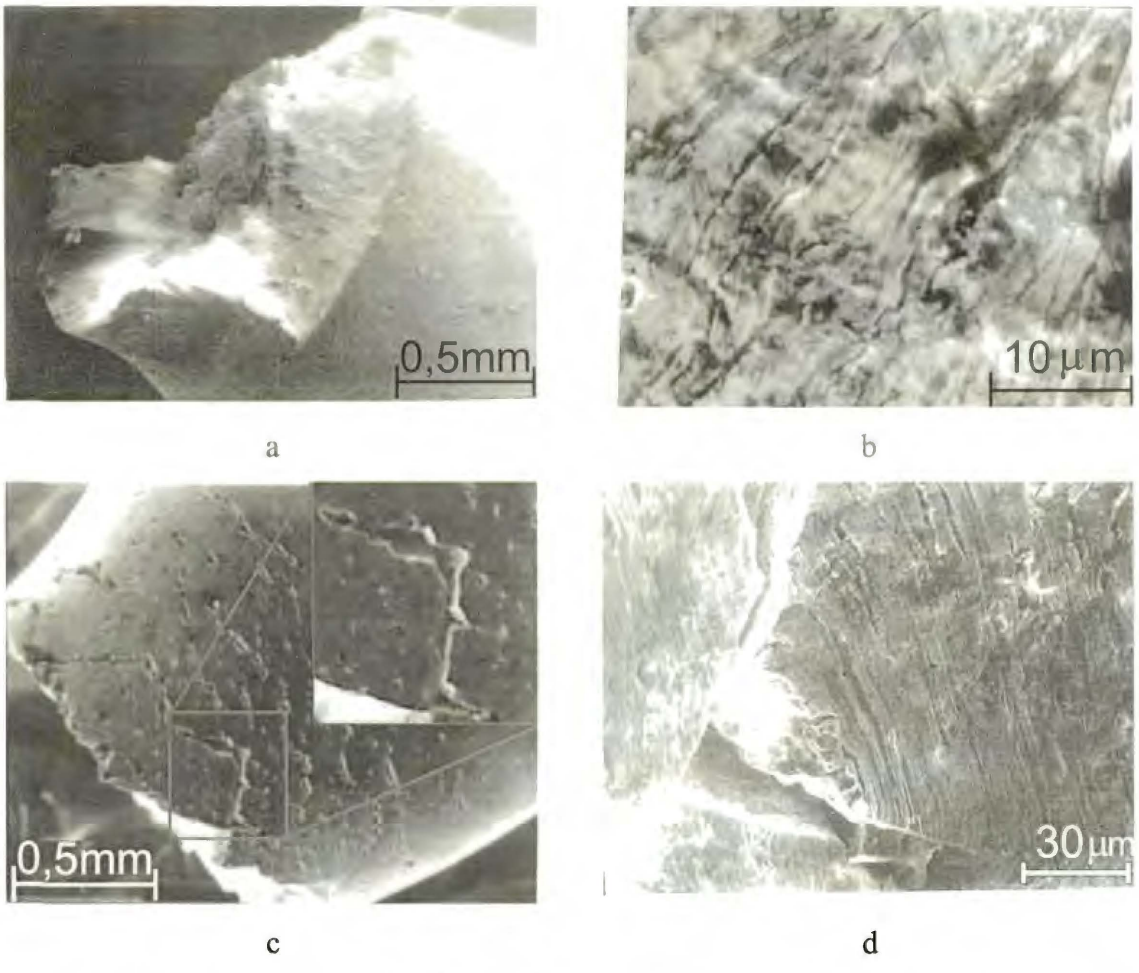

Figure 5.21. Appearance of the side surface of the specimens fractured under the open circuit conditions in NaCl (a, b) and in NaCl+Na_2SO_4 (c, d) solutions.

Cathodic polarization. At application of cathodic polarization the specimens exhibited the mixed, ductile and brittle type of fracture. The share of the ductile fracture decreased with the increase in polarization. As seen in Figure 5.23 in the case of normalized steel, the brittle fracture had transgranular appearance (Figure 5.23a), whereas in the case of bainite steel rather the intergranular brittle fracture occurred (Figure 5.23b). No apparent effect of the shot peening on the appearance of the fracture surface has been observed.

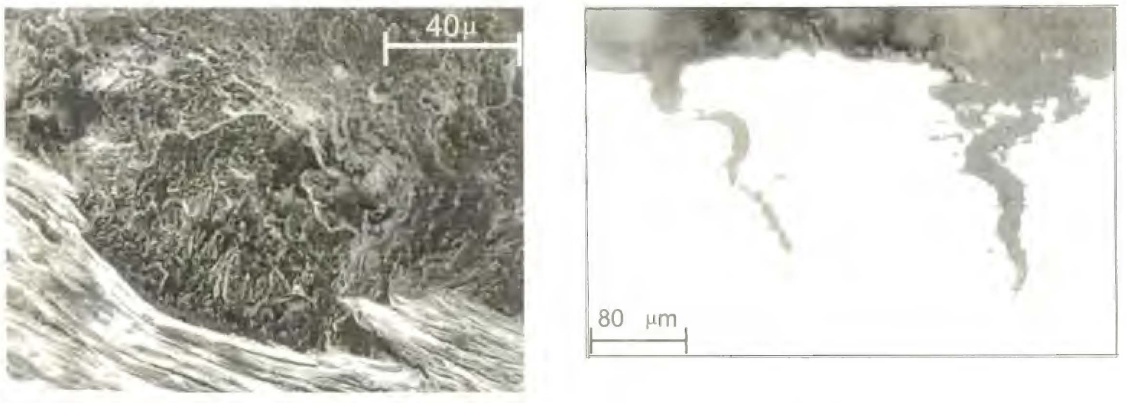

a b

Figure 5.22. Pit seen on the fracture surface (a) and cracks propagated from the pits formed on side surface (b) of the 28QT specimen tensile tested at Eocp in NaCl solution.

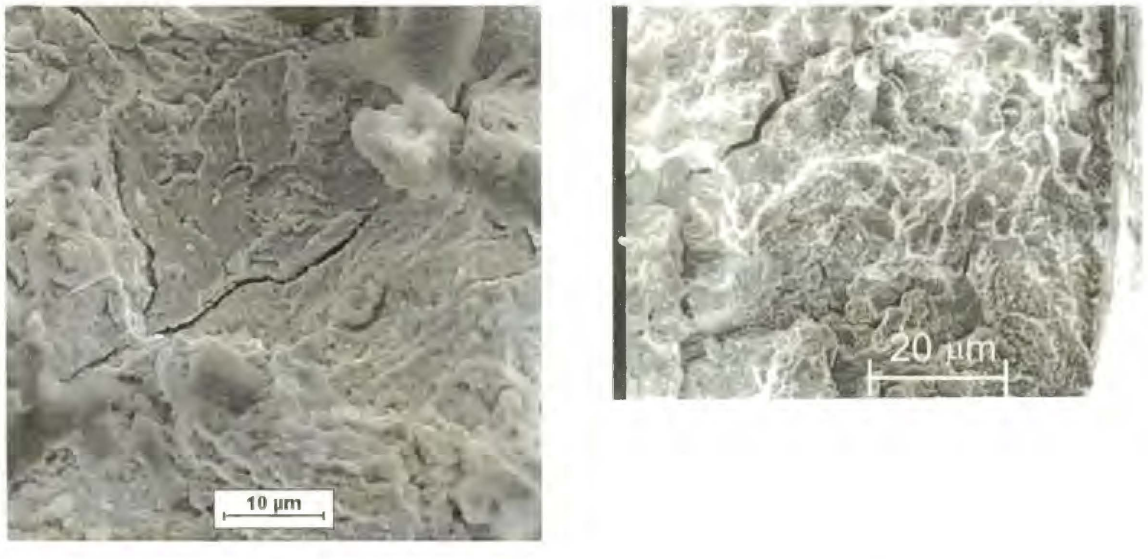

a b

Figure 5.23. Appearance of the brittle part of the fracture surface of 25N (a) and 28QT (b) steels tested at cathodic polarization -1500 mV in NaCl solution.

6. DISCUSSION

Since the mixed mechanism of the stress corrosion cracking involving the local corrosion and the hydrogen embrittlement has been observed, the effects of the carbon content, the heat treatment and the surface modification on both, the resistance to the pitting corrosion and to the hydrogen embrittlement should be considered. In the case of the studied low sulfur steels, not exhibiting the sulfide inclusions, not the sulfides but the other structural features would govern the susceptibility to pitting corrosion, hydrogen embrittlement and to stress corrosion cracking.

6.1. Stress corrosion cracking under the open circuit conditions

6.1.1. Effect of pits on stress corrosion cracking

As seen in Figure 5.22a the fracture surface of the specimens tested under the open circuit conditions revealed the pits. Therefore the susceptibility to stress corrosion cracking of the steels in studied solutions should be associated with the susceptibility to pitting corrosion.

6.1.2. Effect of pit morphology on stress concentration

Pitting corrosion was described by three parameters: pit density, maximum depth and diameter of pits (Table 5.4). As seen in Figures 5.21 and 5.22 the cracks leading to the fracture of the specimens, tensile tested at the open circuit potential in aggressive solution, initiated at the corrosion pits formed on the side surface. Pits served as the notches. From the point of view of the stress corrosion cracking the depth of pits should be a parameter of greater importance than the diameter of pits and their number.

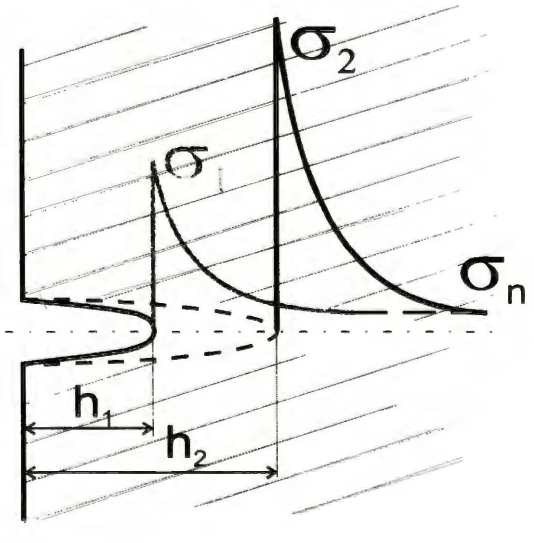

Figure 6.1. Schematic presentation of the effect of notch depth on stress concentration.

In the case of deeper pits the stress concentration was higher (Figure 6.1), so pits became more effective as notches and the cracks were more eager to form. On the other hand, with increased diameter of the pit its notch efficiency decreased [143]. Taking this into account the maximum pit depth was chosen as the parameter to evaluate the pitting corrosion resistance and to compare it with the resistance to SCC.

6.1.3. Relationship between susceptibility to pitting corrosion and to SCC

Figure 6.2 presents the relationship between the relative decrease in elongation to fracture observed at the stress corrosion tests carried out under the open circuit conditions in both test solutions and the maximum pit depth estimated in the pitting corrosion tests, for studied steels.

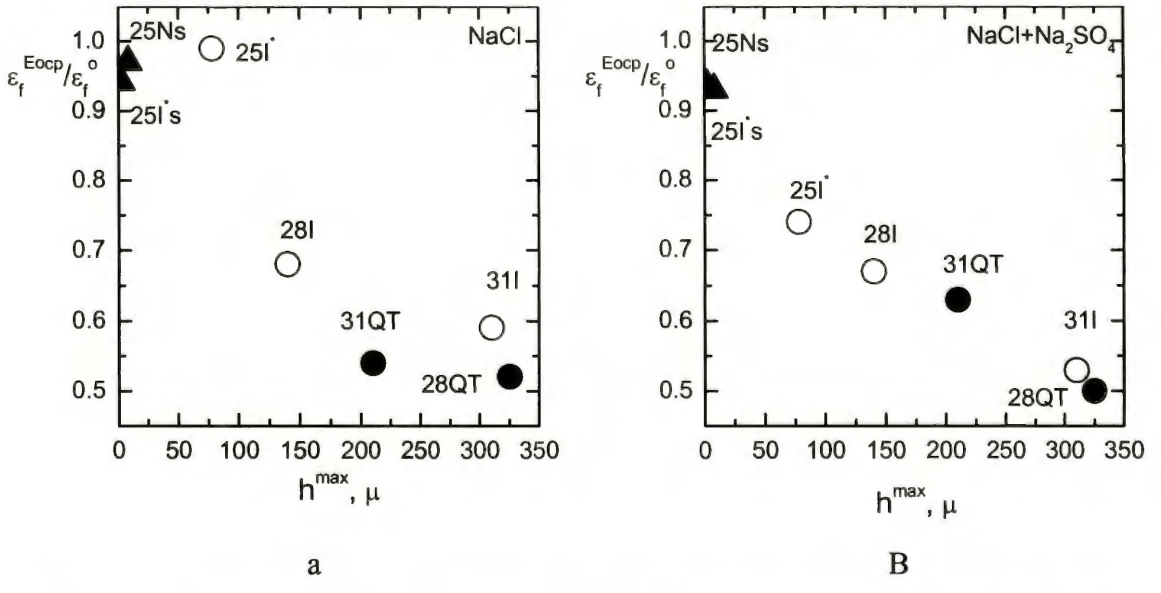

Figure 6.2. Relationship between the maximum pit depth (as measured in $FeCl_3$ solution) and change of the elongation to fracture of studied steels at tensile tests at open circuit potential (Eocp) in studied solutions.

Materials exhibiting the higher resistance to pitting corrosion (as established in $FeCl_3$ solution) revealed also the higher resistance to stress corrosion cracking in both test solutions, despite the chemistry, heat and surface treatment. Resistance to pitting corrosion and thus to stress corrosion cracking was mostly affected by two parameters: carbon content and surface treatment. Lower carbon content in steel and application of shot peening increased the resistance to stress corrosion cracking. Heat treatment had the less pronounced effect in this case, however, normalized steel exhibited no pitting (Table 5.4) and the very low susceptibility to stress corrosion cracking as well (Table 5.11).

6.1.4. Susceptibility to pitting corrosion and stress corrosion cracking of fatigue pretreated material

As shown in Figure 5.6a the surface of the not shot peened specimens subjected to fatigue test exhibited the marks situated perpendicular to the axis of applied stress. Those marks reflected the steps and the grooves formed on the fatigue surface as schematically shown in Figure 6.3a. During the following exposition of such specimens in Cl^- containing solution those grooves served as the pit nucleation sites, as shows Figure 6.3b. The elongated shape of pits (Figure 5.6c) resembling the situation of grooves confirms the above assumption.

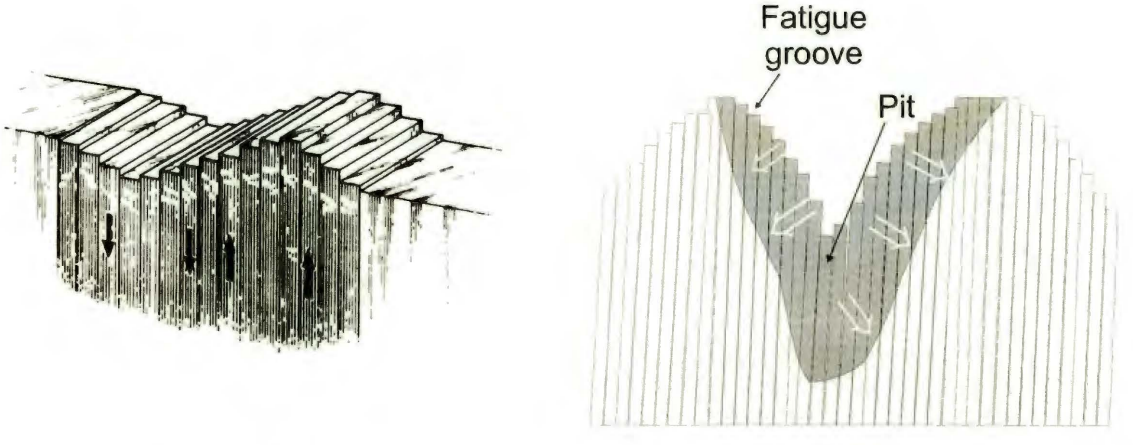

a b

Figure 6.3. Schematic presentation of the surface topography of specimen after fatigue pretreatment tests (a) and after subsequent pitting corrosion tests (b).

Shot peening hindered the formation of fatigue grooves on the specimen surface (Figure 5.6b). However, pits elongated perpendicular to the specimen axis were also observed after exposition of those specimens to the Cl^- containing environment (Figure 5.6d). This means that the uneven deformation which underwent material during fatigue test promoted the pits nucleation, even if there were no apparent change on the surface topography.

Although the shot peened fatigue pretreated material underwent the pitting corrosion similarly as did the not shot peened one, the intensity of pitting corrosion was much lower in the first case. As shown in Table 5.4 the pit density, diameter and maximum depth in the case of fatigue pretreated shot peened material ($25I^*_SF$) were lower than those in the case of fatigue pretreated not shot peened steel ($25I^*F$).

From the obtained above (Figure 6.2) relationship between the susceptibility to the pitting corrosion and to the stress corrosion cracking it may be concluded that the fatigue pretreated shot peened material should exhibit the higher resistance to stress corrosion cracking than the fatigue pretreated not shot peened ones.

6.2. Stress corrosion cracking at cathodic polarization of not shot peened bainite steels

At cathodic polarization stress corrosion cracking has been governed by the hydrogen embrittlement mechanism and, therefore, should be associated with the transport and the behavior of the hydrogen in the metal. Those parameters, in turn, are affected by the chemistry and the microstructure of the steels subjected to the different heat and surface treatments.

6.2.1. Hydrogen transport and trapping in not shot peened materials

6.2.1.1 Hydrogen diffusivity

Figure 6.4 shows the calculated values of hydrogen apparent diffusivity for the heat treated materials, depending on the carbon content. Under the applied experimental procedure the values of D_{tb} were established from the beginning of the decay permeation transients. Those transients revealed the beginning of the hydrogen desorption from the materials with filled hydrogen traps. Therefore, the data were not affected by the hydrogen-traps interaction [144]. Those values cannot be accounted for the "lattice diffusivity" of hydrogen in the ferrite in terms of paper [101], since they are much lower than the hydrogen diffusivity in ferrite [101] or even in the studied normalized 25N steel (Table 5.8). However, the D_{tb} values can be determined as the hydrogen "intrinsic diffusivity" in the given bainite ferrite.

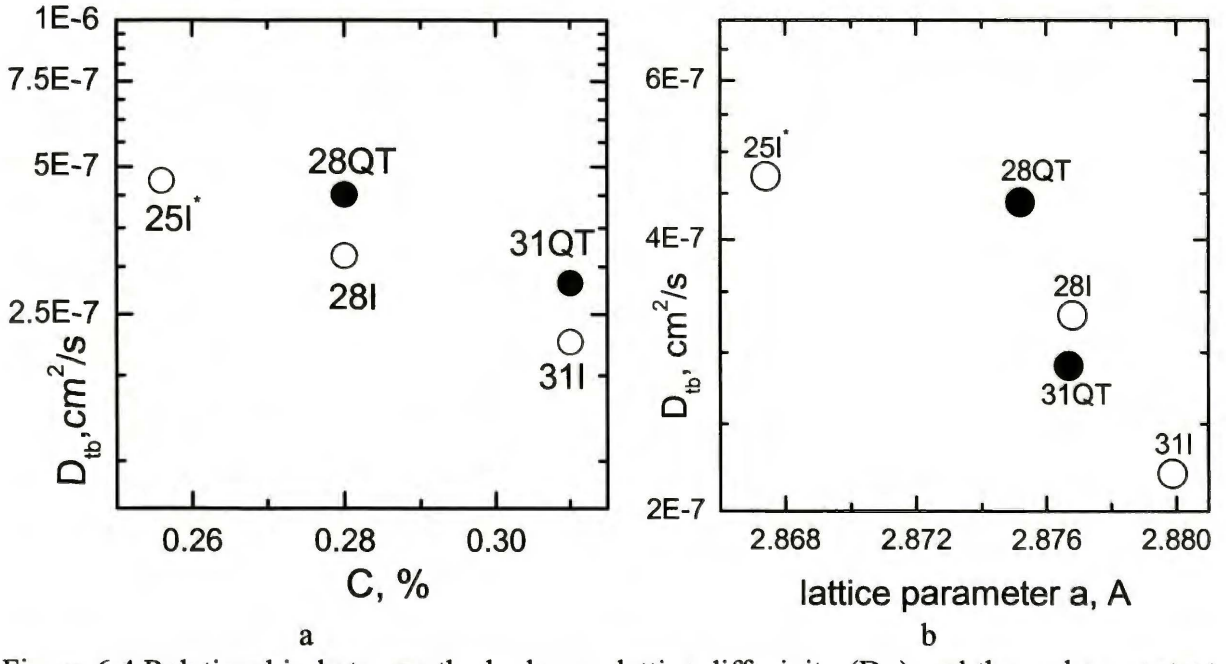

Figure 6.4.Relationship between the hydrogen lattice diffusivity (D_{tb}) and the carbon content (a) and between the hydrogen lattice diffusivity (D_{tb}) and the ferrite bainite lattice parameter (b) of steels.

As seen in Figure 6.4a the hydrogen diffusivity D_{tb} decreased with increasing of carbon content, similar as has been found in [103]. This might be associated with the increasing of deformation (expansion) of the bainite-ferrite lattice due to the increase in the carbon content. It also follows from Figure 6.4a that hydrogen diffusivity was higher in the quenched and tempered materials than in isothermally treated ones. In Figure 6.4b the hydrogen apparent diffusivity has been compared with the lattice parameters of the studied bainite steels. It is seen that hydrogen diffusivity roughly decreases with the increase in the lattice parameter. The tendency was especially apparent for the isothermally quenched steels.

6.2.1.2 Hydrogen trapping

In Figure 6.5 the hydrogen apparent diffusion coefficient D^*_{-1500} is shown for not shot peened materials. Coefficient D^*_{-1500} (Figure 6.5a) established from the buildup transient (Figure 4.8) according to equation (4.1) resembled the hydrogen transport affected by the interaction with hydrogen traps [39]. Hampering of the hydrogen transport due to the trapping has been confirmed by the lower values of D^*_{-1500} in comparison with the values of D_{tb} for all the studied materials, cf. Table 5.8.

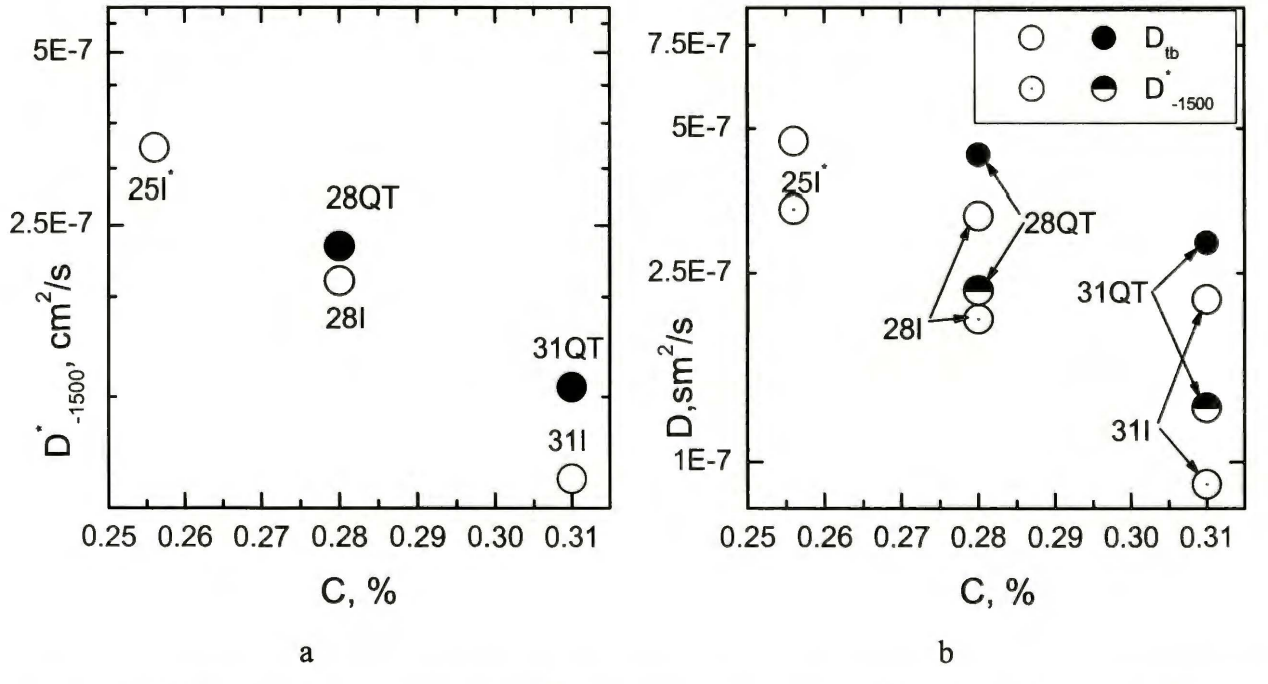

Figure 6.5.Effect of the carbon content on the apparent hydrogen diffusivity (D^*_{-1500}) (a) and on the difference between the lattice diffusivity (D_{tb}) and apparent diffusivity (D^*_{-1500}) (b)

With increase in the carbon content, the D^*_{-1500} values decreased and the difference between D^*_{-1500} and D_{tb} values increased (Figure 6.5b). This revealed the increase in the hydrogen trapping with the increase in the carbon content for similarly treated steels.

Trapping has been known [97] to affect the steady state hydrogen permeation measured under the similar charging conditions. Hydrogen steady state permeation decreased at the increase in the carbon content (Figure 6.6). This finding also confirmed the assumption on the increasing hydrogen trapping with the increase in carbon content for the specimens of the same heat treatment.

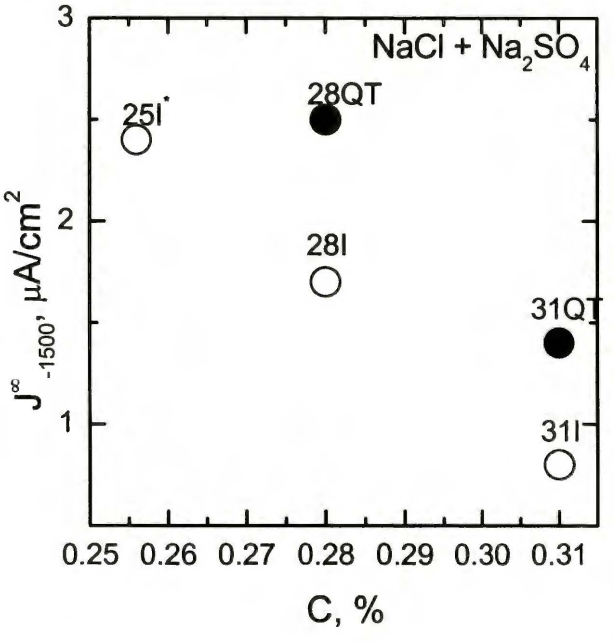

Figure 6.6. Effect of the carbon content on steady state hydrogen permeation through the studied not shot peened steels.

6.2.1.3 Hydrogen trapping efficiency

The effect of the trapping on the hydrogen transport may be estimated using the following relationship [101]:

$$\frac{D_{tb}}{D^*} = 1 + \frac{k}{p}N \qquad (6.1)$$

where: {k/p}*N – the trapping efficiency;

k and *p* - the kinetic parameters of capture and release of hydrogen from traps;

N – the density of traps.

In order to correlate the hydrogen trapping with microstructure features the observation of the fracture surface of the membrane subjected to high cathodic polarization may be used. At high cathodic polarization the microcracks and the peeling–off the surface layer at the ingress side of the membrane occurred as schematically shown in Figure 6.7. Under the conditions of present experiments the formation of the cracks leading to the peeling-off the membrane ingress surface occurred without application of the external stresses. Therefore, the cracking was a result of the local segregation and accumulation of trapped hydrogen.

Figure 6.7. Schematic presentation of cracks and peeled-off surface layer at the ingress side of membrane subjected to high cathodic polarization.

As seen in Figure 5.9 the microcracks have been formed along the grain boundaries of the bainite laths and the parent austenite grains. The observed resemblance of the marks on the surface peeled-off after the cathodic polarization with the steel microstructure geometry (Figures 5.11, 5.12) suggested in accordance with literature data [30, 145] that metal decohesion occurred at those grain boundaries. Therefore, the boundaries of the bainite laths and of the parent austenite grains served as the hydrogen traps.

Figure 6.8a shows the estimated trapping efficiency of steels ((k/p)*N) vs. the relative length of the boundaries calculated by quantitative metallography. Unexpectedly the hydrogen trapping efficiency decreased with the increase in the relative length of the boundaries, i.e. with the increase in the density of the possible traps. However, on the surface of the peeled-off metal (Figure 5.10, 5.12) the carbide particles have been observed. This may reveal the effect of the carbides on the hydrogen induced decohesion and thus on the hydrogen trapping. Therefore, the hydrogen trapping efficiency might be associated not with the relative length of the boundaries itself, but rather with the presence of the carbon [59] and the carbides [27, 68] on those boundaries. The occupancy of the grain boundaries by the carbon was calculated assuming that all the carbon segregated on the boundaries of the bainite laths and the parent austenite grains. As seen in Figure 6.8b the hydrogen trapping efficiency increased with the increase in the carbon density at the grain boundaries, i.e. with the trap sites density. This confirmed the above suggestions on the effect of the carbon segregation on the hydrogen trapping.

Irreversibly trapped hydrogen may be associated with the content of the residual hydrogen in membrane (V_H) measured after the switching off the cathodic polarization. According to the permeation test scheme (Figure 4.7) all the movable hydrogen desorbed from the membrane and only remained irreversibly trapped hydrogen was measured in the vacuum extraction test. As seen in Figure 6.9 the residual hydrogen content in the bainite steel roughly increased with the increasing carbon content, revealing the enhancement of irreversible hydrogen trapping in steel containing the higher carbon amount.

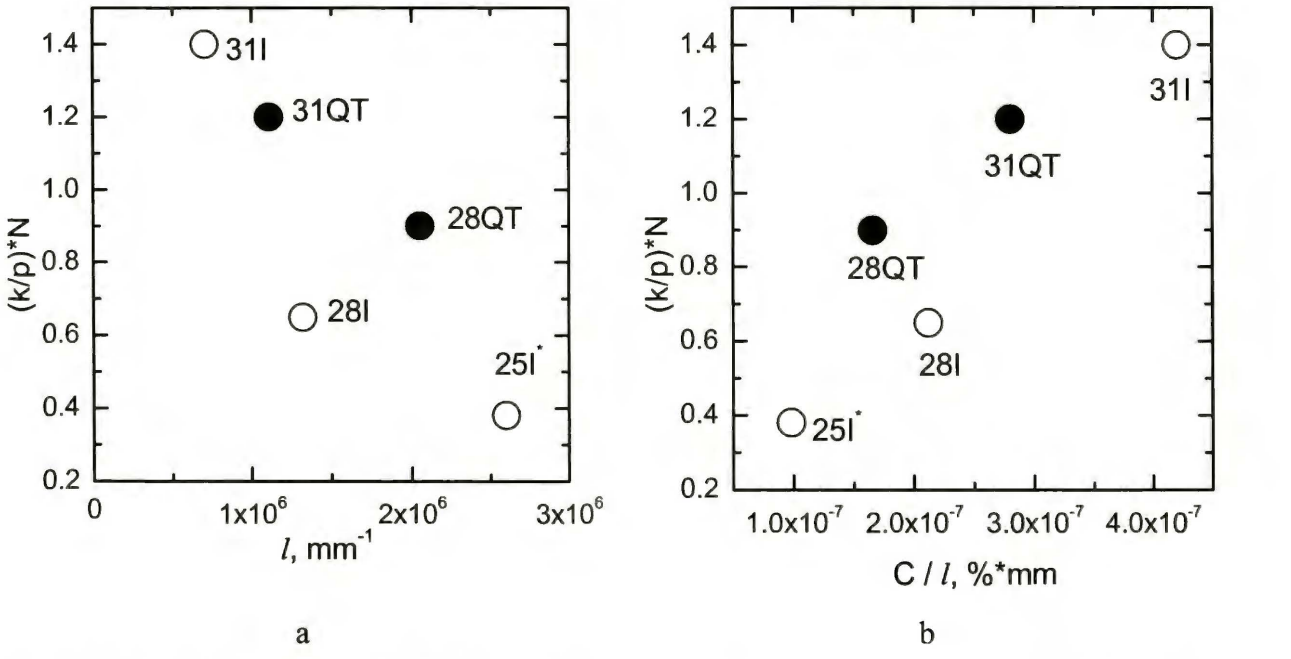

a b

Figure 6.8. (a) - relationship between the hydrogen trapping efficiency and the relative length of the boundaries of bainite laths and parent austenite grains;

(b) - relationship between the hydrogen trapping efficiency and the carbon segregation on the boundaries of bainite laths and parent austenite grains.

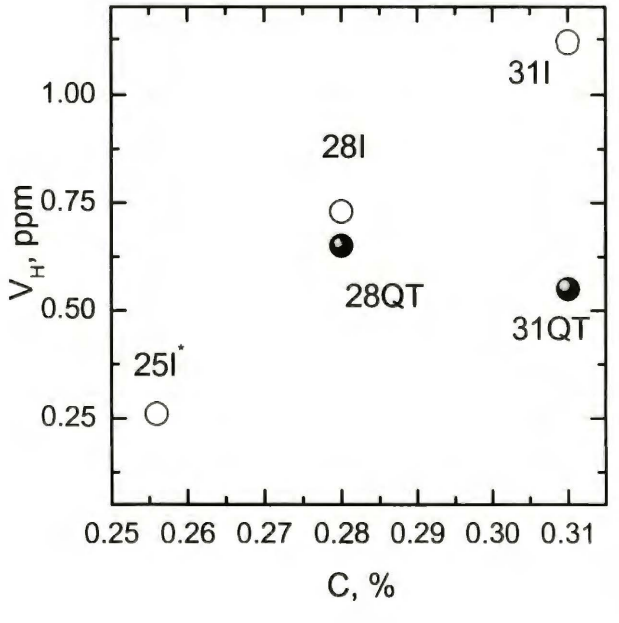

Figure 6.9. Effect of the carbon concentration on the residual hydrogen content in studied steels.

6.2.2 Susceptibility to hydrogen embrittlement

As it has been discussed earlier susceptibility to hydrogen embrittlement of high strength steels generally increases with the increase in the steel strength [25, 28,]. In the case of studied bainite steels there was no clear and apparent relationship between the strength and the susceptibility to stress corrosion cracking at cathodic polarization, cf. data in Table 5.1-5.3 and Table 5.11. The hydrogen mobility and its distribution between the different states should play an essential role in hydrogen embrittlement of studied steels.

According to [68, 90, 114] susceptibility to hydrogen induced cracking of high strength steels has been affected by the hydrogen diffusivity determining the rate of hydrogen to reach the hydrogen traps and by the hydrogen entry flux determining the accumulation of trapped hydrogen to critical level for cracking.

In Figures 6.10-6.12 susceptibility to hydrogen embrittlement has been compared with the evaluated hydrogen transport parameters. As seen in Figure 6.10 susceptibility to hydrogen embrittlement increased with decrease in the hydrogen diffusivity. This revealed that the hydrogen diffusivity itself did not govern the hydrogen embrittlement in the studied steels.

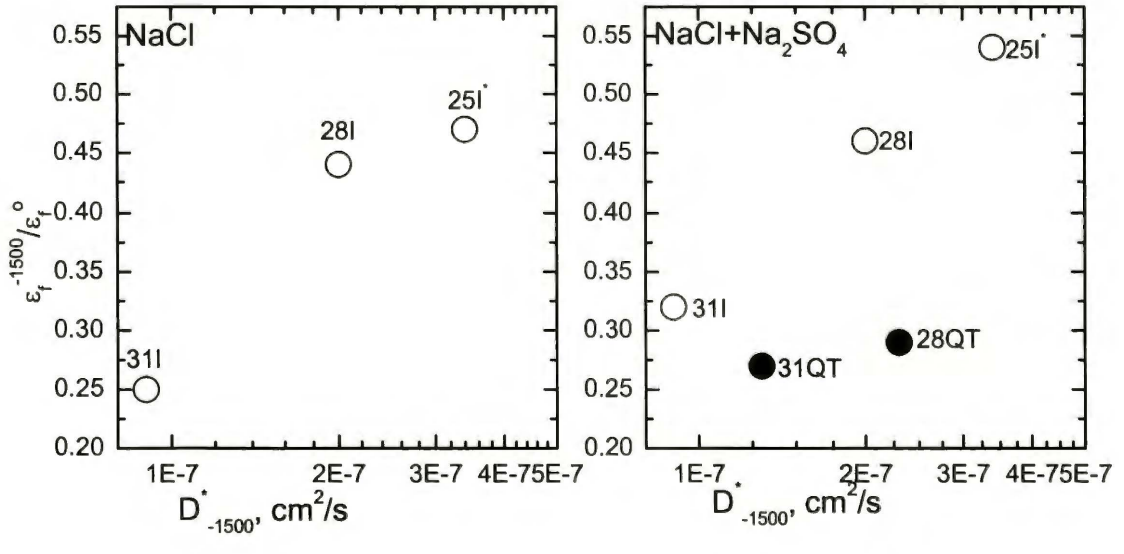

Figure 6.10. Relationship between the susceptibility to stress corrosion cracking at cathodic polarization in studied solutions and the hydrogen transport.

Susceptibility to the hydrogen embrittlement increased with decrease in the steady state hydrogen permeation (Figure 6.11). This relation seems to be in contradictory with the mentioned above effect of the hydrogen entry flux on the cracking. It should be emphasized, however, that the hydrogen permeation current measured in the permeation tests did not correspond to the hydrogen entry flux.

Due to the similar electrochemical conditions at the surface of studied steels at cathodic polarization -1500mV Hg/HgO (Figure 5.7) the similar hydrogen flux can be expected to enter the metals. On the other hand, the measured hydrogen permeation flux has been affected by the hydrogen trapping [97]. Therefore, the higher resistance to hydrogen embrittlement should have not been expected with the decrease in the hydrogen permeation rate. The relationship seen in Figure 6.11 reveals the effect of trapping.

Predominant effect of the trapping on the hydrogen induced stress corrosion cracking of the bainite steels follows from the data in Figure 6.12. It is seen that susceptibility to hydrogen embrittlement and thus to stress corrosion cracking at cathodic polarization in Cl^- containing solutions increased with the increase in hydrogen trapping efficiency.

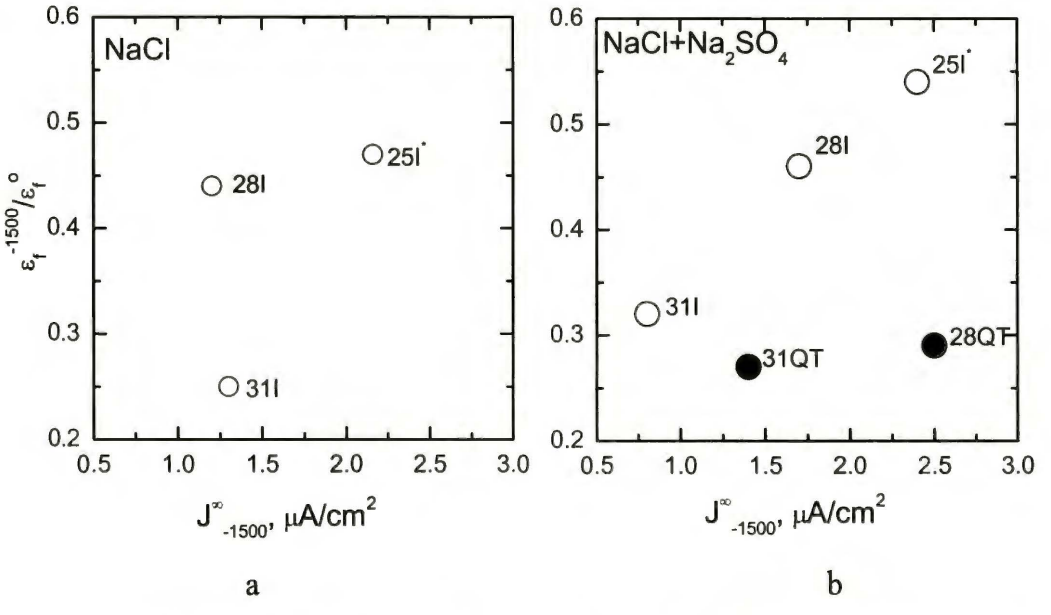

Figure 6.11. Relationship between the susceptibility to stress corrosion cracking at cathodic polarization in studied solutions and the steady state hydrogen permeation.

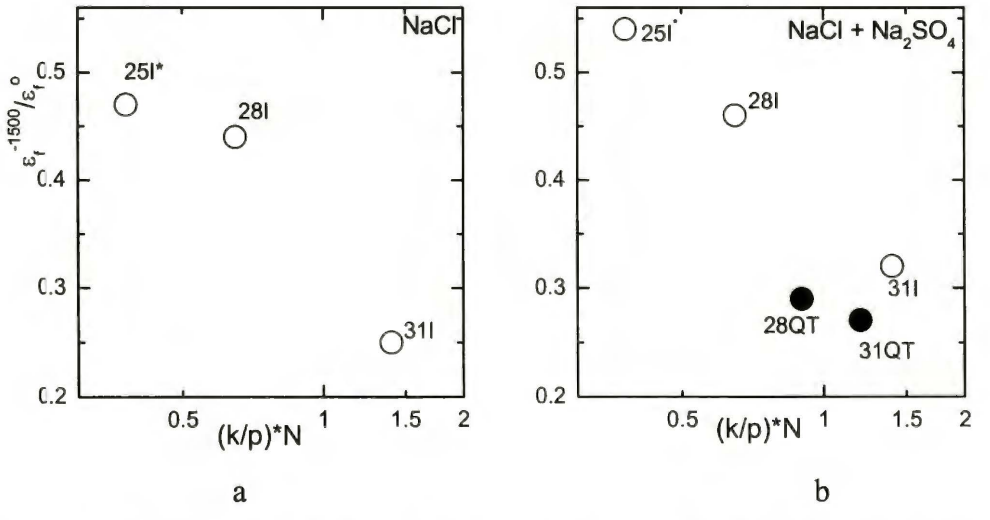

Figure 6.12. Relationship between the susceptibility to stress corrosion cracking at cathodic polarization in studied solutions and the hydrogen trapping efficiency.

6.3 Stress corrosion cracking at cathodic polarization of shot peened steel

6.3.1 Hydrogen transport in shot peened material

As seen in Figure 6.13a the steady state hydrogen permeation recorded for shot peened materials is lower than for not shot peened ones. This can not be an effect of decrease in hydrogen absorption due to the shot peening. As follows from Figure 5.7 the similar cathodic current density and thus the similar hydrogen evolution have been observed at cathodic polarization for not shot peened and shot peened materials. On the other hand, the much higher content of residual hydrogen measured in shot peened than in not shot peened materials showed that shot peening did not prevent the hydrogen absorption (Figure 6.13b).

The values of J^{∞}_{-1500}, D_{tb} and D^{*}_{-1500} estimated in hydrogen permeation tests carried out for shot peened material reflected the hydrogen transport through the plastically deformed shot peened layer and through the non deformed core as well.

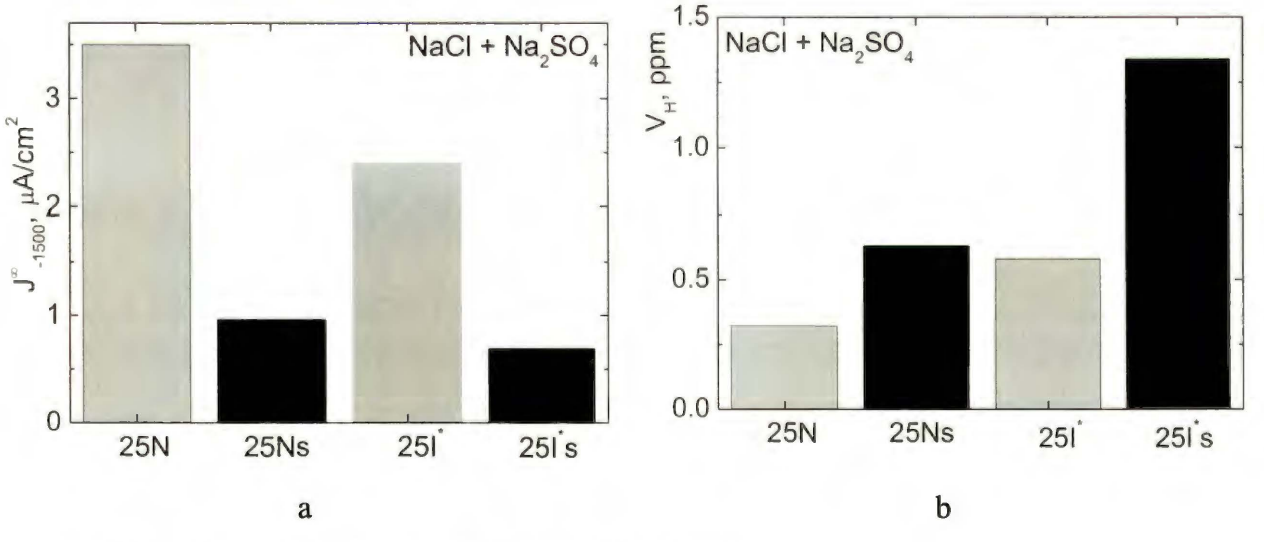

Figure 6.13. Effect of shot peening of 25N and 25I* steels
on the steady state hydrogen permeation (a)
and on the mean value of residual hydrogen content (b).

To estimate the parameters of hydrogen transport in deformed layer, the solution for diffusion through the material consisting of two layers (schematically shown in Figure 6.14) of different transport rate should be used. For the purpose of the present case the solution given in [146] was adopted.

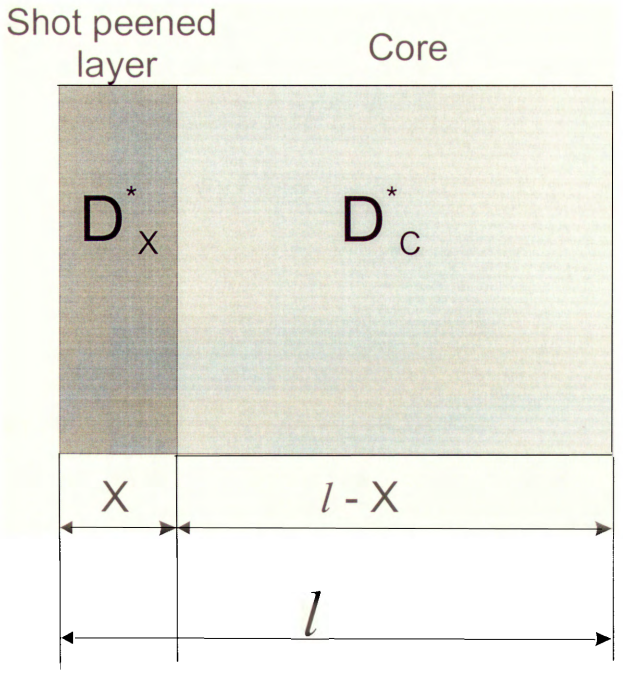

Figure 6.14. Schematic presentation of hydrogen diffusivity in shot peened layer and in the core.

In terms of the present study it can be written:

$$\tau_{0.63} = \frac{\left\{\frac{X^2}{D^*x}\left(\frac{X}{6D^*x} + \frac{lc}{2D^*c}\right) + \frac{l_C^2}{D^*c}\left(\frac{lc}{6D^*_c} + \frac{X}{2D^*x}\right)\right\}}{\frac{X}{D^*x} + \frac{lc}{D^*c}} \qquad (6.2)$$

where: $\tau_{0.63}$ – time to archive 0.63 of steady state permeation measured for shot the peened material from the buildup permeation transient at polarization -1500mV;

D^*_X – hydrogen apparent diffusivity in shot peened layer;

D^*_C – hydrogen apparent diffusivity in core;

X – thickness of the shot peened layer(Table 5.2);

$l_C = l - X$ – thickness of the core.

The hydrogen apparent diffusivity within the core (D^*_C) might be associated with the values of D^*_{-1500} estimated for respective not shot peened materials 25N and 25I*. The calculated hydrogen apparent diffusivity within the shot peened layer (D^*_x) is presented in Table 6.1. From the comparison of those values with the values of hydrogen lattice diffusivity (D_{tb}) for respected not shot peened materials (Table 5.8) the very high trapping efficiency (k/p)*N within the deformed layer has been estimated, as shown in Table 6.1. The lower steady state hydrogen permeation through the shot peened material than through the not shot peened one (Figure 6.13a) should be accounted for the retardation of hydrogen transport within the shot peened layer due to the hydrogen-traps interaction.

Table 6.1

Hydrogen diffusivity and trapping parameters in shot peened layers of studied steels.

Material	D^*_X	(k/p)/N	V_X	V_x/V_c
$25N_s$	$2.56*10^{-7}$	13.6	2.73	8.5
$25I^*_s$	$2.1*10^{-8}$	22.3	9.44	16.3

The content of residual hydrogen measured by vacuum extraction in the shot peened specimen is the mean value of irreversible trapped hydrogen content in the layer and in the core. The distribution of irreversible hydrogen between the shot peened layer and the core may be estimate using the scheme shown in Figure 6.15. The content of irreversibly trapped hydrogen in the layer (V_X) may be calculated according to the equation:

$$V_x = \frac{l \cdot V_H - (l - x)V_c}{x} \tag{6.3}$$

where : V_H- the mean content of residual hydrogen measured in shot peened steel (Table 5.9)

V_c – the content of residual hydrogen in core.

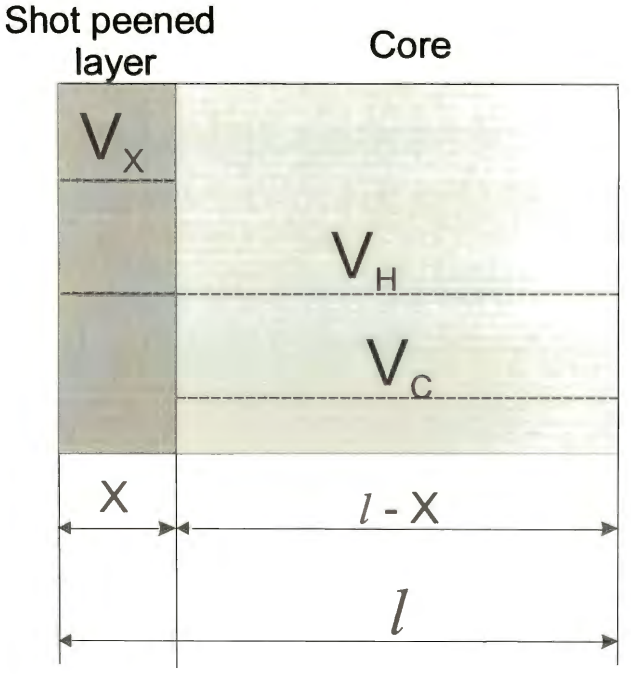

Figure 6.15. Distribution of the mean content of residual hydrogen between the shot peened layer and the core.

Assuming that V_C corresponded to the residual hydrogen content (V_H) measured for the not shot peened materials (Table 5.9) the content of irreversibly trapped hydrogen within the shot peened layer has been calculated, as shown in Table 6.1. Almost one order of magnitude higher content of residual hydrogen in the shot peened layer in comparison with not shot peened one (Table 6.1) revealed the high segregation of hydrogen within the deformed layer.

Shop peening did not change the steel chemistry. The retardation of hydrogen transport and the hydrogen segregation within deformed layer have been caused by intensification of hydrogen trapping due to the change of the microstructure produced by the shot peening. As seen in Figure 5.4 shot peening of normalized steel produced the heavy plastic deformation bands. This structure resembled the appearance of the surface peeled-off due to the high cathodic polarization (Figure 5.10). The formation of hydrogen induced cracks along the plastic deformation bands suggested that the increased dislocation density promoted the hydrogen trapping. In the case of bainite 25I* steel shot peening produced also the refinement of the bainite laths (Figure 5.3) and hence caused the increase in relative length of the boundaries and the number of the possible hydrogen traps. The increased relative length of the bainite laths boundaries and the increase in dislocation density occurred due to shot peening increased the reversible [30, 68, 97] and irreversible [114] hydrogen trapping within the shot peened layer.

6.3.2 Susceptibility to hydrogen embrittlement

The shot peened steels exhibited the lower resistance to hydrogen embrittlement in comparison with the not shot peened ones (Table 5.11). This is in agreement with the estimated higher efficiency of hydrogen trapping within the shot peened layer than within the bulk, and with the discussed above effect of the hydrogen trapping on susceptibility to hydrogen embrittlement.

However, the effect of surface deformation on the trapping efficiency was much higher than that on the susceptibility to hydrogen embrittlement. Increase in the trapping efficiency was about one order of magnitude whereas decrease in the resistance to hydrogen embrittlement was only about 35%. Susceptibility of shot peened material to hydrogen embrittlement has been affected by the hydrogen behavior in the shot peened layer and in the core. The segregation of hydrogen and the retardation of its transport within deformed layer decreased the hydrogen flux entering the core, which manifested itself in the lower value of the hydrogen permeation rate measured for shot peened material (Table 5.6). Therefore, under the similar charging conditions the flux of the hydrogen entering the core of the shot peened material was much lower than the hydrogen flux entering the not shot peened material. As a result, the possibility of hydrogen embrittlement of the core decreased.

6.4. Hydrogen behavior in fatigue pretreated steel

As it has been known [65] and as it has been confirmed in the present study of the shot peened materials the plastic deformation of steel resulted in the hindering of hydrogen transport and in the increase in its segregation. The similar effects could be traced also in the case of fatigue pretreated material, as seen in Tables 5.7 and 5.8. It has been also observed that with the increase in the maximum stress applied at fatigue tests the hydrogen permeation (Table 5.7), the hydrogen diffusivity D_{tb} (Table 5.8) and the hydrogen apparent diffusivity D^*_{-1500} decreased (Table 5.8), whereas the residual hydrogen content increased (Table 5.9).

In the case of fatigue the very specific dislocation structure has been known to form in materials. In Fe and Fe-0.11%C materials subjected to fatigue [79] the persistent dislocation bands have been formed instead the dislocation cells. The bands are few microns long with the distance between them about 1-3 μm. Within the bands the dislocations strips and walls are organized in the ladder like structure. Fatigue causes the refinement, scattering and even replacement of carbides in the ferrite-pearlite steels [79].

Although in the case of bainite structure the much complex dislocation structure should be expected, some resemblance to the dislocation structure caused by fatigue in pearlite-ferrite steels may occur. The formation of specific slip band structure and the deformation of the carbides due to fatigue tests may be supported by the appearance of the fracture surface of membranes cut from the fatigue pretreated specimens subjected to high cathodic polarization. As seen in Figure 5.17 peeled-off surface exhibits the fracture surface different from that observed in the case of other studied materials, including the shot peened ones (Figures 5.11 and 5.12). Surface revealed the ladder like appearance (Figure 5.17 c) which may resemble the specific appearance of the deformation structure formed during the fatigue.

From the results obtained for the differently cold worked materials it is seen that the hydrogen induced cracking followed the local deformation paths and, therefore, the kind of the applied cold work determined the mode of the hydrogen induced fracture of metal and the appearance of the fracture surface.

6.5. Effect of electrolyte chemistry on the susceptibility to SCC and HE of studied steels

As follows from the electrochemical measurement (Table 5.5) all the studied materials exhibited generally the more cathodic values of E_{ocp} potential and the higher values of corrosion current density in the NaCl+Na_2SO_4 solution than in the NaCl one. Susceptibility to SCC at open circuit potential as determined by the ratio of elongation to fracture in solution to that in air showed very close values for studied materials in both solutions (Table 5.11). Only 25I* steel was more susceptible to SCC in NaCl+Na_2SO_4 solution. However, as seen in Figure 5.18a, the NaCl+Na_2SO_4 solution produced the more pronounce deterioration effect on the reduction area. The mechanism of the crack initiation and propagation was similar in both solutions.

At cathodic polarization at -1500 mV hydrogen permeation current was slightly higher in the NaCl+Na_2SO_4 solution (Table 5.6). Although taking into account the scattering of the results the difference was not dramatic. Also susceptibility to SCC at the application of cathodic polarization determined by the ratio of elongation to fracture in solution to that in air did not differ considerably (Table 5.11). No substantial difference was also measured in RA of steels tested in both solutions, cf. Figure 5.18. The negligible effect of the chemistry and pH of the studied Cl^- containing solutions may be explained by specific conditions established within the cracks. Electrochemical conditions within the cracks differed from those maintained on the surface and were similar in the case of both solutions [83, 123].

Taking into account the higher corrosiveness of the NaCl+Na_2SO_4, the more pronounced effect of NaCl+Na_2SO_4 solution at Eocp on RA as well as the data revealing the more intensive pitting in the NaCl+Na_2SO_4 than in NaCl solution [129], the higher detrimental effect of the NaCl+Na_2SO_4 environment on the studied steel can be stated.

7. CONCLUSIONS

On the base of the discussion of the results obtained at testing the ferrite-pearlite and bainite 30HGSNAŻ type steels containing 0.25-0.31% C in the solutions simulating the sea shore atmosphere and the acid rain (acid dew) the following conclusions concerning the susceptibility to SCC and HE can be drawn :

1. In the low sulfur steel, not the sulfide inclusions but the other structure features govern the susceptibility to pitting corrosion, hydrogen embrittlement and stress corrosion cracking.
2. Susceptibility to stress corrosion cracking of the 30HGSNAŻ type steel in the NaCl and Na_2SO_4 + NaCl solutions under the open circuit conditions has been associated with the susceptibility of the steels to the pitting corrosion established in the tests chlorine containing solution.
3. Resistance to both, the pitting corrosion and the SCC increases with decreasing content of C in steel of similar microstructure.
4. Shot peening of the 30HGSNAŻ type steel with decreased carbon content allows increase mechanical properties of steel in order to fulfill the requirements.
5. The shot peening improves the resistance to pitting corrosion and to SCC of steel under the open circuit conditions.
6. Pitting resembles the deformation paths formed at the fatigue tests even if no apparent marks are seen on the surface of the specimens subjected to fatigue pretreatment.
7. Shot peening of material decreases the susceptibility to the pitting of the fatigue pretreated material and, thus, the decreasing in susceptibility to SCC of the material undergone the fatigue can be expected.
8. Susceptibility to hydrogen embrittlement of studied steels has been mainly governed by the hydrogen trapping efficiency, which is accounted by the carbon segregation at the boundaries of the bainite laths and the parent austenite grains.
9. Decrease in the carbon content in steel results in decrease in the hydrogen trapping and, thus, in lower susceptibility to hydrogen embrittlement.
10. Both kinds of the applied cold work (shot peening and fatigue) result in the increase in the hydrogen trapping by steel.
11. Shot peening increases the trapping efficiency within the deformed layer and, thus, hampers the hydrogen transport through the layer and causes the segregation of hydrogen within the layer.

12. Presence of the shot peened layer decreases the hydrogen flux entering the core and thus decreases the susceptibility of core to hydrogen embrittlement.
13. The appearance of the peeled-off fracture surface of the cold work materials resembles the pattern of the local increase in plastic deformation formed at prestressing. The mode of the fracture of cold work material depends on the kind of the applied cold work treatment.
14. The normalized ferrite-pearlite steel exhibits the lower susceptibility to pitting corrosion, stress corrosion cracking and hydrogen embrittlement in comparison with the bainite one of the similar chemistry.
15. Na_2SO_4 + NaCl solution simulating the acid rain or acid dew is more aggressive than NaCl solution, especially under the open circuit conditions. At cathodic polarization the effect of the solution chemistry is negligible.
16. The 30HGSNAŻ steel with carbon content below the lower limit required by the Standard for the 30HGSNAŻ steel subjected to surface modification by shot peening exhibited the mechanical properties required by the Polish standard, the resistance to pitting corrosion and to stress corrosion cracking at open circuit potential higher and the resistance to hydrogen embrittlement similar to those established for the standard steel.
17. Application of the modified 30HGSNAŻ steel for the aircraft parts might be considered.

8. REFERENCIES

1 Denny A. Jones, *Principles and Prevention of Corrosion*, Prentice hall, NJ, 1996.

2 J. Flis in *Wodorowe i korozyjne niszczenie metali*, PWN, 1979, p.174.

3 P.Aaltonen et al, *Selective dissolution-vacancy-creep model for EAC of brass*, in Proc. of **CDI'96**, Nice, France, 1996, p. 35.

4 A.R. Trojanoj, **Trans. ASM.**, *52*, 1960, p.54.

5 S. L. Lee, **Engineering Fracture mechanics**, *31*, 4, 1988, p.647.

6 R.A. Oriani in Proc. of **Stress Corrosion Cracking and Hydrogen Embrittlement of Iron Base Alloys, NACE-5**, Houston, 1977, p.351.

7 G.V. Karpenko, I.I., Wasilenko, *Korrozionnoe rastreskiwanie stalej*, Tehnika, Kiev, 1971.

8 S.P. Lynch, *A commentary on mechanism of environment assisted cracking*, in Proc. of **CDI'96**, Nice, France, 1996, p. 206.

9 E. Lunarska in *Hydrogen degradation of ferrous alloys*, Noyes Publ., NJ, 1985, p.321.

10 T. Tabata, H.K. Birnbaum, **Scripta metal.**, *17*, 1983, p.947.

11 T. Magnin et al, *The corrosion enhanced plasticity model: single crystal experiments and numerical simulation*, in Proc. of **CDI'96**, Nice, France, 1996, p. 12.

12 C.E. Sims, **Trans. AIME**, *215*, 1959, p. 367.

13 Z. Szklarska-Smialowska, **Corrosion**, *27*, 1971, 223.

14 Z.A. Jofa, G.N. Tomashowa, **Z. Fiz Chim** (russ), *21*, 1947, p.201.

15 Z.A. Jofa, V.V. Batrakov, Ba Cho Ngok, **Zashita Metallow** (russ), *1*, 1965, p. 55.

16 H. Holtan, H. Sigurdsson, **Werkstoffe und Korrosion**, *28*, 1977, p.475.

17 P. Poyet, A. Dessedtret, **Mem. Sc. Rev. Met.**, *72*, 1975, p.133.

18 P.E. Manning, D.J. Duquette, W.F. Savage, **Corrosion**, *35*, 1979, p.151.

19 W.L. Clarke, G.M. Gordon, **Corrosion**, *29*, 1973, p.1.

20 T. Murata in *Current Japanese Material Research, Vol.4: Localized Corrosion*, Elsevier Applied Science, London & New York, 1988, p. 17

21 B.F. Brown, *Stress corrosion cracking of high strength steels. The theory of stress corrosion cracking in alloys*, in Proc. of **NATO science committee research evaluation conference**, Brussels, 1971, p.186.

22 V.J. Colangelo, M.S. Ferguson, **Corrosion**, *25*, 1969, p.509.

23 G.E.Kerns, *Ph.D. thesis*, The Ohio State University, Columbus, Ohio, 1973.

24 G. Sandoz, **Met. Trans.**, *3*, 1972, p.1169.

25 P McIntyre in *Hydrogen Degradation of Ferrous Alloys*, Noyes Publ., NJ, 1985, p.763.

26 K. Farrel, A.G. Quarrell, **J. Iron Steel Instr.**, *202*, 1964, p.1002.

27 P.Manolatos, C.Duret-Thual, J.Le Coze, M.Jerome, E.Bollinger, **Corrosion Sci.**, *37*, 1995, p.1785.

28 G.E.Kerns, M.T.Wang, R.W.Staehle, *Stress corrosion cracking and hydrogen embrittlement in high strength steels* in Proc. of **Stress Corrosion Cracking and Hydrogen Embrittlement of Iron Base Alloys, NACE-5**, Houston, 1977, p.700.

29 B.E.Wilde, C.D.Kim, E.H.Phelps, **Corrosion**, *36*, 1980, p.625.

30 M.I.Luppo, J.Ovejero-Garcia, **Corrosion Sci.**, *32*, 1991, p.1125.

31 V. Pokhmurski, **FHMM** (russ), *4*, 1997, p.25.

32 M.T. Wang, R.W. Staehle, *Effect of heat treatment and stress intensity parmeters on crack velocity and fractografy of AISI 4340 steel* in Proc. of **International Conference on Hydrogen in Metal**, Paris, France, 1972, p.342.

33 A. Zielinski, E. Lunarska, P. Michalak, W. Serbinski, **FHMM**, to be published.

34 P. Timmins, *Solutions to Hydrogen Attack in Steels*, Materials Park,ASM, 1997.

35 Fragilisation par l`hydrogene et corrosion sous contrainte. Phenomenologie et mecanismes, Bombannes: Edit. Phys. 1990, p. 397.

36 E. Sitko, *Badanie przyczyn pękania wysokowytrzymałej stali konstrukcyjnej w warunkach działanai naprężeń i czynników korozijnych*, Ph.D thesis, IChF, Warszawa, 1980.

37 D.N.Williams, **Oil &Gas Journal**, *3*, 1981, p. 86.

38 M. Margot-Marette, T. Jossic, J.L. Caplet, J.C. Charbonnier, A.M. Brass, *Application of electrochemical permeation technique to hydrogen trapping in steels correlation with hydrogen induced cracking resistance*, in Proc. of **Hydrogen-4**, Beijing, 1988, p.168.

39 I.M.Bernstein, G.M.Pressouyre in *Hydrogen degradation of ferrous alloys*, Noyes Publ., NJ, 1985, p.641.

40 R.T. Ault, K.L. McDowell, P.L. Hendricks, T.M.F. Ronald, **Trans. ASM**, *60*, 1967, p.79.

41 A.Chavane, M. Habashi, G.M. Pressouyre, J. Galland, ***Corrosion***, *42*, 1, 1986. p.54.

42 P. Lillys, A.E. Nehrenberg, **Trans ASM**, *48*, 1956, p.327.

43 R.A.Davis, **Corrosion**, *19*, 1966, p.323.

44 W.A. Van der Sluys, **Eng. Fract. Mech.**, *1*, 1969, p.447.

45 D.P.Williams, H.G. Nelson, **Met. Trans.**, *1*, 1970, p.63.

46 V.R.Sawicki, Jr. *Ph.D. Thesis*, Cornell University, Ithaca, NY, 1971.

47 R.P.M. Proctor, H.W. Paxton, **Trans. ASM**, *62*, 1969, p.989.

48 M.J. Morgan, C. J. McMahon in *Hydrogen degradation of ferrous alloys*, Noyes Publ., NJ, 1985, p.608.

49 B. D. Craig, **Corrosion**, *34*, 1978, p. 282.

50 J. C. M. Ferrar, R.E. Dolby in *Sulfide inclusions in steel*, American Soc. for Metal, Materials/Metalworking Technology Ser., 6, 1975, p.252.

51 B.E. Wilde, C.D. Kim, E.H. Helps, **Corrosion**, *36*, 1980, p.625.

52 J.E. French, P.F. Weinrich, C.W. Weaver, **Scripta Met.**, *13*, 1979, p.285.

53 J.C.M. Li, R.A. Oriani, L.S. Darken, **Z. Phys. Chem. (N.F.)**, *49*, 1966, p.271.

54 A. Ciszewski, T. Radomski, M. Smialowski in Proc. of **Stress Corrosion Cracking and Hydrogen Embrittlement of Iron Base Alloys, NACE-5**, Houston, 1977, p.671.

55 I.P. Zhegina, E.B. Chabina, L.N. Beljakov, N.G.Orehov, N.G. Pokrowskaja, **FHMM** (russ), *5*, 1991, p.89.

56 G. Sandoz, *Stress corrosion cracking in high strength steels and in titanium and aluminum alloys*, Naval Research Laboratory, Washington, DC, 1972, p.79.

57 C.S. Carter, **Corrosion**, *25*, 1969, p.423.

58 T. Hyodo, M. Iino, A. Ikeda, M. Kinura, M. Shimizu, **Corrosion Scence**, *27*, 10, 1987, p.1077

59 I.I.Dikij, **FHMM** (russ), *17*, 1981, p.108.

60 E.E. Glikman, E.R. Bruwer, K.J. Sarychew, **Doklady AN SSSR** (russ), *200*, 1971, p.1055.

61 K. Yokogawa, S. Fukuyama, K. Kudo, *Hydrogen environment embrittlement of carbon steels at room temperature* in Proc. of **2-nd JIM international symposium**, Minakami, Japan, 1979, p.417.

62 S.C. Chang, J.P.Hirth, **Metal. Trans. A**, *17A*, 1986, p.1485.

63 Y. Sakamoto, K. Takao, *Effect of quenching and tempering on diffusion of hydrogen in high-strenght alloy steels* in Proc. of **Second international congress on hydrogen in metals**, Paris, France, 1977, 1A8.

64 E. Sato, M. Hashimoto, T. Murata, **Trans ISIJ**, *21*, 2, 1981, p.151.

65 B. Marandet in Proc. of **Stress Corrosion Cracking and Hydrogen Embrittlement of Iron Base Alloys, NACE-5**, Houston, 1977, p.774.

66 S. F. Floreen in *Hydrogen degradation of ferrous alloys*, Noyes Publ., NJ, 1985, p.799.

67 Z. Szklarska-Smialowska, Z. Xia, **Corrosion Science**, *39*, 12, 1997, p.2171.

68 Z.Szklarska-Smialowska, *Susceptibility of steels to hydrogen trapping evaluated by potentiostatic double pulse technique* in Proc. of **Polish-Japan symposium "Enviromental effects in high technology materials"**, Zakopane, 1997, p.131.

69 W. Dietzel, M. Pfuff, G.G. Juilfus, *Investigation of hydrogen transport in plastically deformed steel membranes*, in Proc. of **EDEM-2003**, Bordeaux, France, 2003, KN3-3-3.

70 P.G.Bailey, J.M. Whalen in *Surface Engineering*, Elsevier Applied Science, London, 1990, p.379.

71 D.W.Hammond, S.A.Meguid in *Surface Engineering*, Elsevier Applied Science, London, 1990, p.386.

72 A. Nakoneczny, W. Szyrle, *Właściwości eksploatacyjne materiałów obrobionych dynamiczną powierzchniową obróbką plastyczną* in Proc. of **Nowoczesne procesy specjalne w obróbce metali**, Rzeszów, Poland, 1998, p.51.

73 M. Koma, V. Dinar, R. Mardarevic, A. Nakoneczny, L. Kwiatkowski, O. Kowtun, *Mechanoelektrohimichni wlastiwosti splawu D16T pislja riznyh wydiw powerhnewoi obrobki* in Proc. of **Korozia-2004**, Lviv, Ukraina, 2004, p.698.

74 E. Łunarska, O. Czerniajewa, A. Nakonieczny, **Inzynieria Powierzchni**, *22*, 2000, p.12.

75 P. O'Hara, *Stress corrosion, fretting and fatigue control by surface pre-stressing*, Surface Engineering Practice, Ellies Horwood Publ, London, 1990.

76 J. Labanowski, A. Ossowska, J.Cwiek, *Influence of cold worked laser on stress corrosion cracking susceptibility of duplex stainless steel*, in Proc. of **II Pomorska konferencja naukowa**, Gdansk-Sobieszewo, Poland, 2001, p.148.

77 C.L. Ho, S.L.I. Chan, J.Y. Lin, *Evaluation of three different surface modification technique for resisting hydrogen embrittlement in steel*, in Proc. of **12th International Corrosion Congress**, Houston, TX, 1993, p. 2367.

78 M. Smialowski, *Wodor w stali*, WNT, Warszawa, 1961.

79 S.Kocanda, *Fatigue failure of metals*, Sijthoff & Noordhoff International Publishers, Alphen aan den Rijn, 1978.

80 J. Toribio, V. Kharin, **FHMM** (russ), *4*, 2002, p.43.

81 P.C. Hughes, I.R. Lamborn, B.B. Liebert, **J.I.S.I.**, *203*, 1965, p.156.

82 R.S. Treseder, T.M. Swanson, **Corrosion**, *24*, 1968, p.31.

83 O.N. Romaniv, G.N. Nikiforchin, A.T. Tsyrulnik, **FHMM** (russ), *2*, 1984, p.3.

84 C.F. Barth, E.A. Steigerwald, A.R. Troianoj, **Corrosion**, *25*, 1969, p. 353.

85 M.F. McGUire, R.F. Hehemann, A.R. Troianoj, *Stress corrosion cracking and hydrogen embrittlement in 410 stainless steel*, in Proc. of **International Conference on Hydrogen in Metal**, Paris, France, 1972, p.325.

86 T.P. Radhakrishnan, L.L. Shreir, **Electrochimica acta**, *11*, 1966, p.1007.

87 G.B. Wood, **J. Electrochemical Soc.**, *110*, 1963, p.867.

88 C.M. Hudgins, R.L. McGlasson, P. Mehdizadeh, W.M. Rosborough, **Corrosion**, *22*, 1966, p.238.

89 Z. Szklarska-Smialowska, *Pitting corrosion of metals*, NACE, 1986.

90 A. Turnbull, **Materials Science Forum**, *192-194*, 1995, p.63.

91 A. I. Shirley, C.K. Hall, **Scripta Metallurgica**, *17*, 1983, p.1003.

92 B.G. Pound, *Predicting the susceptibility to hydrogen embrittlement*, in Proc. of **12th International Corrosion Congress**, Houston, TX, 1993, p.2356.

93 M.A.V Devanathan, Z Stachurski, **J. Electrochemical Soc**., *121*, 1964, p.619.

94 B.G. Pound, *Evaluation of diffusion/trapping model of hydrogen ingress in high strength alloys*, SRI International, Final report to the office of Naval Research, contract No. N00014-86-C-0233, 1988.

95 B.G. Pound, **Acta Metall.**, *18*, 1990, p.2373.

96 B.G. Pound, R.M. Sharp, G.A. Wright, **Acta Metall.**, *35*, 1987, p.263.

97 M. Iino, **Acta Metall.** *30*, 1982, p.377.

98 R.D. McCright in Proc. of **Stress Corrosion Cracking and Hydrogen Embrittlement of Iron Base Alloys, NACE-5**, Houston, 1977, p.308.

99 G.W. Hong, J.Y. Lee, **Mat. Sci & Eng.**, *61*, 1983, p.219.

100 S.M. Lee, J.Y. Lee, **Met. Trans. A**, *17A*, 1986, p.181.

101 G.M. Pressouyre, I.M. Bernstein, **Metall. Trans. A**, *9A*, 1978, p.1571.

102 R.F. Blundy, R. Royce, P.Poole, L.L. Shreir, in Proc. of **Stress Corrosion Cracking and Hydrogen Embrittlement of Iron Base Alloys, NACE-5**, Houston, 1977, p.636.

103 W.C. Luu, J.K. Wu, **Corrosion science**, *38*, 2, 1996, p.239.

104 T.K. Sergeeva, E.F. Petrowa, L.A. Swartsman, N.A. Pawlenko, **Metally** (russ), *6*, 1986, p.133.

105 M. Iino, **Metall. Trans. A**, *16A*, 1985, p.401.

106 A.A. Knjazev, V.A. Volkov, L.G. Chernuha, **Metally** (russ), *4*, 1984, p.43.

107 A.R. Elsea, E.E. Fletcher, *DMIC Report 219*, Battelle memorial institute, 1965.

108 U.V. Baht, H.K.Lloyd, **J.Iron and Steel Institute**, *165*, 1950, p.382.

109 C.D. Kim, A.W. Loginow, **Corrosion**, *24*, 1968, p.313.

110 M.I.Luppo, J. Ovejero-Garcia, **Corrosion Science**, *32*, 10, 1991, p.1125.

111 C.S.Kortovich, E.A.Staigerwald, **Engn. Fract. Mech.**, *4*, 1972, p. 637

112 L.Nannis, T.K.G.Namboodhiri, in Proc. of **Stress Corrosion Cracking and Hydrogen Embrittlement of Iron Base Alloys, NACE-5**, Houston, 1977, p.432.

113 J.O'M. Bockris, P.K. Subramanyan, **J. Electrochem. Soc**., *118*, 7, 1971, p.1114.

114 A.Turnbull, M.W, Carroll, D.H.Ferriss, **Acta metall.**, *37*, 1989, p.2039.

115 G.M.Pressouyre, I.M.Bernstein, **Acta metall.**, *27*, 1979, p. 89

116 R.B. Rebak, L. Muchjin, Z. Szklarska-Smialowska, **Corrosion**, *53*, 6, 1997, p.481.

117 B.G.Pound, **Corrosion**, *45*, 1989, p. 18.

118 J. Cwiek, K. Nikiforow, **FHMM** (russ), to be published.

119 G.M. Pressouyre, **Metall. Trans. A**, *10A*, 1979, p.1571.

120 E. Lunarska, K. Nikiforow, A. Zieliński, P. Domżalicki, E. Sitko, **Ochrona przed korozją,** wydanie specjalne, **XLII**, 1999, p.462

121 E.S. Ivanov, **FHMM** (russ), *6*, 1989, p. 92.

122 A.I. Basarab, W.M. Zhovnirchuk, O.T. Tsirulkik, **FHMM** (russ), *5*, 2001, p.106.

123 W.I. Kampinos, **FHMM** (russ), *3*, 1981, p.115.

124 Yu. A. Krupin, I.K. Kiselev, **FHMM** (russ), *5*, 1990, p. 36.

125 A.Ju. Kazanskaja, M.A. Smirnov, V.V. Zabilski, **FHMM** (russ), *8*, 1990, p.201.

126 E.Lunarska, K. Nikiforow, E. Sitko, *Wpływ obróbki cieplnej stali lotniczej 30HGSHA na absorpcję i przenikanie wodoru* in Proc. of **V Ogłnopolski Sympozjum Naukowo-Techniczne Nowe osiągnięcia w badaniach i inżynierii korozyjnej**, Poraj, Poland, 1998, p. 209.

127 Łunarska E., Nikiforow K., Czerniajewa O., Sitko E., *Hydrogen embrittlement of 30HGSNA aircraft steel in Cl^- containing environments* in Proc. of **Intern. Conf. EDEM-99**, Gdańsk-Jurata, 1999, *1*, p.32-37.

128 V.V. Velichko, G.M. Miheev, V.V. Zabilskij, D.I. Maleew, **FHMM** (russ), *1*, 1991, p.112.

129 W. Karliński, *Odporność stali 30HGSNA na korozję naprężeniwą*, Internal report, Instytut Lotnictwa Warszawa, 1999.

130 *Analiza przyczyn korozyjnego pękania elementów samolotów na przykładzie wybranej wysokowytrzymałej stali konstrukcyjnej*, Grant KBN T129713, Head: E.Sitko, Report ITWL, Warsaw, 2001

131 *Analiza trwałości i wytrzymałości stali 25HGSNAŻ przewidzianej do remontu wysokoobciążonych elementów konstrukcyjnych eksploatowanych samolotów i śmigłowców*, Grant KBN T12C06219, Head: E.Sitko, Report ITWL, Warsaw, 2003.

132 *Acid Reign '95*, Abstract Book, Kluwier Academic Publ., 1996.

133 D.T. DeHoff, F.N. Rhines, *Quantitative Microscopy*, McGraw-Hill, NY, 1973.

134 E. Łunarska, K. Nikiforow, **Ochrona przed Korozją**, *44*, 2001, p. 115.

135 M.A.V.Devanathan, Z.Stachurski, **Proceed. Roy. Soc.**, *270*, 1962, p.351.

136 E.Gileadi, M.A.Fullenwider, J.O'M.Bockris, **J. Electrochem. Soc.**, *113*, 1966, p.926.

137 J.McBreen, L.Nanis, W.Beck, **J. Electrochem. Soc.**, *113*, 1966, p.1218.

138 T.Zakroczymski, Wnikanie i transport wodoru w żelazie i jego stopach, Wydawnictwo IChF PAN, Warsaw, 1990.

139 N.Boes and H.Zuchner, **J. Less Comm. Met.**, *49*, 1976, p.223.

140 L.Habraken, J.-.L de Brouwe, *Fundamentals of Metallography*, Presses Academiques Europeennes, Bruxelles, 1975.

141 E. Lunarska, Y. Ososkov, *Change in structure of pipeline steels due to subcritical hydrogen charging*, in Proc. of **CDI'96**, Nice, France, 1996, p. 271.

142 E. Lunarska, J. Jagodzinski, K. Nikiforow, **J. Alloys and Compounds**, *310*, 2000, p.205.

143 S. Katarzyński, S. Kociańda, M. Zakrzewski, *Badanie własności mechanicznych metali*, WNT, Warszawa, 1967.

144 J.O'M.Bockris, in Proc. of **Stress Corrosion Cracking and Hydrogen Embrittlement of Iron Base Alloys, NACE-5**, Houston, 1977, p.286.

145 J.Yao, J.R.Cahoon, **Acta metall. mater.**, *39*, 1991, p.119.

146 R. Ash, R.M. Barrer, D.G. Palmer, **Brit. J. Appl. Phys.**, *16*, 1965, p. 873.